Lehrstuhl für Fluidmechanik und Prozessautomation der Technischen Universität München

Mathematically Based Management of *Saccharomyces sp.* Batch Propagations and Fermentations

Tomas Kurz

Vollständiger Abdruck der von der Fakultät Wissenschaftszentrum Weihenstephan für Ernährung, Landnutzung und Umwelt der Technischen Universität München zur Erlangung des akademischen Grades eines

Doktor-Ingenieurs (Dr.-Ing.)

genehmigten Dissertation.

Vorsitzender:	Univ.-Prof. Dr. rer. nat. habil. R. F. Vogel
Prüfer der Dissertation:	1. Univ.-Prof. Dr.-Ing. habil. A. Delgado
	2. Univ.-Prof. Dr.-Ing. E. Geiger
	3. Prof. Dr.-Ir. A. Debourg / Freie Universität Brüssel (schriftliche Beurteilung)

Die Dissertation wurde am 23.10.2002 bei der Technischen Universität München eingereicht und durch die Fakultät Wissenschaftszentrum Weihenstephan für Ernährung, Landnutzung und Umwelt am 07.11.2002 angenommen.

This thesis was published with the same title in the series 14, number 112 of the “VDI Fortschrittsberichte” (VDI proceedings) by the VDI Verlag, Düsseldorf.

ISBN 3-18-311214-0

Acknowledgements

This thesis was made from 1997 to 2002 at the “Lehrstuhl für Fluidmechanik und Prozessautomation” at the “Technische Universität München”. My thank goes to all, who have supported me in this time.

First, I want to thank Eva Fischer who supported and motivated me in an unique manner.

Especially, I want to thank my “Doktorvater” Prof. Dr.-Ing. A. Delgado for his confidence and support. He made this work possible and allowed me wide academic freedom. I also want to thank PD Dr.-Ing. T. Becker for his advice and my colleagues Dr.-Ing. E. Murnleitner and Dr.-Ing. S. Arnold for the productive discussions.

I also wish to thank W. Seidl and J. Rohrer who supported me in construction of the pilot plant, as well as A. Lorenz, who supported me in electrical affairs.

Parts of this work follow directly from master or students thesis. Here, I want to thank Dipl.-Ing. T. Becher, Dipl.-Ing. J. Mieleitner and Dipl. Braum. T. Bollinger as well as D. Wagenknecht, B. Balg, D. Wallerius and B. Huehnlein who supported this work in an excellent manner. I also want to thank C. Mutzel and H. Teichert who supported this work as collegiate assistants.

Industrial aspects of this work were notably supported by different breweries. Especially, I want to thank Dr.-Ing. U. Peters, Dr.-Ing. G. Stettner, Dipl.-Ing.H. Wolfinger, Dipl.-Ing. F. Peifer, Dipl.-Ing. W. Viehhauser and Dipl.-Ing. P. Winter.

I wish to thank Birgit and Marc McMahon as well as Katharina Fischer for the correction concerning the English language.

Further, I wish to thank Prof. Dr.-Ing. E. Geiger and Prof. Dr.-Ir. A. Debourg for their interest in my work and for their audit, as well as Prof. Dr. rer. nat. R.F. Vogel for taking the chair of the examination board.

Parts of this work were supported by the Wissenschaftsförderung der Deutschen Brauwirtschaft e.V. (B68).

Last, but not least, I wish to thank all my colleagues at the LFP for the friendly climate I could experience here.

Freising, November 2002 Tomas Kurz

Meinen Eltern gewidmet.

For my parents.

Table of Contents

ABBREVIATIONS AND SYMBOLS VIII

ABSTRACT X

ZUSAMMENFASSUNG XI

PUBLICATIONS XIII

1 INTRODUCTION AND CONCEPTIONAL FORMULATION 1

1.1 Introduction 1

1.2 The scope of the thesis 3

2 BASIC CONSIDERATIONS 4

2.1 Modelling 4
2.1.1 General considerations 4
2.1.2 Deterministic mathematical modelling 5
2.1.2.1 Unstructured Models 7
2.1.2.2 Structured models 9
2.1.2.3 Segregated models 9
2.1.3 Modelling approaches for temperature influence in biotechnology 9
2.1.3.1 Models of the Arrhenius type 9
2.1.3.2 Bělehrádek type models 14

2.2 Relevant aspects to Saccharomyces cerevisiae 15
2.2.1 Yeast metabolism 15
2.2.1.1 Catabolism 15
2.2.1.2 Anabolism and maintenance 19
2.2.1.3 Metabolism regulation phenomena 19
2.2.2 Substrate uptake mechanisms 22
2.2.2.1 Sugar uptake 22
2.2.2.2 Oxygen uptake 23
2.2.3 Yeast batch propagation and fermentation 24

3 PRESENTATION AND DISCUSSION OF RESULTS 27

3.1 Mathematical modelling of Saccharomyces sp. metabolism 27
3.1.1 Requirements for the modelling approach 27
3.1.1.1 General requirements 27
3.1.1.2 Specific conditions in brewing industry 28
3.1.2 Existent modelling approaches for yeast growth and fermentation 29
3.1.3 Black-Box modelling approach 30
3.1.3.1 Stoichiometry 32
3.1.3.2 Kinetics 33
3.1.4 Metabolic modelling approach 38

3.1.4.1 Stoichiometry 39

3.2 Validation of simulations of yeast propagations 43
3.2.1 Validation using literature data 44
3.2.2 Simulations of experiments A 47
3.2.3 Simulations of experiments B 49
3.2.4 Simulations of experiments C 51
3.2.5 Simulations of experiments D 53
3.2.6 Sensitivity Analysis 54

3.3 Technological and mathematical validation of the influence of manipulated variables 64
3.3.1 Technological validation of the influence of temperature as manipulated variable 65
3.3.2 Modelling the temperature dependency of substrate and oxygen uptake kinetics and specific growth rate 69
3.3.2.1 Square-root- model 69
3.3.2.2 Bělehrádek-Model 70
3.3.2.3 Schoolfield-Modell 71
3.3.2.4 Model of Mohr and Krawiec 71
3.3.2.5 Comparison and evaluation of the results 72
3.3.3 Validation of the influence of oxygen as manipulated variable 76

3.4 Process control scenarios for brewing yeast propagations 77
3.4.1 Temperature control scenarios 78
3.4.2 Dissolved oxygen scenarios 80

3.5 Simulations of industrial batch propagations 82
3.5.1 Isothermal propagations 82
3.5.1.1 Results of experiments E 82
3.5.1.2 Results of experiments F 83
3.5.1.3 Results of experiments G 84
3.5.2 Sequencing batch propagations 86
3.5.3 Non-isothermal propagations 87

3.6 Simulation of brewing fermentations 89

4 CONCLUSIONS AND OUTLOOK 93

5 MATERIALS AND METHODS 96

5.1 Yeast propagation system 96
5.1.1 Yeast propagation system 1 96
5.1.1.1 Experimental Set Up 96
5.1.1.2 CIP and supply 98
5.1.1.3 Temperature control of the propagation system 98
5.1.1.4 Aeration and dissolved oxygen control 100
5.1.1.5 Implementation of PLC and the Human Machine Interface 100
5.1.2 Propagation plant 2 101
5.1.3 Propagation plant 3 101
5.1.4 Propagation plant 4 101
5.1.5 Propagation plant 5 102
5.1.6 Propagation plant 6 102

5.2 Online measurement and calibration 102

5.3 Analytical methods 103
5.3.1 Offline measurement 103
5.3.2 Offline data processing 104
5.3.2.1 Specific growth rate 104
5.3.2.2 Biomass concentration 104
5.3.2.3 Fermentable gravity and glucose equivalent 104

5.4 Microorganisms and medium 105

5.5 Computational methods 106
5.5.1 Aquasim modelling software 106
5.5.2 Parameter determination for temperature model (Newton approach) 107

APPENDIX 108

Additional Figures 108

Validation of the models 111

Modelling of temperature dependency 115

Process control scenarios 119

Industrial Propagations 120

Tables to materials and methods 121

REFERENCES 122

ABBREVIATIONS AND SYMBOLS

δ	P/O-Relation
μ	Specific growth rate
μ_{eth}	Specific growth rate for growth on ethanol
$\mu_{s,f}$	Specific growth rate for fermentative growth on glucose
$\mu_{s,ox}$	Specific growth rate for oxidative growth on glucose
A	Stoichiometry matrix
a, b, ...	Stoichiometric coefficients
ATP_i	Stoichiometric coefficient
CCF	Cylindroconical fermentation tank
E	Ethanol concentration
f_{temp}	Coefficient for temperature dependency of the specific substrate uptake rate
HX	Hydrogen portion of the biomass composition (mol/c-mol)
IL	instruction list
K_e	Half saturation constatnt for limitation of ethanol uptake
$K_{i,s}$	Half saturation constant for glucose inhibition of the ethanol uptake
$K_{i,eth}$	Half saturation constant for ethanol inhibition of the substrate uptake (glucose)
$K_{i,eth,o}$	Half saturation constant for ethanol inhibition of the oxygen uptakel
K_n	Half saturation constant for nitrogen limitation of the glucose uptake
K_o	Half saturation constant for oxygen limitation of the oxygen uptake
K_s	Half saturation constant for glucose limitation of the glucose uptake
L_t	Lag time function for the growth on glucose
$L_{t,eth}$	Lag time function for the growth on ethanol
m_{ATP}	Energy demand for maintenance
N	Concentration of assimilable nitrogen
NAD	nicotinamide adenine dinucleotide, oxidised
$NADH_2$/ $NADH/H^+$	nicotinamide adenine dinucleotide, reduced
NX	Nitrogen portion of the biomass composition (mol/c-mol)
O	Oxygen concentration
OX	Oxygen portion of the biomass composition (mol/c-mol)
PC	Personal computer
PI	Proportional – integral controller
PLC	Programmable logic controller
q_e	Specific ethanol uptake rate
$q_{e,gr}$	Specific ethanol uptake rate for growth
$q_{e,main}$	Specific ethanol uptake rate for maintenance
$q_{e,max}$	Maximum specific ethanol uptake rate
q_{O2}	Specific oxygen uptake rate
$q_{O2,e}$	Specific oxygen uptake rate for oxidation of ethanol
$q_{O2,e,gr}$	Specific oxygen uptake rate for oxidative growth on ethanol
$q_{O2,e,main}$	Specific oxygen uptake rate for oxidative maintenance on ethanol
$q_{O2,max}$	Maximum specific oxygen uptake rate
$q_{O2,s}$	Specific oxygen uptake rate for oxidation of glucose
$q_{O2,s,gr}$	Specific oxygen uptake rate for oxidative growth on glucose
$q_{O2,s,main}$	Specific oxygen uptake rate for oxidative maintenance on glucose
q_s	Specific glucose uptake rate
$q_{s,f,gr}$	Specific glucose uptake rate for fermentative growth
$q_{s,f,main}$	Specific glucose uptake rate for fermentative maintenance
$q_{s,gr}$	Specific glucose uptake rate for growth
$q_{s,main}$	Specific glucose uptake rate for maintenance

$q_{s,max}$	Maximum specific glucose uptake rate
$q_{s,ox,gr}$	Specific glucose uptake rate for oxidative growth
$q_{s,ox,main}$	Specific glucose uptake rate for oxidative maintenance
r	Vector for turnover rates of the single substances
S ; C_s	Glucose concentration
t	Time
t_{lag}; $t_{lag,eth}$	Lag-time
v	Vector for reaction rates
X	Biomass concentration
$Y_{X/E}$	Yield coefficient mol biomass/mol ethanol
$Y_{X/Sf}$	Yield coefficient mol biomass/mol glucose, fermentative growth
$Y_{X/Sox}$	Yield coefficient mol biomass/mol glucose, oxidative growth

ABSTRACT

Yeast propagation increasingly stands for a central step in beer production and emprises an important economical and technological factor in brewing practice. Vitality and quality of the propagated yeast exerts a relevant influence on the subsequent fermentation run and the resulting beer quality. Therefore, the yeast inoculum must be available at pitching time in the right amount and especially in the right quality.

To guarantee this by process management tools, in particular by modelling and active process control, is a main feature of this work. Two kinetic models of yeast propagation are introduced. These modelling approaches represent the basis for a control strategy aiming on the provision of an optimal inoculum at the starting time of subsequent industrial fermentations. Both models, a Black Box model and a metabolic model, include respiratory metabolism on sugars and ethanol as well as fermentative metabolism on sugars. Limitation effects, occurring due to specific nutritional data of the growth medium beer wort, were taken into account for sugar, nitrogen, ethanol and oxygen concentrations. Correspondingly, inhibitions of the metabolism by ethanol and high sugar concentrations were formulated. The models especially represent the Crabtree-effect.

For model validation, literature data were used and selected experiments within the relevant range of manipulated variables (temperature, dissolved oxygen) were conducted for different yeast strains and propagation strategies. In a sensitivity analysis three parameters were identified as particularly relevant. After adaptation of these parameters on data sets, simulations, based on the suggested models, matched these data with a deviation below 10 mmol/L (0.2% w/w for sugar concentrations and $6.2*10^6$ cells/mL for biomass concentration).

The variable parameters showed a characteristic temperature dependency, which could be described by mathematical functions. The implementation of these functions in both models allowed predictive simulations of the yeast propagation process even applying non-isothermal trajectories. During experiments it was proved that in ideally mixed fermenters the dissolved oxygen concentration affects the yeast growth only below concentrations of 0.1 ppm.

Predictive simulations allowed an active process control by a precise adjustment of trajectories of both, temperature and dissolved oxygen concentration. Thus, the optimal crop time of the inoculum could be varied within a period of two days in order to maintain high fermentation activity for the subsequent anaerobic fermentation. The validity of the modelling approaches was proved for industrial propagations and fermentations in breweries as well. In particular for the industrial propagations above mentioned accuracies were achieved. Accuracies of the simulation of brewing yeast fermentations resulted in a practicable range not before a sedimentation model was included in the process models.

ZUSAMMENFASSUNG

Die Hefeherführung gilt zunehmend als zentraler Teilprozess im Rahmen der Bierbereitung. Sie stellt somit einen wichtigen technologischen und wirtschaftlichen Faktor in der Brauindustrie dar. Die Qualität und Vitalität der hergeführten Hefe beeinflusst in einem hohen Maße die nachfolgende Gärung und die Qualität des fertigen Bieres. Deshalb muss zum Anstellzeitpunkt stets die richtige Menge an Hefe in der richtigen Qualität vorliegen.

In dieser Arbeit wurden in Form von Modellierung und modellbasierter aktiver Prozessführung Management-Instrumente zur Prozesssimulation und -optimierung entwickelt. Das Hefewachstum wird in zwei kinetischen Modellen beschrieben. Die Modellierungsansätze bilden die Basis für eine Prozessführungsstrategie, die auf die Bereitstellung einer vitalen Hefe für die nachfolgende Gärung abzielt. Beide Modelle, ein Black Box Modell und ein metabolischer Ansatz, umfassen sowohl den oxidativen Stoffwechselweg mit Nutzung von Glucose oder Ethanol als Hauptsubstrat als auch den fermentativen Stoffwechselweg mit ausschließlicher Nutzung von Glucose. Limitierungseffekte, die aufgrund der Eigenschaften des Wachstumsmediums Bierwürze auftreten, wurden für Konzentrationen von Zuckern, Stickstoffquelle, Ethanol und Sauerstoff berücksichtigt. Analog sind Inhibierungseffekte durch Ethanol und hohe Zuckerkonzentrationen integriert. Besondere Berücksichtigung in den Modellen findet der Crabtree Effekt.

Zur Validierung der Prozessmodelle wurden Literaturdaten herangezogen sowie ausgesuchte Experimente aus dem relevanten Parameterraum der Stellgrößen Temperatur und Gelöstsauerstoffkonzentration mit verschiedenen Hefestämmen und Propagationsanlagen durchgeführt. In einer Sensitivitätsanalyse wurden für beide Modelle drei Parameter als besonders relevant identifiziert. Nach Anpassung dieser Parameter an die Datensätze gaben auf den Modellen basierende Simulationen die experimentellen Daten mit einer Abweichung von weniger als 10 mmol/L (0.2% G/G Extraktkonzentration und $6.2*10^6$ Zellen/ml) wieder.

Die variablen Parameter zeigten eine charakteristische Temperaturabhängigkeit, die durch eine mathematische Funktion beschrieben werden konnte. Der Einsatz dieser Funktionen für die variablen Parameter ermöglichte prädiktive Simulationen, auch unter Anwendung von nicht isothermen Trajektorien. Im Rahmen der Experimente wurde der Beweis erbracht, dass das Hefewachstum in einem ideal durchmischten Fermenter erst durch Sauerstoffkonzentrationen unterhalb von 0.1 ppm beeinträchtigt wird.

Die prädiktive Simulation ermöglichte eine aktive Prozessführung durch zielgerichtete Anpassung der Stellgrößenprofile für Temperatur und Sauerstoffkonzentration. Dadurch konnte der optimale Entnahmezeitpunkt der Hefe innerhalb eines Zeitfensters von zwei Tagen verschoben und stets eine aktive Hefe für die nachfolgende Fermentation bereitgestellt werden. Die Gültigkeit des Modellierungsansatzes konnte ebenso für industrielle

Propagations- und Fermentationsanlagen in Brauereien gezeigt werden. Dabei wurden insbesondere für Simulationen von Hefepropagationen in der Industrie eine Genauigkeit ähnlich der oben genannten erreicht. Die Genauigkeit der Simulationen von Gärungen in Brauereien lag erst nach Integration eines Sedimentationsmodells in praktikablen Grenzen.

PUBLICATIONS

Paper in Refereed Journals:

Kurz, T., Fellner, M., Becker, T., Delgado, A. (2001) Observation and Control of the Beer Fermentation Using Cognitive Methods. Journal of the Institute of Brewing, Vol. 107 (4), 241-252.

Kurz, T., Mieleitner, J., Becker, T., Delgado, A. (2002) Model Based Simulation of Brewing Yeast Propagation. Journal of the Institute of Brewing, Vol. 108 (2), 248-255.

Conference Papers:

Kurz, T., Fellner, M., Becker, T., Delgado, A. (1999) Praxiseinführung eines Systems zur Online-Messung und Prozeßführung bei der Biergärung. In: Handbuch zum 32. Technologischen Seminar Weihenstephan, Freising, Germany.

Kurz, T., Fellner, M., Becker, T., Delgado, A. (1999) Praxiseinsatz einer aktiven Prozessführung bei der Gärung und Reifung von Bier. In: European Brewery Convention. Proceedings of the 27th congress, Cannes, France, 743-750.

Kurz T., Becker T., Fellner M., Schmitz M., Delgado A., Murnleitner E. (1999) Cognitive Computing in Brewing Technology. In: 7th European Congress on Intelligent Techniques & Soft Computing (EUFIT), Aachen, Germany, September 13 –16, 1999, 235 - 236.

Kurz T., Fellner M., Becker T., Delgado A. (2000) Aktive Prozessführung bei der Fermentation von Bier. GVC-Fachausschuß Lebensmittelverfahrenstechnik und Trocknungstechnik, Würzburg, Germany, March 29 – 31, 2000.

Kurz, T.; Becker, T.; Delgado, A.: Propagation of brewery yeast – modelling and simulation. Proceedings of the 28th EBC Congress, Budapest, Hungary, May 12 – 17, 2001, Verlag Hans Carl, Nürnberg, Germany, 29.

Kurz, T., Delgado, A. (2002) Hefeherführung – Modell und Experiment. In: Handbuch 35. Technologisches Seminar Weihenstephan, Freising, Germany.

Kurz, T., Delgado, A. (2002) Model based control of Saccharomyces cerevisiae cultivation under growth limiting conditions. International congress on the process industries, Mexico City, Mexico, March 18 – 20, 2002

Kurz, T., Arnold. S., Fellner, M., Murnleitner, E., Mitzscherling, M., Becker, T., Delgado, A. (2002) Modelling and Optimisation Approaches in Industrial Fermentation Processes. FOODSIM'2002, 2nd International Conference on Simulation in Food and Bio Industries, Cork, Ireland, June 17-18, 2002.

Other:

Kurz, T., Becher, T., Becker, T., Delgado, A. (2001) Hefeanzucht – Einfluss der Stellgrößen und aktive Prozessführung. Der Weihenstephaner, Vol. 69, 124-130.

1 Introduction and Conceptional Formulation

1.1 Introduction

Saccharomyces sp. comprise a variety of species and sub-species. The best known species in biotechnology and food-technology is *Saccharomyces cerevisiae* (bakers' yeast) which has been object of intensive research activities since the 1950s. Here, the production of recombinant proteins or secondary metabolites using (recombinant) *Saccharomyces cerevisiae* is of increasing importance. The species is also applied in many industrial processes. Examples are bakers' yeast production or more traditional industrial branches in fermentation industries for wine (*Saccharomyces cerevisiae*), sake and beer.

Management as it is defined can be seen as an act to supervise, to plan, to give strategies, and to control systems [98]. The transfer of these aspects to the regarded bioprocesses propagation and fermentation of *Saccharomyces species (sp*.) in general is aim of this work. A main aspect, in particular, is the transfer of the mentioned aspects to yeast propagation and fermentation in the brewing industry.

Yeast propagation increasingly stands for a central step in beer production and emprises an important economical and technological factor in brewing practice. Vitality and quality of the propagated yeast exerts a relevant influence on the subsequent fermentation run and the resulting beer quality [6, 9, 10, 69, 85, 87, 90, 102, 138]. Therefore, the yeast inoculum must be available at pitching time in the right amount and especially in the right quality. This prerequisite potentiates an optimal exploitation of economical and technological advantages [6, 9, 56, 87, 136]. To guarantee this by process management tools, in particular by modelling and active process control, is a main feature of this work.

Up to now process technology in breweries does not allow to compensate disturbances in the production plan or in the yeast propagation. For example, variations of up to 2 - 3 days have to be compensated due to changes in the production plan. As a result, no adequate inoculum will be delivered for the subsequent fermentation, which entails extensive consequences for following production steps until the resulting beer [9, 10, 69, 85, 87, 102, 136, 138].

The vital motivation for this work bases in the development of a practicable system, which allows to evaluate proposals for an active process control regime during yeast propagation. Aim of the process control is the provision of the right amount of yeast in the right quality at the right time, even if disturbances in the production process occur. The economical and technological potential of an optimised process regime for yeast propagation emanates from the illustrated advantages of using a vital yeast for fermentation. Fermentation times will be

reduced, tank capacity increased, risk of contamination decreased, fermentation faults avoided and, finally, the quality of the resulting beer will be improved.

In this regard, modelling and optimisation are rather described in the area of bakers' yeast propagation [19, 21, 44, 96, 111, 127, 128, 129, 130, 145]. It is known that the fundamental pathways of metabolism of brewers' and bakers' yeast are comparable [5, 6, 87]. Therefore, in this work relevant aspects are singled out and transferred to the concerns of brewing yeast propagation. The development of a process model provides a tool for the simulation of propagation and fermentation runs, which is not available so far. Planned control actions, e.g. for changes in propagation or fermentation procedures, can be evaluated concerning the effects on command variables [96, 106, 129, 130]. The simulation tool allows to create scenarios and thus, the prevention of consequential costs or a reduction of beer quality, due to mistakes in the process regime.

The topic „yeast propagation and fermentation" is discussed extensively in literature out of different industrial and scientific points of view. Concerning brewery research, microbial and physiological aspects were examined in detail [5, 6, 9, 10, 22, 56, 69, 78,85, 87, 90, 102, 122, 136, 139]. The key position of yeast propagation and fermentation is described principally. Besides, options are introduced to propagate yeast according to the technological demands [6, 9, 56, 69, 74, 85, 136, 138]. An integration of these methods in a model as a fundament of an active control system, however, is not existent. Process control is based almost solely on empirical, technological knowledge [6, 85, 136]. Single approaches deal with modelling of selected aspects as yeast vitality or optimised aeration strategies. Usually, the latter can not be applied as a basis for a comprehensive and precise process control, because they consider only single aspects or pursue different objective targets [5, 6, 19, 21, 44, 59, 87, 96, 106, 111, 127, 128, 129, 130]. However, a multitude of approaches indicate the potential of a comprehensive model based process control [5, 87, 136]. The feasibility of a model based control system is verified by several known approaches out of the fermentation industry, especially bakers' yeast industry or penicillin production [19, 21, 96, 105, 129]. Despite aggravating differences considering boundary conditions, principally overlappings of aims and applied methods are existent. From this, the possibility of knowledge transfer to the regarded applications results.

Prerequisite of a precise process control is the observability and controllability of the process. In the regarded case of yeast propagation or fermentation in bioreactors the observation is rendered more difficult by matrix effects and cross-sensitivities of the online sensor devices. In literature, several methodics are illustrated [5, 69, 87]. However, the latter predominantly serve for monitoring, without an application for process modelling or process control in the breweries.

Principally, manipulated variables, e.g. temperature or dissolved oxygen concentration, allow to control the process of yeast propagation and fermentation [5, 69, 85, 87, 136]. Possible variables are illustrated in literature [5, 6, 9, 59, 69, 85, 87, 102, 136, 138]. In brewing industry, setcurves for the manipulated variables are mainly fixed recipes based on technological knowledge. Adaptations can be made only offline after evaluation of data of further process runs. But, it was shown that for an active process control an exact adaptation of the manipulated variables is necessary, in order to achieve pitching yeast with a high physiological activity [136]. The lack of comprehensive process knowledge is reflected in contradictory process strategies or in a missing integration in an automation conception in the brewery [9, 56, 87].

In biotechnology, however, different methods for model based active control systems are known, which range from periodical offline to online optimisation instruments. Applied are mathematical and cognitive methods or even combinations (hybrid) [15, 19, 21, 96, 135].

1.2 The scope of the thesis

As mentioned above, an active process control of the yeast propagation and fermentation in brewing industry derives technological and economical advantages. Prerequisite for an active control system is a comprehensive knowledge of the system behaviour, which can be abstracted in a process model.

As no comprehensive modelling approach was available for the description of brewing yeast metabolism, the first objective of this work was to develop a modelling approach for the brewing yeast propagation process considering limiting and inhibiting effects of industrial media and to validate the model based on literature and experimental data. For brewing yeast propagation, metabolism regulation effects, as for example the Crabtree effect, which were not relevant for existing models, had to be considered particularly. The second target was to show the potential of a model based predictive simulation to evaluate process control strategies and to extract the limits of controllability using practice relevant case scenarios. An important aspect of this work was the development of a simulation tool, which could be applied for process simulation as well as for scheduling and error estimation, in order to allow a cost saving evaluation and modification of recipes or technologies in a plant.

The following tasks were necessary to meet the requirements:

- Development of a comprehensive modelling approach for the yeast metabolism,
- Validation of the process model with data from bakers' and brewing yeast propagations,
- Analysis of the dependency of the yeast metabolism on the manipulated variables and integration in the modelling approach,
- Application of the modelling approach for industrial propagations and fermentations with different technologies.

2 Basic considerations

2.1 Modelling

2.1.1 General considerations

According to Bellgardt [17],

a model is an image of a real system that shows analogous behaviour in the important properties, and that allows within a limited region a prediction of the behaviour of the original system.

Thus, the model sufficiently replaces experimental studies of the regarded system. Considering economic aspects, a model acts simpler, cheaper and faster than the original system. In particular for research applications it is important that a model is less complex than reality and therefore, a clear view of complex mechanisms can be obtained. Especially, as in a model certain effects can be isolated and emphasised or suppressed [17, 18]. A further aspect of modelling exists in the identification of sites of change in a system studied under different conditions. The model helps to identify, which parameters change between the conditions [15]. Possible benefits of modelling embody a better understanding of process behaviour, a more effective planning of experiments, extrapolation of results, prediction and process optimisation [64].

In literature, three groups of models are distinguished, physical, verbal, and mathematical models. An overview is given by Bellgardt [17] and Becker [15]. Physical models usually realise the original system in a smaller scale or by turning to a different physical system. Verbal models give a linguistic representation of process knowledge, usually as rules. Herein expert systems contain knowledge as “if....then....” relations. Mathematical models describe the behaviour of the original system by mathematical equations. Fuzzy-Logic, which allows a translation of qualitative and rule-based knowledge into mathematical equations, represents a link between the latter two approaches. A further classification of mathematical models depends on the mathematical formalism or the methods for model building. Theoretical models as mechanistic models base on physical and chemical laws and the knowledge about the inner structure and function of the system, e.g. flows of mass and energy. Therefore, they often provide far reaching predictions of the system behaviour [17]. In contrast, experimental or non-mechanistic models try to give a description of the observed system reaction in response to a certain forcing signal, disregarding intrinsic characteristics of the system. These types of models are called “black-box models”. Very typical black box-models are Artificial Neural Networks, which have found a wide application in biotechnology also.

Usually, the selection of a model type depends on the available process knowledge (see Table 1). With the availability of very detailed knowledge, which can be formulated in mathematical equations, a mathematical, mechanistic approach is preferred. Black box models as artificial neural networks are preferenced if no explicit knowledge but representative experimental data is existent.

Table 1: Guideline for the selection of model type. Dependent on the system knowledge different model types are selectable. CFD: Computional fluid dynamics. PLS: Partial least square, PCR: Prinicpal component regression [15].

	high	**system knowledge**			**low**
Model type	Deterministic	Stochastic, Statistical	Expertsystems	Approximation	Classification
Examples	unstructured, structured, CFD	Markov Chains, Maximum Likelihood, Kalman,	Fuzzy models, Set theory	Neural networks, PLS, PCR	Pattern recognition

2.1.2 Deterministic mathematical modelling

In this work deterministic models were developed. Figure 1 illustrates the general structure of a model for a bioreactor with gas phase and liquid phase and including the biotic phase.

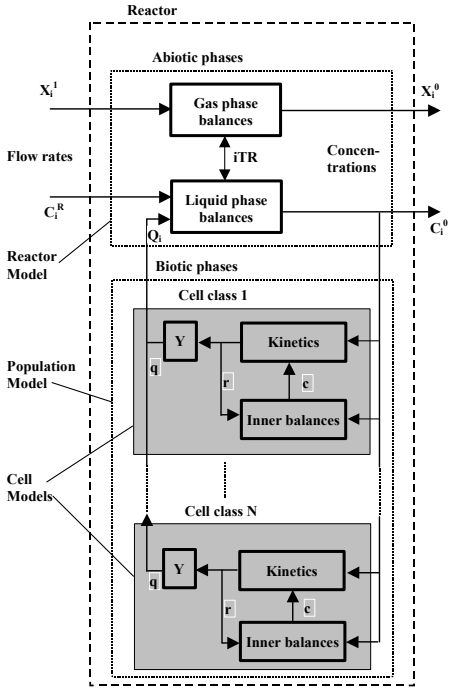

Figure 1: General model structure for biotechnological processes. x: external flow and transport rates, c: concentration of the component (·)I Inlet, (·)O Outlet, TR: transfer rates, Q: volumetric reaction rate, q: specific reaction rate, Y: yield coefficient, r: intrinsic reaction rate, (·)i: Index for quantity i, (·)j: Index for quantity j [17].

Models for bioreactors provide the concentrations of substrates, products and cells as input variables to the models of the biotic phase. To accomplish this, the reactor model needs to know the actual reaction rates, which are the output of the biological models. A required feature of mathematical models is to describe temporal and local changes of relevant chemical and physical quantities. For each quantity (e.g. concentrations) in the regarded subsystems of Figure 1, a balance equation has to be formulated. Exemplarily, a macroscopic bilance is illustrated in Figure 2.

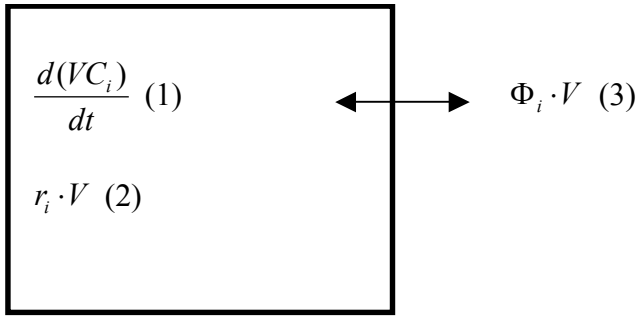

Figure 2: Macroscopic balance in a bioreactor with volume (V), concentration of component I (C_i), specific turnover rate of component I (r_i) and the specific transport rate of component I (Φ_I).

In this balance, the accumulation (1) of a component sums up turnover (2) and transport (3) of a specific component. The relation is valid for an ideally mixed system. Non-ideally mixed systems require a subdivision in several units. A system of differential equations results. r_i and Φ_i are net rates of turnover and transport. The net rate represents the sum of all rates of processes involving component i [64]. For each equation the turnover rate and the transport rate have to be defined, for example by kinetic equations. These reaction kinetics characterise the dependency on temperature, pressure and concentrations of relevant quantities [64].

Biochemical reaction equations base on the law of mass conservation. Thus, considering the stoichiometry of the reactions, relations for the turnover rates of the single components derive. [18].

In this work, the main aspect features the development of a biological model. The reactor is considered to be ideally mixed and no input or output occurs, except for the modelling of sequencing batch propagation in chapter 3.5.2. Different types of biological models are distinguished, according to the level of the modelling and its degree of detail and desired accuracy [17, 18]. Table 2 illustrates a classification based on approximations concerning balanced growth and average cell approximation. Referring to this, a classification is made in unstructured and structured as well as segregated and unsegregated approaches [30]. In reality, cells have to be regarded as multicomponent systems. Unstructured models disregard this fact and consider the cell as one component. Structured models take also into account intracellular structures or concentrations of metabolites. If heterogeneity in the cell population

is considered, a model additionally is denoted as segregated. Summarising, an unstructured, unsegregated model offers a view with the highest idealisation. The real biological system matches best with a structured, segregated process model.

Table 2: Different levels of deterministic modelling of biological systems. Unstructured and structured as well as segregated and unsegregated models are distinguished. [30]

	unstructured	structured
unsegregated	**Highest degree of idealisation** Cell population is regarded as one component	Multicomponent treatment of an average cell
segregated	Single component, heterogenous, individual cells	Multicomponent. Consideation of cell heterogeneity **Reality**

„Average cell" approximation (↑)

Balanced growth approximation (→)

2.1.2.1 Unstructured Models

Bellgardt provides a comprehensive definition of unstructured models [18]. In unstructured models, the biological reaction depends directly and only on macroscopic variables, the conditions in the bioreactor. Therefore, unstructured models are essentially combinations of elementary kinetics that mainly describe the influence of substrate and product concentrations or other variables, such as pH value or temperature. The only biological state variable is the cell mass concentration. Beside the cell mass, the model considers only those other process variables that show great variations during the regarded process and have significant influence on the microbial behaviour.

The most simple approaches of this type are for example the Logistic Law or the Cube-Root Law. This approaches disregard substrate limitation kinetics, but solely depend on cell mass. Applications exists in such biotechnological processes, where no information about substrates are available or growth is not dependent on substrate concentrations or is not limited by the available substrate.

Another unstructured approach was formulated by Monod. He found in experiments in a stirred fermenter a relation between the specific growth rate μ and the concentration of the limiting substrate C_S:

$$\mu = \mu_{\max} \frac{C_S}{K_S + C_S} \,. \tag{1}$$

Figure 3 illustrates this relation graphically. The kinetic equation of Monod only comprises the constant maximum specific growth rate μ_{max} and the half saturation constant K_S, which represents the substrate concentration belonging to the half maximum growth rate. Other external or internal substances or reactions are not considered.

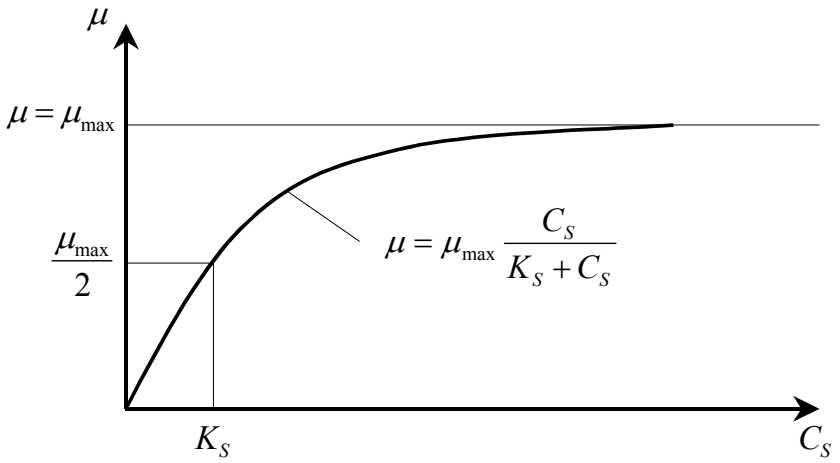

Figure 3: Dependency of the microbial growth in bioreactors on the concentration of the limiting substrate according to Monod.

Therefore, this unstructured approach solely describes exponential growth and the transition to stationary phase during cell growth (see chapter 2.2.3). A lag phase, as it initially occurs, if microorganisms are inoculated in a growth medium, or the stationary phase are not describable by an unstructured model. These states have to be modelled in a structured model, which also considers intracellular (biochemical) processes.

Substrate limitation is not necessarily the only aspect affecting yeast growth. For example volumetric or cell mass related limitation effects are known. Other approaches as well describe growth limitations or product inhibitions during microbial growth. An overview to kinetic relations, which describe the dependency of microbial growth on limiting or inhibiting substrates is given in literature [17, 30, 143].

Usually, all mentioned unstructured models are simple and contain easy quantifiable parameters. In this work especially the sequential usage of different substrates (diauxic use of glucose and ethanol) by the yeast cell is regarded. Therefore, the intrinsic enzymatic processes during the lag phases have to be taken into consideration in more detail. However, if

intracellular reactions affect the growth process, unstructured models no longer present the reality.

2.1.2.2 Structured models

Structured models consider the internal structural elements of the cells that may be metabolites, enzymes, or other cell constituents. By interaction of these elements, which are described by inner balances and related intrinsic reactions, the properties of the cells become variable in time. Structured models possess the capability to describe these dynamics of metabolic regulation, e.g. during lag phases of growth. Similarly to unstructured models, structured models take the growth process as continuous and the population as homogenous [17].

Metabolic models belong to the group of structured models. A metabolic model bases on the principle that the metabolism of microorganisms comprises a limited number of universal metabolic pathways accessible for modelling. Characteristic reactions describe the exchange of compounds with the surrounding medium. So, additionally to extracellular substances in a metabolic model also intracellular reaction and components are considered (metabolic intermediates, reduction equivalents or ATP). The knowledge of the metabolic pathways enables the formulation of stoichiometric relations for involved substances. Analogue to unstructured models, kinetic equations have to be defined for the unknown reaction rates [65].

2.1.2.3 Segregated models

Segregated models discriminate inhomogeneous population in classes with different properties. The classes represent different species, or within one species differences of physiological, morphological or genetic nature. In most segregated approaches it is assumed that the cell classes themselves are homogenous and thus can be represented by structured or unstructured models [17].

2.1.3 Modelling approaches for temperature influence in biotechnology

In literature, principally, modelling approaches for the description of temperature dependencies in biotechnology are distinguished in Arrhenius type models or Bêlehrádek type models. The former are based on different theories out of the field of physical chemistry. The approaches are described in the following.

2.1.3.1 Models of the Arrhenius type

Experiments revealed for many reactions the validity of the Arrhenius equation for the temperature dependency of the rate constant

$$k = A \cdot \exp\left(-\frac{E_a}{R \cdot T} \right) \quad (2)$$

with E_a activation energy ($J*mol^{-1}$), A preexponential coefficient (h^{-1}) and R universal gas constant (8.314 $J*mol^{-1}K^{-1}$) [8].

By substitution of k in equation 2 by the specific growth rate μ ($\mu = dX / (dt \cdot X)$), with biomass concentration X [mmol/L], the Arrhenius relation was introduced to microbiology and food technology for the description of the temperature dependency of microbial growth [39, 58, 81, 118, 142] and particularly for a kinetic model of wine fermentation [25]. The application of the Arrhenius equation, however, was often critisised, because the equation described only a single reaction whereas microbial growth is influenced by several factors [16, 112]. In the studied approach, the growth is assumed to be a single enzymatic reaction (master reaction).

2.1.3.1.1 Theoretical approaches

Equation 2 bases on theoretical approaches, the activated complex and the collision rate theory, which are introduced shortly in the following. In both cases a simple reaction

$$A + B \rightarrow P \quad (3)$$

is considered. The collision rate theory originally was developed for reactions in gas phase, but has been transferred to reactions in solutions as well [8]. Two assumptions are made. The reaction rate is (a) proportional to the number of collisions of the reactants and (b) proportional to the probability that during a collision a sufficient kinetic energy was available for the reaction. In a first step, the number of actual collisions of a single molecule A (particle with radius r_A) and molecules B (radius r_B) in a fictive cylinder was determined for a time interval. This was realised by calculation of a mean speed of molecules based on the Maxwellian velocity distribution and the number of particles B in the considered volume. The volumetric product of the number of collisions and the number of particles A represents a collision number

$$Z_{AB} = \sigma \cdot \sqrt{\frac{8 \cdot k_B \cdot T}{\pi \cdot \mu}} \cdot N_A^2 \cdot [A] \cdot [B] \quad (4)$$

per time interval and volume at temperature T and dependent on the molar particle concentrations ($\mu = m_A * m_B / (m_A + m_B)$ reduced mass, k_B Boltzmann constant, σ cross section of collision, N_A Avogadro constant).

The particles need a certain activation energy E to perform a reaction. The Boltzmann distribution describes the portion n* of particles n containing this energy dependent on the temperature T:

$$\frac{n^*}{n} = \exp\left(-\frac{E}{R \cdot T}\right). \tag{5}$$

The product of collision number Z_{AB} and the portion of collisions relevant for the reaction divided by the Avogadro constant represents the change in the molar concentration of A (reaction rate). The latter is defined as $-dA/dt = k^*[A]^*[B]$. Thus, the reaction rate k is given as

$$k = \sigma \cdot \sqrt{\frac{8 \cdot k_B \cdot T}{\pi \cdot \mu}} \cdot N_A \cdot \exp\left(-\frac{E}{R \cdot T}\right) \cdot P\,. \tag{6}$$

An additional coefficient P was introduced in order to fit the function to measurement values. P can be interpreted as a steric coefficient, because for a reaction the molecules need a certain steric orientation [8].

The theory of the activated complex emanates from the field of statistical thermodynamics as well [124]. It is assumed, that the master reaction progresses along a reaction coordinate from the educt via a transition state (activated complex) to the final product. This is illustrated graphically in Figure 4.

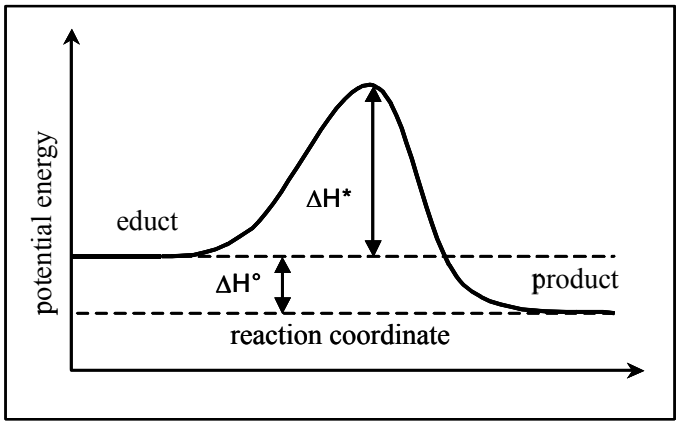

Figure 4: Energy diagram for a simple exothermic reaction [8].

If a constant pressure is applied during the reaction the usage of enthalpies is recommended. The molar difference between educts and products correspond with the reaction enthalpy ΔH°. By analogy, the difference between educt and activated complex corresponds with the activation enthalpy ΔH*. Assuming an equilibrium of educts and activated complex, the regarded reaction can be formulated as

$$A + B \underset{k^-}{\overset{k^+}{\rightleftarrows}} (AB)^* \xrightarrow{k^*} P\,. \tag{7}$$

If $k_+ + k_- >> k^*$ and $K = k_+ / k_- << 1$, i.e. in the equilibrium predominantly educts are existent and P is produced very slowly, in an approximation the effective reaction rate

$$k = k^* \cdot K \tag{8}$$

is resulting (detailed description in [124]). The equilibrium constant K is related to the free reaction enthalpy ΔG*:

$$\ln(K) = -\frac{\Delta G^*}{R \cdot T}. \tag{9}$$

The free reaction enthalpy

$$\Delta G^* = \Delta H^* - T \cdot \Delta S^* \tag{10}$$

can be expressed by the activation enthalpy ΔH* and the activation entropy ΔS*. Eyring suggested to formulate the rate constant k* as k_B*T/h, with the Planck constant h [51]. Together with equations 8 - 10 the Eyring equation for the effective reaction rate

$$k = \frac{k_B \cdot T}{h} \cdot \exp\left(\frac{\Delta S^*}{R}\right) \cdot \exp\left(-\frac{\Delta H^*}{R \cdot T}\right) \tag{11}$$

is resulting.

In order to compare both theories, the differential d(ln[k])/dT was applied for equations 2, 6 and 11. If these differentials were equated the activation energy

$$E_a = E + \frac{1}{2} \cdot R \cdot T = \Delta H^* + R \cdot T \tag{12}$$

(see equation 2) could be expressed by parameters of both theories. This proved that the activation energy itself is dependent on the temperature.

If E or ΔH* in equations 6 or 11 is expressed by E_a in equation 12, for the preexponential coefficient A similar expressions are resulting. Remarkable is that for the collision theory, A is proportional to the square root of the temperature T and direct proportional to the Temperature in the case of the activated complex. In both cases, however, the temperature dependency of A and E_a was negligible compared to the exponential expression.

2.1.3.1.2 The model of Mohr and Krawiec

Regarding microbial growth as a simple reaction, it can be assumed that the growth rate is resulting from two processes, which are influenced by the temperature in a different manner, a process for synthesis of new biomass and a process for irreversible inactivation of biomass (decay) [20]. If growth rates are plotted half logarithmically versus temperature (Arrhenius plot) curves are obtained instead of straight lines especially for growth rates in the suboptimal range. Mohr and Krawiec found for several bacteria two ranges, for which different slopes in the Arrhenius plot resulted below and above a critical temperature T_{krit} [100]. This was interpreted as a change in the internal organisation of the microorganisms. Another approach,

considering a coexistence of different organisations in an equilibrium at suboptimal temperatures, was integrated in the model for the specific growth rate

$$\mu(T) = \frac{1}{A_1 \cdot \exp\left(\frac{E_{a1}}{R \cdot T}\right) + A_2 \cdot \exp\left(\frac{E_{a2}}{R \cdot T}\right)} - B \cdot \exp\left(-\frac{E_b}{R \cdot T}\right) \tag{13}$$

with E_{a1} and E_{a2} as activation energy [J·mol^{-1}] for both ranges below a growth optimum T_{opt} and E_b as inactivation energy [J·mol^{-1}] above T_{opt} as well as coefficients A_1, A_2 [h] and B [h^{-1}].

2.1.3.1.3 Schoolfield model

This model as well is founded on the assumption of a master reaction, which determines the growth rate in a sequence of enzymatic reactions. According to Sharpe and DeMichele growth is proportional to the concentration of the rate determining enzyme E, which, however, is in an equilibrium with two inactivated forms, caused by low and high temperatures [126]. Additionally, it is assumed that the inactivated forms themselves are not in an equilibrium and transition periods between the different forms are distributed exponentially. Thus, a probability P_i can be computed, based on rate constants of these equilibrium reactions. Regarding steady state conditions, finally a Monod expression results, which indicate the probability P_{active} that enzyme E exists in an activated form [67, 126]:

$$P_{active} = \frac{1}{1 + K_T + K_H}. \tag{14}$$

K_T and K_H represent equilibrium constants for the inactivation of enzyme E at high or low temperatures. Summarising, the specific growth rate μ then can be formulated as

$$\mu = [E] \cdot P_{active} \cdot k. \tag{15}$$

Sharpe und DeMichele replaced the rate constants of the equilibrium reactions and the rate constant k by the Eyring relation (see equation 11) [126]. This modelling approach was modified by Schoolfield et al. by the introduction of new parameters [125]:

$$\mu(T) = \frac{r_{(15^\circ C)} \cdot \frac{T}{288K} \cdot \exp\left[\frac{\Delta H^\circ}{R} \cdot \left(\frac{1}{288K} - \frac{1}{T}\right)\right]}{1 + \exp\left[\frac{\Delta H^\circ_T}{R} \cdot \left(\frac{1}{T_{0,5\,T}} - \frac{1}{T}\right)\right] + \exp\left[\frac{\Delta H^\circ_H}{R} \cdot \left(\frac{1}{T_{0,5\,H}} - \frac{1}{T}\right)\right]} \tag{16}$$

with $r_{(15°C)}$ specific growth rate at 15°C [h^{-1}], ΔH° activation enthalpy of the limiting enzyme reaction [J·mol^{-1}], ΔH_T° change of the activation enthalpy by inactivation of the enzyme at low temperatures [J·mol^{-1}], $T_{0,5\,T}$ temperature [K], when half of the enzymes are inactivated

by low temperatures, $\Delta H_H°$ change of the activation enthalpy by inactivation of the enzyme at high temperatures [$J \cdot mol^{-1}$] and $T_{0,5\,H}$ temperature [K], when half of the enzymes are inactivated by high temperatures. The rate of the enzyme catalysed reaction (growth rate) is modelled only by the numerator, if all enzymes are active. The exponential expressions in the denominator model the transition in an inactive form caused by high or low temperatures. Also, for this model three ranges with a constant slope in the Arrhenius plot are resulting. A major advantage of the Schoolfield model compared to the approach of Sharpe [126] appears in the easy biological interpretation of parameters [125].

2.1.3.2 Bělehrádek type models

No theoretical background is available for these kind of models. Arrhenius relations for modelling microbial growth were discussed critically in literature, because the activation energy appeared to be variable for different temperature ranges. Therefore, Bělehrádek examined different mathematical relations for a description of microbial growth.

2.1.3.2.1 Bělehrádek relations

Originally, Bělehrádek formulated the relation between temperature T and duration t of a biological process as [16]:

$$t = \frac{a}{T^{\alpha}}. \tag{17}$$

The constants a and α could be determined graphically. By substitution of t by the specific growth rate μ ($\mu = t^{-1}$) the model could be applied for the specific growth rate

$$\mu(T) = \left[b \cdot (T - T_0)\right]^{\alpha}. \tag{18}$$

Temperature T here is used in °C. The coefficient b results from a substitution of a ($b = a^{-1/\alpha}$). A third parameter T_0 was added, in order to be able to consider other temperatures as 0°C, which result a zero growth rate. The model is applicable for the suboptimal temperature range only, however can be extended similar to the square root model (see chapter 2.1.3.2.2).

2.1.3.2.2 Square root model

This model is a special case of the Bělehrádek relation with the coefficient $\alpha = 2$. Ratkowsky et al. [113] applied the approach for modelling of bacterial growth rates in the suboptimal temperature range:

$$\sqrt{\mu(T)} = b \cdot (T - T_0). \tag{19}$$

Similar to equation 18, b is a regression coefficient and T_0 the minimum temperature for growth. Additionally, Ratkowsky et al. extended the model for the whole temperature range [114]:

$$\sqrt{\mu(T)} = b \cdot (T - T_{min}) \cdot \{1 - \exp[c \cdot (T - T_{max})]\} \quad \textbf{(20)}$$

with c representing a further regression coefficient. T_{min} and T_{max} are temperatures, where no growth can be observed. As the parameters are easy to determine and data sets can be represented sufficiently, the modelling approach is often used in microbiology, despite the lacking theoretical or biological background [112, 142].

2.2 Relevant aspects to Saccharomyces cerevisiae

Saccharomyces cerevisiae is found in various industrial applications as bakers' yeast, distillery yeast, and brewery yeast and therefore has a great economical importance. Also *Saccharomyces sp.* is object of basic microbial research as eucaryothic model microorganism. Hence, growth and metabolism of this yeast type is of great interest and has been object of numerous examinations.

In the following chapters the relevant aspects for modelling are described. Considered are aspects of yeast metabolism (chapter 2.2.1) and substrate uptake (chapter 2.2.2), as well as a short description of yeast propagation and fermentation in brewing technology (chapter 2.2.3).

2.2.1 Yeast metabolism

At present, approximately 600 yeast species are known and these possess widely diverging capacities for metabolising specific carbohydrates. Each species has a characteristic pattern of sugars that can be metabolised via oxidative, oxidoreductive or fermentative pathways. The metabolic processes provide the yeast with energy and building blocks for growth and other vital activities. Processes leading to energy production are indicated as catabolism or dissimilation, whereas those converting the substrate to building blocks for synthesis of cell material are designated anabolism or assimilation [121].

In this subchapter, for the description of yeast metabolism, energy producing steps in catabolism (degradation) and energy consuming reactions for anabolism (synthesis) and maintenance are distinguished. Also, occuring regulation phenomena as Pasteur effect and Crabtree effect are described.

2.2.1.1 Catabolism

The oxidation of an organic C-source by dehydrogenation represents the basic process during the production of cellular energy in the yeast cell (C-heterotrophic organisms). The separated substrate–hydrogen is transferred finally to different acceptors, dependent on the

cultivation conditions. Catabolic pathways are distinguished by these hydrogen acceptors, main substrate and the degree of substrate degradation. Regarding yeast catabolism, the most important pathways are the oxidative (respirative) and the fermentative (ethanol fermentation) pathway. *Saccharomyces cerevisiae* belongs to the group of facultative anaerobic microorganisms. The latter are characterised by the ability to use the oxidative and the fermentative pathway for substrate degradation and energy production, dependent on the actual substrate conditions. In the case of *Saccharomyces sp*. both pathways, oxidative glucose degradation and fermentative ethanol formation may also be followed simultaneously (**oxidoreductive metabolism**).

According to the enthalpy and entropy difference, during the catabolic reactions energy is produced. Part of this energy is used to produce the major portion of the cell's ATP (Adenosine-tri-Phosphate), which is provided as energy reservoir by the cell. The remaining part is liberated as heat [3]. Preserved energy is released, for example, in the anabolism by separation of phosphate from ATP forming ADP. Based on this reaction endergonic biomass synthesis is facilitated [61, 122].

Figure 5 presents an overview of relevant biochemical pathways and intermediate products during the catabolism of Saccharomyces cerevisiae growing on glucose or ethanol as main substrate.

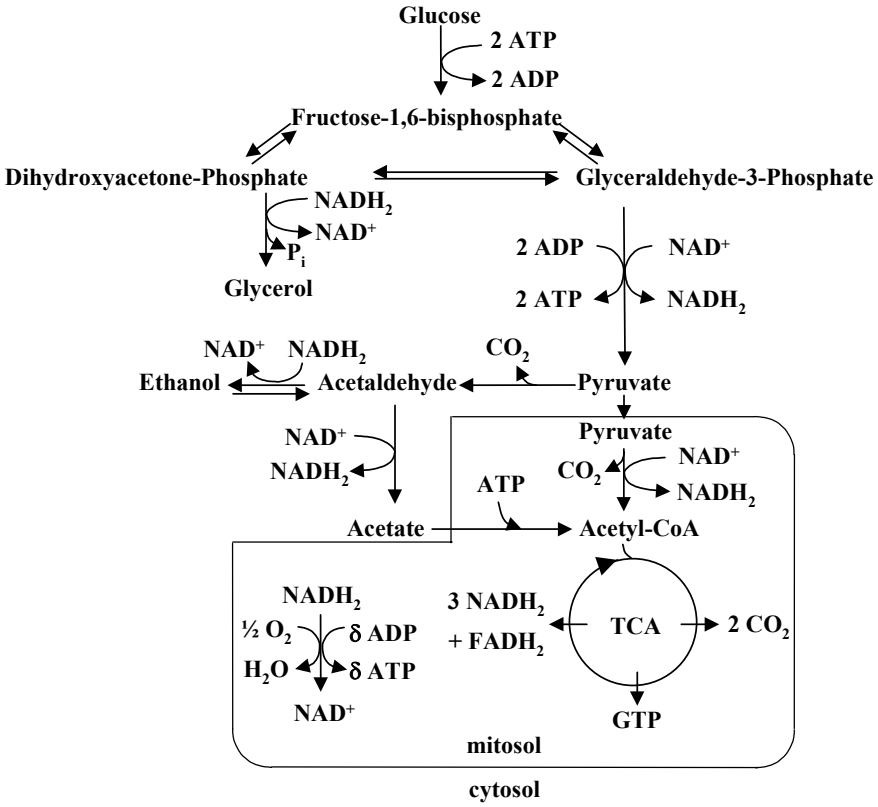

Figure 5: Relevant pathways and intermediate products during catabolism in *Saccharomyces sp.*

In the case of **oxidative growth on glucose**, the pyruvate which is produced in glycolysis quickly enters the mitochondria to be completely oxidised to CO_2 and H_2O. $NADH/H^+$, a reduction equivalent, which is formed during this step, is regenerated to NAD^+ by transferring electrons to O_2. During **fermentative growth** on glucose, glycolysis becomes a main source of the yeast's ATP. Anaerobic energy yielding reactions of this type are called fermentations. Here, pyruvate molecules are converted into ethanol plus CO_2. $NADH/H^+$ synthesised during glycolysis can not be regenerated by O_2. Therefore, regeneration is realised by hydrogenation of intermediate products as pyruvate or glyceron-phosphate in order to maintain glycolysis. In case of **oxidative growth on ethanol**, the latter is degraded to acetate and processed via the aerobic pathway. Glycolysis and further steps of the anaerobic pathway occur in the cytosol of the yeast cell, whereas in the oxidative pathway, after glycolysis, pyruvate or acetate are transported into the mitochondria for further degradation. These steps are illustrated in the following.

In the process of **glycolysis**, a glucose molecule with six carbon atoms is converted into two molecules of pyruvate, each with three carbon atoms. The cell hydrolyses two molecules of ATP to drive the early steps but produces four molecules of ATP in the later steps, so that a net gain of ATP results by the end of glycolysis.

Logically, the sequence of reactions in the glycolysis is divided into three parts. Glucose is converted into glyceraldehyde-3-phosphate. The conversion requires an investment of energy, in form of ATP hydrolysis, in order to provide two phosphate molecules. Subsequently, the aldehyde group of glyceraldehyde-3-phosphate is oxidised to a carboxylic acid. The energy of this reaction serves to create a high energy phosphate linkage (ATP) from inorganic phosphate and ADP. During the third part the invested phosphate molecules are transferred back to ADP.

The overall result is that an aldehyde group of a sugar is oxidised to a carboxylic acid and an inorganic phosphate group is transferred to a high-energy linkage (ATP). Additionally, a molecule of NAD^+ is reduced to $NADH/H^+$. According to reaction 21, per mol glucose two mol ATP and two mol $NADH/H^+$ are formed.

$$C_6H_{12}O_6 + 2\ ADP + 2\ P_i + 2\ NAD^+ \rightarrow 2\ Pyruvate + 2\ ATP + 2\ NADH_2 + 2\ H_2O \qquad (21)$$

Under aerobic conditions, pyruvate is dehydrogenised and decarboxylated to actetyl CoA and CO_2 (**oxidative decarboxylation**). Hydrogen is transferred to NAD^+. This reaction, located in the mitochondria, is catalysed by the multi enzyme complex pyruvate dehydrogenase.

$$Pyruvate + HSCoA + NAD^+ \rightarrow C_2H_3O\text{-}SCoA + CO_2 + NADH/H^+ \qquad (22)$$

During the subsequent **citric acid cycle** (CAC or TCA) acetyl CoA is oxidised to CO_2 in multiple dyhydrogenation steps. Hydrogen acceptors are 3 NAD^+ and 1 FAD. Per mol acetyl CoA, 3 mol $NADH/H^+$, 1 mol $FADH_2$ and 1 mol GTP are produced (see Figure 5):

$$C_2H_3O\text{-}SCoA + 3\ H_2O + 3\ NAD^+ + FAD^+ + GDP \rightarrow$$
$$2\ CO_2 + 3\ NADH/H^+ + FADH_2 + GTP + HSCoA. \qquad (23)$$

Oxidative phosphorylation represents the last step in oxidative catabolism and the point, at which the major portion of metabolic energy is released. Reduction equivalents $NADH/H^+$ and $FADH_2$ transfer the electrons to molecular oxygen forming H_2O. This reaction formally is equivalent to the burning of hydrogen in air to form water. In the course of oxidative phosphorylation, electrons from $NADH/H^+$ and $FADH_2$ pass down a chain of carrier molecules that are known as the electron transport chain. The latter is located in the inner membrane of the yeast mitochondria. At each step of the transfer, the electrons fall to a lower energy state, until they are transferred finally to oxygen molecules. The electron transfer causes protons to be pumped across the membrane from the inner mitochondrial compartment to the outside. An electrochemical proton gradient is thereby generated across the mitochondrial membrane. This, in turn, drives a flux of protons back through a special enzyme complex in the same membrane, causing the enzyme (ATP synthase) to add a phosphate group to ADP and thereby forming ATP (theory of Mitchell) [88]. Summarising, the oxidative phosphorylation is formulated as

$$½\ O_2 + NADH_2 + \delta\ ADP + \delta\ P_i \rightarrow H_2O + NAD^+ + \delta\ ATP. \qquad (24)$$

δ mol ATP are generated per mol $NADH/H^+$. The relation $\delta = ATP/NADH/H^+$ is known as P/O-relation (ATP per oxygen). Concerning Saccharomyces cerevisiae, van Gulik [131] found a value $\delta = 1.5$ in theoretical and $\delta = 1.2$ in practical examinations.

If no glucose (below 2.8 mmol/L [60, 127]) is available, the yeast cell switches to ethanol as main substrate. According to Figure 5, ethanol reacts to acetyl CoA in a two step dehydrogenation via acetaldehyde and acetate. Acetyl CoA is then directly introduced to citric acid cycle [108]:

$$C_2H_5OH + 2\ NAD^+ + HSCoA \rightarrow C_2H_3O\text{-}SCoA + 2\ NADH/H^+. \qquad (25)$$

Along the fermentative pathway, substrate degradation is not completed. The final hydrogen acceptor is acetaldehyde, a metabolic intermediate product, and ethanol is resulting. Reduction equivalents from the glycolysis can be regenerated by transferring the hydrogen to pyruvate. In a first step pyruvate is decarboxylated to acetaldehyde by the enzyme pyruvate decarboxylase. Afterwards $NADH/H^+$ is regenerated by hydrogenation of acetaldehyde to ethanol by alcohol dehydrogenase (see Figure 5). A balance can be formulated as:

$$Pyruvate + NADH/H^+ \rightarrow C_2H_5OH + CO_2 + NAD^+. \qquad (26)$$

In anaerobic conditions, the regeneration of $NADH/H^+$ by ethanol formation is not sufficient. Here, the regeneration of $NADH/H^+$ is strongly dependent on the amount of $NADH/H^+$ consumed in glycolysis. However, during biomass formation additional $NADH/H^+$ is produced, which has to be regenerated. Therefore, the hydrogen is transferred to glyceron phosphate alternatively. Glycerol phospate is formed, which further reacts to glycerol by separation of phosphate (see Figure 5). The mentioned reactions are summarised as follows:

$$C_6H_{12}O_6 + 2\ NADH_2 + 2\ ATP \rightarrow 2\ C_3H_8O_3. \quad (27)$$

2.2.1.2 Anabolism and maintenance

In catabolism, substrate is degraded in order to produce energy for maintenance and the synthesis of biomass. Regarding known yield coefficients ($Y_{X/Sox} \approx 0.5$ g biomass / g glucose, $Y_{X/Sf} \approx 0.1$ g biomass / g glucose, $Y_{X/e} \approx 0{,}5$ g biomass / g ethanol), the portion of substrate needed for energy production in catabolism becomes obvious. The remaining part of substrate can be used in anabolism.

The yeast cell consists of macromolecules. The latter are polymerised from monomers, which are synthesised from various intermediate products of the catabolism. The entirety of these complex reactions can be expressed in a simplified manner according to the following equation [65]:

$$g\ C_6H_{12}O_6 + 0{,}15\ [NH_3] + K\ ATP \rightarrow$$
$$CH_{1,79}O_{0,57}N_{0,15} + c\ CO_2 + n\ NADH/H^+ + w\ H_2O. \quad (28)$$

CO_2 is formed by decarboxylation during anabolism. The stoichiometry of the CO_2 production is primarily dependent on the carbon source. According to Heijnen [65] during growth on glucose c = 0.095 - 0.22 mol CO_2/mol biomass are produced. For ethanol as carbon source $c_E = 0.266$ (- 0.285 mol) mol CO_2/mol ethanol was found [64, 86]. Anabolic reactions require energy in form of ATP. Heijnen [65] found a value of K = 1.7 mol ATP/C-mol biomass for this demand.

Energy in form of ATP is not only required for growth but also for maintenance (non growth associated maintenance). Heijnen [65] specifies an energy demand of m_{ATP} = 0,007 - 0,018 mol ATP/(C-mol biomass*h). According to Heijnen [66] the maintenance related energy demand is only dependent on biomass concentration and temperature.

2.2.1.3 Metabolism regulation phenomena

Saccharomyces cerevisiae uses various regulation mechanisms in order to adapt the rates of the mentioned pathways of catabolism to the actual substrate conditions. The most important basic mechanisms are the Pasteur effect and the Crabtree effect. Both effects are control functions of the metabolism considering the actual glucose and oxygen concentration in the growth medium and are therefore important for the development of a process model.

The **Pasteur effect** is found in all facultative anaerobic microorganisms. Louis Pasteur described this effect the first time for the yeast Saccharomyces cerevisiae [122]. He observed that the glucose uptake rate and also the rate of glycolysis is higher in anaerobic conditions then in aerobic conditions. If oxygen is added to an anaerobic yeast fermentation, glucose uptake rate is decreasing [61]. Several reasons for this effect are discussed in literature. It is possible that several regulation mechanisms are involved.

One mechanism is explained with the competition on ADP and inorganic phosphate for ATP formation. Without ADP and phosphate the dehydrogenation of glyceral-3-phosphate in glycolysis is interrupted (see Figure 5). Under aerobic conditions the oxidative phosphorylation in the mitochondria is also competing on ADP and inorganic phosphate for ATP formation. Therefore, the concentration of ADP and phosphate in the cytosol as well as the glycolysis rate are decreasing [61, 122].

Another explanation is the allosteric inhibition of phosphofructokinase, an enzyme in the glycolysis, by ATP. Additional ATP is formed in the oxidative phosphorylation step under aerobic growth conditions, which causes a decrease in glycolysis rate [122].

The **Crabtree effect** was observed the first time in cancer cells by Crabtree in 1929 [35]. Crabtree positive yeasts as Saccharomyces sp. form ethanol even under fully aerobic conditions, if glucose concentration in the growth medium exceeds a critical value. Hence, a portion of the available substrate glucose is degraded following the fermentative pathway. This phenomenon is known as **overflow metabolism**, **catabolite repression**, **aerobic fermentation** or **oxidoreductive metabolism** [60, 61, 108]. Similar to the Pasteur effect different explanations are discussed in literature.

In a first approach a repression of enzymes out of the oxidative pathway of catabolism by glucose or other intermediate products was presumed. Therefore, the Crabtree effect was first known as catabolite repression [60]. However, the effect occurs within seconds after exceeding the critical glucose concentration in the growth medium. Therefore, according to Gschwend-Petrik [60] and Pham et. al. [108] the Crabtree effect is not explainable by long term mechanisms like repression or adaptation. Ethanol formation due to a repression of the enzymes of respirative glucose degradation is excluded.

A further explanation including short term regulation is delivered with the bottleneck hypothesis. According to this hypothesis, the rate of the aerobic catabolic pathway is limited and therefore, because of a higher rate of glycolysis compared to the rate following the oxidative pathway, an overflow reaction for the degradation of excessive pyruvate occurs. Concerning the rate limiting critical reaction for the oxidative pathway, different theories are reported in literature [60, 108].

According to Sonnleitner and Käppeli [127] the respirative capacity represents the limit. Thus the limiting reaction is the oxygen uptake rate in the oxidative phosphorylation.

Meanwhile, it was proved that oxygen uptake rate is not limited to the observed maximum value for growth on glucose. Verdun et al. [134] reached in experiments with uncoupling substances, e.g. benzoic acid, higher respirative rates. Thus, the oxidative phosphorylation is not a limiting instance. As long term regulation effects like repression and adaptation can be excluded, the reason for a limited oxygen uptake rate must lie in a limited availability of $NADH/H^+$ or ADP and inorganic phosphate in the mitochondria.

Gschwend-Petrik [60], Hartmeier [61] and Pham et al. [108] suppose a limited turnover rate of the enzyme complex pyruvate dehydrogenase as a reason for the Crabtree effect. Pyruvate is the starting point for the fermentative and the oxidative pathway of the yeast catabolism. The turnover rate for the degradation of pyruvate via the citric acid cycle (oxidative pathway) is limited by pyruvate dehydrogenase with a half saturation constant $K_m = 10^{-4}$ mol/L. The fermentative turnover to acetaldehyde is catalysed by pyruvate decarboxylase with a $K_m = 10^{-3}$ mol/L (see Figure 6). At low glucose and analogue pyruvate concentrations, pyruvate is degraded mainly via the pyruvate dehydrogenase due to the lower K_m-value (higher affinity to the substrate). With increasing substrate concentrations the degradation via pyruvate decarboxylase is installed additionally. At a pyruvate concentration of about 10^{-3} mol/L the pyruvate dehydrogenase is reaching substrate saturation and maximum turnover rate. However, pyruvate decarboxylase reaches only the half maximum turnover rate at this point. Therefore, with increasing substrate concentrations only the turnover rate via the fermentative pathway is increasable. With a concentration of 1 g / 100 mL the pyruvate decarboxylase is saturated as well [60, 61, 70].

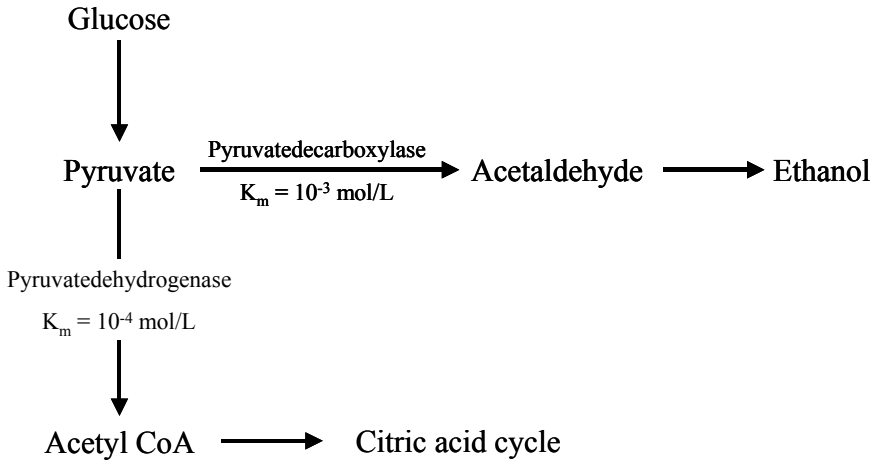

Figure 6: Pathways for the turnover of pyruvate to acetaldehyde and acetyl CoA. The reactions are catalysed by the enzymes pyruvate decarboxylase or pyruvate dehydrogenase.

As mentioned above, a further explanation is the competition on ADP and inorganic phosphate in cytosol and mitochondria. During respiration the main part of ATP is formed in the mitochondria, but usage takes place in the cytosol as well. Additionally, due to the increasing glycolysis rate, in the cytosol more ATP is formed. Because of this additional

energy production, the supply of the ATP consuming reactions can be optimised and the growth rate increases [61].

According to Gschwend-Petrik [60] for the examination of the Crabtree effect short term regulation mechanisms (see above) and long term effects, as e.g. adaptation of enzyme activities to substrate conditions, must be distinguished.

2.2.2 Substrate uptake mechanisms

The behaviour of a yeast towards a specific substrate is not only governed by the genetic information available in the DNA, but by the environmental conditions also. Important parameters are the qualitative and quantitative composition of the culture medium, temperature, and the availability of dissolved oxygen [121].

2.2.2.1 Sugar uptake

Transport of glucose across the cell membrane is supposed to follow a facilitated diffusion mechanism. Here, a selective permease transports glucose along the concentration gradient. In contrast to molecular diffusion, the mechanism is characterised by a substrate saturation. Additionally, transport is inhibited by glucose-6-phosphate in the cytosol [3, 11].

In literature, Monod-kinetics are often supposed for glucose uptake of *Saccharomyces cerevisiae* [108, 127, 129]. The glucose uptake rate is limited for low glucose concentrations, above $C_s = 1$ g/100 mL glucose uptake is saturated. In between $C_s = 1$ g/100 mL to $C_s = 10$ g/100 mL glucose concentration has no influence on the yeast metabolism and glucose uptake rate remains at maximum. Higher concentrations of glucose $C_s > 10$ g/100 mL cause inhibition effects due to osmotic pressure [61]. Hartmeier [61] defines a critical range for glucose concentration $C_s = 0{,}02$-1 g/100 mL as transition range from oxidative to oxidoreductive metabolism.

Glucose uptake is dependent on the nitrogen concentration in the growth medium. Without assimilable nitrogen sources, neither glucose nor other sugars will be transported across the membrane of *Saccharomyces cerevisiae*, because above mentioned selective permeases are inactivated without current protein formation [24, 140]. Ethanol in the growth medium inhibits glucose uptake due to toxic effects. According to Aiba [2], the inhibition effect is non-competitive.

Malt wort comprises a variety of sugars, which are sequentially transported and metabolised by the yeast in the approximate order glucose (also fructose or sucrose), maltose and maltotriose. Maltose, a disaccharide, is the most abundant fermentable sugar present in brewers' wort. *Saccharomyces cerevisiae* transports maltose by an energy dependent proton symport mechanism and hydrolyses the sugar by an intracellular maltase into two molecules of glucose. Maltose is existent at much higher concentrations than glucose, but glucose

regulates the rate at which maltose is utilised and thus, the overall rate of propagation or fermentation [140].

2.2.2.2 Oxygen uptake

Oxygen uptake follows a diffusion mechanism [61]. Hartmeier [61] described the kinetic of oxygen uptake in yeasts and other microorganisms. Under low oxygen concentrations the oxygen uptake rate is limited by oxygen concentration in the growth medium. With increasing oxygen concentrations the rate is asymptotically approaching to a maximum value. This critical oxygen concentration was determined as 22 µmol/L. Only at very high oxygen concentrations the respiration is inhibited and the oxygen uptake rate is decreasing [61]. According to Hartmeier for aerobic yeast growth a narrow range of oxygen concentrations slightly above the critical concentration is optimal. Oxygen uptake rate is limited or inhibited below or above this range.

Monod kinetics are presumed in most cases for oxygen uptake in yeasts [108, 127, 129]. However, Hartmeier [61] found significant deviations from Monod kinetics for very low oxygen concentrations during his examinations with yeasts and mould fungi. In contrast to this result, bacteria show only very small deviation from Monod kinetics. A possible reason is the diffusion resistance in the eucaryotic yeast across several membranes. The last step in oxidative catabolism, the transfer of electrons from Cytochrom C to molecular oxygen in the oxidative phosphorylation show Monod characteristics as well as the oxygen uptake of mitochondria. However, the uptake kinetic of the complete cell deviates from this behaviour.

Oxygen uptake is influenced by growth medium conditions and temperature. For example, if hydrogen supply out of the substrate dehydrogenation is not sufficient, the latter step becomes a limiting factor. Therefore, the actual maximum oxygen uptake rate is dependent on substrate type and concentration. Also pH-values outside a range between pH 4.5 and 6.5 decrease the oxygen uptake rate [61].

The maximum specific oxygen uptake rate is strongly dependent on the temperature. Until temperatures of 30°C, the maximum oxygen uptake rate increases with the temperature. Above 30°C differences appear between yeast cells adapted or not adapted to high temperatures (see Figure 7) [61].

Without oxygen supply, the growth of Saccharomyces cerevisiae is stopped after several generations [138]. Oxygen even in small quantities, which are not relevant concerning energetical aspects, is necessary for anabolism, e.g. for the formation of specific unsaturated fatty acids, sterols or DNA. Usually beer wort contains merely a small amount of sterols and unsaturated fatty acids. Both are components of the plasma membrane of the cell and sustain their fluidity and function [141]. Oxygen is required for the formation of sterols. If oxygen is limiting, the sterol content decreases during yeast growth. Below a threshold of 0.1% w/w no

further growth is possible [7]. Thus, the demanded oxygen supply depends on the yeast type and the characteristic threshold for sterol concentrations in the growth medium [80].

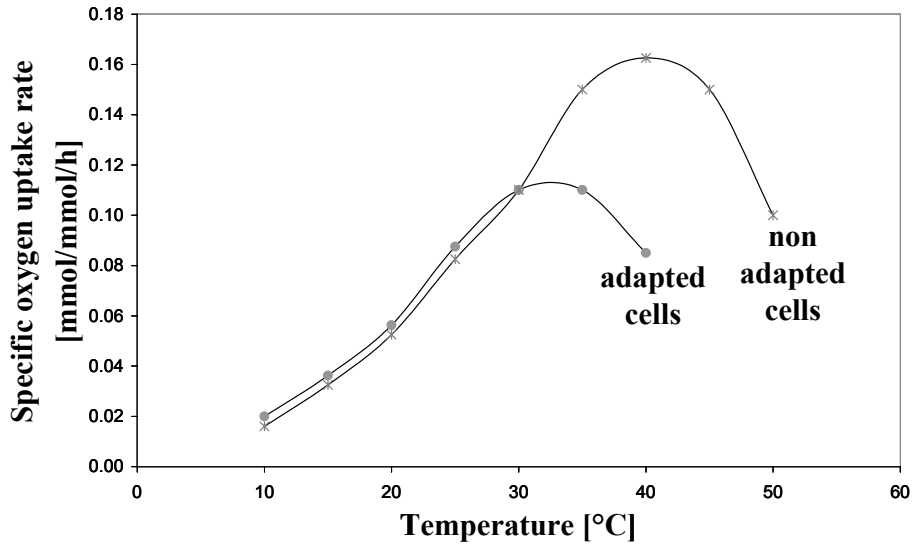

Figure 7: Maximum specific oxygen uptake rate of S. cerevisiae for temperature adapted and non adapted cells [61].

For both aspects, the substrate uptake and the oxygen uptake, an influence of the pH value can not be expected. Bronn [22] found in pH range of 3.0 – 6.6 no influence on the yeast metabolism. Yeast demands a wide variety of trace elements for enzymatic and structural purposes. Usually, the beer wort supplies a sufficient mineral concentration. However, concentrations of zinc in most industrial worts lie below a treshold of 0.15 mg/L [50]. A lack of zinc leads to a decreased growth rate, longer fermentation periods and an undesired flavour composition in the resulting beer [95].

2.2.3 Yeast batch propagation and fermentation

Usually, yeast propagation and fermentation in breweries are realised as batch or sequencing batch processes. Hereby, the yeast passes through different growth phases of a static culture. The period from inoculation until the appearance of the maximum growth rate is denoted as lag phase. During this time the yeast becomes adapted to the growth medium by synthesis of nucleic acids, ribosoms and enzymes. The duration of the lag phase depends on the physiological state of the inoculum and the specific growth medium [122]. A subsequent exponential phase (log phase) is characterised by a nearly constant growth rate on a high level. Limiting factors in the growth medium beer wort, e.g. assimilable nitrogen, zinc or vitamins (pantothenic acid), or exhausted substrate (sugar) cause a decrease in growth rate. Additionally, the accumulation of metabolic products as ethanol and CO_2 as well as a high population density inhibits yeast growth. Therefore, yeast growth changes to a stationary phase, where no cell growth can be observed. In this phase, cells can survive for a longer period. Not until the entire fermentable sugar is consumed, the population changes to a

quiescent phase. With the exploitation of reserve carbohydrates, e.g. glycogen, the degeneration of the cell starts [75, 85, 102].

As mentioned above, yeast vitality exerts a relevant influence on the subsequent fermentation and the resulting beer quality, the inoculum is aspired to be harvested from the exponential phase of a propagation [10, 74, 101]. The aim of yeast propagation is to conserve the yeast cells in the exponential phase, by different feeding strategies of substrates, e.g. sugars, nitrogen, or oxygen, and elimination strategies for metabolic products as ethanol, CO_2 and yeast biomass. In practice, different strategies were developed in this regard. They replaced the common strategy of yeast culturing in open vessels or pure cultures using doubling strategy. The latter were cost intensive and implied a high risk of microbiological contaminations.

Brewery yeast propagation is unlike biomass propagation systems used in other fermentation industries. Baker's yeast for example, has been focus of much research and is normally produced in highly aerated fed-batch systems, maximising biomass yield and minimising ethanol production [109, 120, 132]. This process eliminates fermentative metabolism in *Saccharomyces cerevisiae*. Brewers' yeast, however, is propagated in standard brewery wort with a variety of aeration regimes. The degree of aeration and mixing used in brewery propagations is likely to lead to oxygen-limited growth [79]. Likewise, the growth medium itself is high in sugars and therefore, due to the limited oxidative capacity of *Saccharomyces cerevisiae*, significant quantities of wort sugars are converted to metabolic endproducts by oxidoreductive metabolism [60, 61]. To overcome these difficulties, some breweries import yeast as an alternative to yeast propagation [89].

In modern brewing practice propagation strategies according to Geiger, Back or Wackerbauer are often applied. Following a propagation strategy according to Geiger [56], in a propagation tank yeast is inoculated in sterile brewing wort at a defined temperature. The yeast suspension is aerated during circulation in a circulation pipe. Geiger [56] recommended a continuous aeration with a dissolved oxygen concentration in the suspension above the saturation level and a continuous circulation, dependent on the volume of each tank. After a first cultivation (pure culture), subsequent propagations are initiated by adding wort to 10% of the yeast suspension as inoculum. Experiments showed that in propagations at 10°C the desired amount of yeast (around $100*10^6$ cells/mL for a standard wort) could be reached within 36 to 48 h. The avoidance of large amounts of "propagation beer" of low quality, shorter lag phases in subsequent fermentations and a high quality yeast on a constant quality level as well as a more constant beer quality were reported as major advantages of the propagation strategy [56]. Wackerbauer et al. [138] described a strategy similar to Geiger. However, the suspension is not circulated. Homogenisation of the yeast suspension was realised by pulsed aeration using an aeration lancet in the tank. A duration of 48 h for a propagation at 20°C is reported.

The strategy of „Assimilation“ was developed by Back et. al. [9]. Assimilation plants consist of two tanks, which are connected by a circulation pipe including an aeration device. In the first tank beer wort (not sterilised) is inoculated with a pure culture yeast. Aeration is realised during circulation from one tank to the second. Additionally, in both tanks an aeration unit may be implemented as well. Due to foaming, a spare capacity of 40 – 50% of the tanks is recommended. Advantages of the regarded strategy were reported in a high yeast vitality and a high flexibility in the industrial application. However, high costs and the required space turned out to be major drawbacks. Therefore, assimilation was further developed to a single tank strategy [4, 32].

Several developments are described in literature concerning propagation systems using techniques normally employed outside of the brewing industry, e.g. continuous systems [55, 85] or fed batch systems [90]. It is reported, that the latter two systems produce yeast of improved quality in reduced times compared to conventional multi-vessel systems, with standard beer quality resulting from the first fermentation using propagated yeast [90, 138].

In brewing practice for bottom fermenting yeast propagation temperatures of 6 – 18°C are applied [102]. However, according to Manger and Annemüller [91] only in a range of 15 - 25°C an exponential growth is possible. Top fermenting yeast propagation is recommended at 20 – 22°C [102].

Brewing yeast fermentation is a central step in the entire beer production. Most of the relevant flavour components are formed here. Also the fermentation exerts an important influence on quality parameters of a beer, e.g. foam stability as well as physical and chemical stability [69, 83, 84, 85, 102]. During brewing yeast fermentation the same growth phases can be observed as mentioned above. However, for bottom fermenting yeast strains a sedimentation process is initiated due to physiological changes in the yeast cell [85, 102]. Therefore, during fermentations with a low fluid level (small cylindroconical fermentation tanks or horizontal tanks) a decrease in yeast concentration occurs at the end of the fermentation process. In modern brewing practice, fermentations are carried out in cylindroconical fermentation tanks with a volume up to 5000 hL. These tanks replaced fermentations in open vessels. Bottom fermenting yeast is usually applied at temperatures between 5 and 10°C. Accelerated procedures are run at 12 – 20°C [102]. Temperatures for fermentations with top fermenting yeasts range between 20 – 22°C.

3 Presentation and discussion of results

3.1 Mathematical modelling of Saccharomyces sp. metabolism

Since *Saccharomyces cerevisiae* is often applied in traditional fermentation industries, e.g. wine or beer fermentation as well as in research as a eucaryothic model microorganism, *Saccharomyces sp.* metabolism has been the aim of many examinations in biotechnology. In literature, various mathematical modelling approaches can be found, which, however, in most cases are qualified only for specific purposes or metabolic states (see chapter 3.1.2). One topic of the present work was to develop a comprehensive modelling approach, which combines general requirements for a model of Saccharomyces sp. metabolism in biotechnology (see chapter 3.1.1.1) and special requirements for modelling yeast metabolism under industrial conditions. In this regard, chapter 3.1.1.2 especially emphasises the modelling requirements in brewing technology. Two modelling approaches were developed in this work, an unstructured black-box model and a metabolic model (chapters 3.1.3 and 3.1.4). A validation of the modelling approaches for literature data from bakers' yeast and experimental data from brewers' yeast propagations is given in chapter 3.2. Manipulated variables and their influence on the yeast growth are discussed in chapter 3.3. The potential of the application of a simulation tool for process control scenarios illustrates chapter 3.4. Additionally applications in industrial propagation plants were performed (see chapter 3.5). Finally, results concerning model based simulations for brewery yeast fermentations are reported in chapter 3.6.

3.1.1 Requirements for the modelling approach

A comprehensive simulation model of the yeast metabolism should be developed in order to

- gain more insight into the whole process,
- perform sensitivity analysis for the identification of the important parameters and conditions, and
- be able to simulate different reactors and procedures in research and industry.

3.1.1.1 General requirements

The developed model should provide a suitable basis for simulating yeast growth under all relevant conditions in research and industry. This means, metabolic states as oxidative, oxidreductive and fermentative growth on glucose and oxidative growth on ethanol should be represented by the modelling approach. Also, the influence of manipulated variables, e.g. temperature and dissolved oxygen concentration, has to be included, in order to allow predictive simulations as a base for further process optimisation. Growth media in industrial

applications are characterised by limiting or inhibiting substrate conditions. Referring to this, relevant considerations must be implemented in the process model. In a first step, for simplification, biotic and abiotic concentrations can be regarded as homogeneously distributed in the reactor. Batch-processes, fed-batch processes or sequencing batch processes are widely applicated in industry and, therefore, it should be possible to simulate these procedures as well as chemostats. Additionally, as the physiological state of the yeast exerts a relevant influence on the yeast performance, correlations to physiological properties should be integrated. A further important aspect is a low number of state variables and parameters to guarantee clearness of the approach [64].

3.1.1.2 Specific conditions in brewing industry

Most modelling approaches in literature (see chapter 3.1.2) deal with growth of (recombinant) *Saccharomyces cerevisiae.* Here, often chemostat conditions are applied in order to characterise kinetic parameters. In brewing industry, yeast propagation is realised in batch, fed-batch or sequencing batch processes [4, 69, 85, 87, 138]. Processes are carried out without mixing, with bypass circulation [9, 136] or with quasi ideally mixed reactors [97]. Aeration of reactors is realised by Venturi-principle in the bypass or by inline aeration systems, e.g. lancet or impeller [5, 6, 9]. In most reactors oxygen or other biotic or abiotic concentrations are not ideally distributed in the growth medium. Only single systems achieve a quasi ideally mixing [97]. Fermentations are carried out in batch processes in cylindroconical fermentation tanks (CCF) with volumes up to 5000 hL [69, 85, 102]. However, some approaches are known for continuous propagation or fermentation in breweries [69]. For modelling of non-stirred fermentations with bottom fermenting yeasts (brewery fermentation), a sedimentation process is required also to represent the sedimentation of yeast cells conditional upon physiological conditions.

In brewing industry, several yeast strains are applied. They can be divided into different strains of top fermenting yeasts *Saccharomyces cerevisiae cerevisiae* and bottom fermenting yeasts *Saccharomyces cerevisiae uvarum var. carlsbergensis*. In particular, for the bottom fermenting brewing yeast strain modelling approaches or at least kinetic parameters can hardly be found in literature [60]. According to chapter 2, a model enables the detection of sites of change for example in kinetics or yields. Here, by simulations the performances of different yeasts or different substrates in brewing industry should be detected.

No comprehensive modelling approach is available, which takes into account the very limiting composition of the specific growth medium, the beer wort. This medium is characterised by high concentrations of sugar (> 100 g/L), which leads to regulation effects like the Crabtree effect expressed by reductive, oxidoreductive or oxidative growth of *Saccharomyces sp.* [60, 61, 127]. A lack of nitrogen (< 40 mmol/L NH_3-equivalent) [82, 102] and trace elements, e.g. Zinc (< 0.2 mg/L) [95, 144], causes limitation effects along the batch

process. Beyond this, ethanol production during the growth process causes additional inhibition effects [2, 60, 127, 129, 140]. The relation between physiological state of the propagated yeast and its performance in propagation and subsequent fermentation is of special interest in brewing industry, as quality and taste of the resulting beer depends directly on the fermentation performance [10, 44, 50, 72, 85, 100, 102, 138].

The mentioned aspects should be integrated in the modelling approach in order to simulate not only full media in research, but industrial media and different strains of *Saccharomyces cerevisiae*.

3.1.2 Existent modelling approaches for yeast growth and fermentation

Saccharomyces cerevisiae is one of the best examined microorganisms in biotechnology. To describe the growth and the ethanol formation in the bakers' yeast propagation process, many structured and unstructured modelling approaches are known from the literature. Unstructured modelling approaches, based on the Monod equation and its descendants with the assumption of balanced growth and product formation [127], are often reproached with the fact that they inadequately describe the response of a microorganism population to environmental disturbances. According to Sweere et al. [129] available structured models can be distinguished in different types from approaches based on a structured biochemical pathway [34, 119, 131] to more segregated modelling approaches regarding different cell ages [12, 42]. These approaches consider balanced growth, or are specified to describe particular biochemical pathways inside structured models and therefore represent the basis for the modelling approach introduced in this work.

In most cases the validity of these approaches, however, is limited to defined states of the metabolism (oxidative, oxidoreductive, fermentative). Temperature dependency and maintenance energy are not considered. Also, a lag time function to describe the adaptation of the microorganisms to the surrounding growth medium, including the time for formation of enzymes, is merely included in single approaches using different equations [49, 108, 145]. The maintenance energy of the microorganisms is considered in single approaches only, e.g. Pham et al. [108]. However, this approach is only valid if oxygen is available. Most of the reports in literature used full media as a growth medium to avoid undesired limitation effects during the growth process. This is not possible in this application, because industrially produced beer wort is used as growth medium. Combined limitation and inhibition effects, e.g. caused by high ethanol concentrations, are usually not considered. Therefore, the applicability of the mentioned approaches for industrial purposes, in particular considering the usage of nutrient deficient, limiting or inhibiting media, is not guaranteed without qualifications. So, with a comprehensive modelling approach considering the aforementioned

inhibition and limitation effects, knowledge can be gained toward a process control tool for industrial applications.

In particular, for the bottom fermenting brewing yeast strain *Saccharomyces cerevisiae uvarum var. carlsbergensis* required here, no comprehensive modelling approach is available, which takes into account the very limiting composition of the specific growth medium, i.e., brewers' wort. This medium is characterised by high concentrations of sugar (100 g/L), which leads to regulation effects such as the Crabtree effect expressed by reductive, oxidoreductive or oxidative growth of *Saccharomyces sp.* [127]. A lack of nitrogen and trace elements, e.g. zinc, causes limitation effects [24, 91]. Besides, ethanol production during the growth derives additional inhibition effects [2].

Concerning the influence of temperature, in the field of bakers' yeast propagation work was done on a comparably small scale. In contrast to this, several authors described the temperature dependence of microbial growth in general [37, 142, 143] or for specific bacteria. The most common approaches were exponential following the Arrhenius equation [39, 58, 81] or parabolic Bělehrádek-type equations [113, 142]. The latter relation, however, is better suitable for the description of microorganism growth at sub-optimal temperatures. Reliable data considering an Arrhenius approach could not be found in the literature for industrial propagations of *Saccharomyces sp.* in the regarded temperature range. Solely, Manger et al. [91] described the influence of temperature especially for brewing yeast propagations. However, fixed generation times were used to predict the resulting yeast amount after a specific time. The doubling times were varying in a wide range between the different trials even for one temperature (e.g. between 7.2 and 8.5 h at 15°C). So, for an active process control applying variable temperature profiles, this approach could hardly be used.

3.1.3 Black-Box modelling approach

The Black-Box model in essence is an unstructured modelling approach. The developed model based on a kinetic model of overflow mechanism in *Saccharomyces. cerevisiae* developed by Pham et al. [107]. Additionally, features of modelling approaches of Sonnleitner and Käppeli [127] and Sweere et al. [129] are included. Similar to the former approach, the Black-Box model describes oxidative and oxidoreductive growth on glucose as well as oxidative growth on ethanol. Metabolism regulation (Crabtree effect) is taken into account by limiting the specific oxygen uptake rate to a maximum value.

Differences are made in the formulation of the maintenance demands of the yeast cell. Pham et al. [108] only consider a fixed substrate flow for maintenance within the oxidative pathway, because, at least partly, oxidative growth on glucose is assumed in each regarded case. In this work, however, also purely fermentative growth or purely oxidative growth on ethanol are integrated. Therefore, maintenance terms are integrated for all growth conditions. Limitation effects by glucose, oxygen, nitrogen and ethanol are taken into account. Also

inhibition effects caused by ethanol are included. Additionally, temperature dependency and lag times for growth on glucose and diauxic lag phase, respectively, are introduced.

The Black-Box modelling approach is based on several assumptions:

- Only educts and products mentioned in Figure 8 are considered. Other substrates and byproducts are neglected.
- Glucose, ethanol and oxygen uptake follow Monod-kinetics. All sugars are abstracted as glucose equivalents.
- Specific oxygen uptake rate is limited to a maximum value (Crabtree effect). The latter is assumed to be identical for growth on ethanol and glucose.
- If the specific glucose uptake rate is higher than the adequate specific oxygen uptake rate, a overflow reaction occurs. The „overflow“ glucose is degraded following the fermentative pathway. This means, metabolism is changing from oxidative to oxidoreductive, if oxidative capacity of the yeast cell is exceeded.
- Ethanol uptake and degradation is only possible, if the specific glucose uptake rate is low and oxidative capacity is remaining.
- Biomass composition is assumed to be constant. Only the elements C, H, N and O are taken into account. Yield coefficients are constant.
- The regarded systems are assumed to be ideally mixed. No gradients occur for biotic or abiotic concentrations.

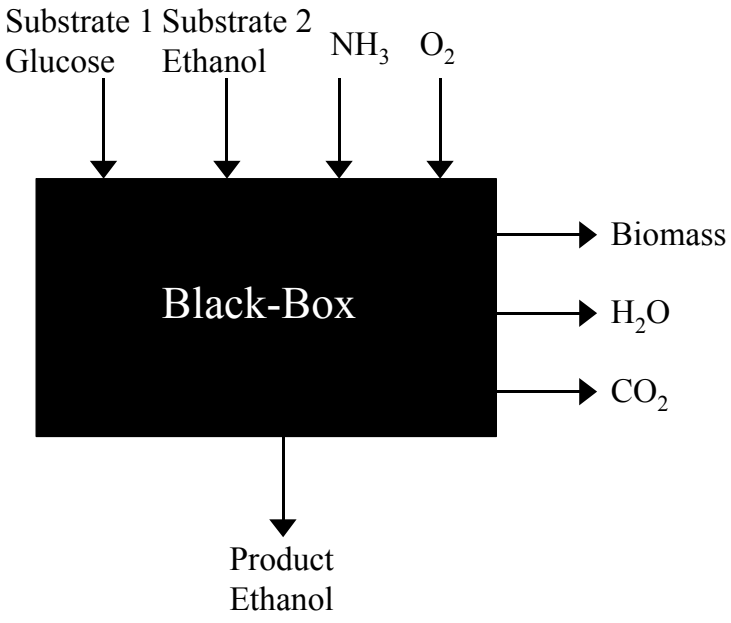

Figure 8: Scheme of the Black-Box modelling approach. Only substances are considered, which interact with the surrounding medium. Educts are glucose (glucose equivalents), ethanol, nitrogen source, and oxygen. Ethanol, biomass, water, and CO_2 are produced.

3.1.3.1 Stoichiometry

In the Black-Box modelling approach growth and energy production for maintenance is abstracted with six reactions, which are described in Table 3. Biomass composition $CH_{HX}O_{OX}N_{NX}$ is adopted from Sonnleitner and Käppeli [127] with HX = 1.79, OX = 0.57 and NX = 0.15.

Table 3: Biochemical reaction equations for growth and maintenance energy production considered in the Black-Box modelling approach. a … n indicate stoichiometric coefficients, ATP_i represents the molar yield of ATP for each substrate.

(I)	Oxidative growth on glucose
	$C_6H_{12}O_6 + a\ O_2 + b\ NX\ [NH_3] \rightarrow b\ C_1H_{HX}O_{OX}N_{NX} + c\ CO_2 + d\ H_2O$
(II)	Fermentative growth on glucose
	$C_6H_{12}O_6 + g\ NX\ [NH_3] \rightarrow g\ C_1H_{HX}O_{OX}N_{NX} + h\ CO_2 + i\ H_2O + j\ C_2H_5OH$
(III)	Growth on ethanol
	$C_2H_5OH + k\ O_2 + l\ NX\ [NH_3] \rightarrow l\ C_1H_{HX}O_{OX}N_{NX} + m\ CO_2 + n\ H_2O$
(IV)	Maintenance (Oxidative energy production on glucose)
	$C_6H_{12}O_6 + 6\ O_2 \rightarrow 6\ CO_2 + 6\ H_2O + ATP_{ox}\ ATP$
(V)	Maintenance (Fermentative energy production on glucose)
	$C_6H_{12}O_6 \rightarrow 2\ CO_2 + 2\ C_2H_5OH + ATP_f\ ATP$
(VI)	Maintenance (Oxidative energy production on ethanol)
	$C_2H_5OH + 3\ O_2 \rightarrow 2\ CO_2 + 3\ H_2O + ATP_{eth}\ ATP$

According to Sonnleitner and Käppeli [127], biomass formation and growth related energy production is realised in three biochemical pathways (see Table 3). Substrate is degraded during oxidative growth on glucose or ethanol to biomass, CO_2 and water (I,III). Under anaerobic conditions biomass, CO_2, water and ethanol is produced from glucose (II).

Table 4: Balance of elements and linear equation systems for calculation of stoichiometric coefficients.

Balance	Oxidative growth on glucose
C	6 = b + c
H	12+3*b*NX = b*HX + 2*d
O	6 + 2*a = b*OX + 2*c + d
	Fermentative growth on glucose
C	6 = g + h + 2*j
H	12 + 3*g*NX = g*HX + 2*i + 6*j
O	6 = g*OX + 2*h + i + j
	Growth on ethanol
C	2 = l + m
H	6 + 3*l*NX = l*HX + 2*n
O	1 + 2*k = l*OX + 2*m + n

The stoichiometric coefficients a to n are calculated balancing the elements in reactions I-III. The three resulting linear equation systems are shown in Table 4. As four unknown coefficients stand opposite to three equations, for each equation system one stoichiometric coefficient must be determined. In this modelling approach, yield coefficients $Y_{biomass/substrate}$,

which are known from literature, are applied. The latter correspond with the coefficients b, g and l:

b = $Y_{X/Sox}$ Yield coefficient mol biomass/mol glucose for oxidative growth on glucose

g = $Y_{X/Sf}$ Yield coefficient mol biomass/mol glucose for fermentative growth on glucose

l = $Y_{X/E}$ Yield coefficient mol biomass/mol ethanol for oxidative growth on ethanol

Analogue to biomass formation, energy for maintenance is produced using the above mentioned pathways, dependent on substrate and availability of oxygen (see Table 3). ATP is formed during the oxidative degradation of glucose (IV). According to chapter 2.2.1.1, here, energy is considered to be delivered from glycolysis (2 mol ATP and 2 mol $NADH/H^+$), oxidative decarboxylation and citric acid cycle (10 mol $NADH/H^+$) as well as along the respiratory chain (δ Mol ATP/mol $NADH/H^+$). Summarising, ATP_{ox} = 2 + δ*12 mol ATP are produced from 1 mol glucose. For calculation GTP production in the citric acid cycle is neglected and $FADH_2$ is set equal to $NADH/H^+$ concerning ATP production in respiratory chain. Under anaerobic conditions glucose is degraded to ethanol and CO_2 (V) producing ATP_f = 2 mol ATP / mol glucose. Ethanol is oxidised to CO_2 during growth on ethanol (VI). During ethanol degradation 6 mol $NADH/H^+$ / mol ethanol and ATP_{eth} = δ * 6 mol ATP, respectively, are formed. For the P/O relation δ (see chapter 3.1.4.1) a fixed value of 1.2 is adopted from literature [63, 86, 131].

3.1.3.2 Kinetics

Dependent on glucose, oxygen, ethanol and nitrogen concentrations in the growth medium, biomass formation and energy production is following the above mentioned pathways. The turnover rates along the pathways are determined by belonging kinetics. Specific uptake rates for glucose q_s, ethanol q_e and oxygen q_O are described with kinetic equations. The formulation of the model kinetics is based on theoretical considerations (see chapter 2.2.2).

The **specific glucose uptake rate q_S** reaches a fixed maximum value $q_{S,max}$ (see Table 12). It is limited by available glucose, ethanol and nitrogen in the growth medium. Inhibition is considered for ethanol. Monod kinetics are assumed for all limitation and inhibition effects. All limitations are formulated as non-interacting [18], i.e. if the specific glucose uptake rate is limited not only by a single nutrient concentration, only the most limiting nutrient will be taken into consideration. Applied half saturation constants for limitations or inhibitions were K_s = 2.8 mmol/L [127], K_n = 2 mmol/L [26] and $K_{i,eth}$ = 500 mmol/L [71]. Additionally, temperature dependency is introduced with a coefficient f_{temp}, which is multiplied by the specific glucose uptake rate

$$q_S = q_{S,\max} \cdot \min\left(\frac{S}{S+K_s}, \frac{N}{N+K_n}\right) \cdot \frac{K_{i,eth}}{K_{i,eth}+E} \cdot f_{temp} \cdot L_t. \qquad (29)$$

Monod kinetics are only able to describe the exponential and stationary states of yeast growth. Therefore, a function for the description of a lag-phase is introduced. The latter covers the period from inoculation until the maximum specific growth rate is reached. A sigmoid lag-time function

$$L_t = \frac{1}{1+e^{-(t-t_{lag})}}, \tag{30}$$

with lag time t_{lag} and time t, is multiplied with the specific glucose uptake rate q_s.

Similar to q_s, the **specific oxygen uptake rate q_{O2}** is characterised by a maximum specific oxygen uptake rate $q_{O2,max}$, which is dependent on temperature [60, 61]. The uptake rate is limited by oxygen concentration and inhibited by ethanol. For the half saturation constant K_o the lowest of all values given in literature was chosen with 0.00121 mmol/L [61]. Ethanol inhibition is formulated with $K_{i,eth,o}$ = 217.35 mmol/L [127]. If the specific substrate uptake rate is exceeding a critical value adequate to the oxidative capacity of the yeast cell $q_{O2,lim}$, according to equation 31 the specific oxygen uptake rate q_{O2} is reaching a maximum value $q_{O2,lim}$. Metabolism then changes from oxidative to oxidoreductive:

$$q_{O2} \le q_{O2,max} \frac{O}{O+K_O} \cdot \frac{K_{i,eth,o}}{K_{i,eth,o}+E} = q_{O2,lim}. \tag{31}$$

Otherwise, with a lower q_s, the oxidative capacity is not utilised and the specific oxgen uptake rate q_{O2} is not reaching $q_{O2,lim}$. In this case, the actual rate can be calculated from q_s and stoichiometric coefficients (see Table 5).

The **specific ethanol uptake rate** is limited by a maximum rate $q_{e,max}$. Limitation terms for ethanol and assimilable nitrogen sources are included using Monod kinetics (K_e = 2.2 mmol/L [108, 127] and K_n = 2 mmol/L [26]). Similar to q_s, only the most limiting nutrient is considered for calculation. During adaptation of the enzyme pool to the substrate ethanol, a (diauxic) lag phase occurs. Analogue to equation 30, the latter is described with a sigmoid lag time function

$$L_{t,eth} = \frac{1}{1+e^{-(t-t_{lag,eth})}} \tag{32}$$

with time t and lag time $t_{lag,eth}$, which is multiplied by the specific uptake rate q_e. Dependent on substrate conditions, a specific ethanol uptake rate $q_{e,lim}$ results. Ethanol uptake by *Saccharomyces. sp*. is only possible, if glucose concentration is very low and oxidative capacity is left. In this approach glucose is assumed to be the preferred substrate and oxidative capacity is used by glucose first. So, the specific ethanol uptake rate

$$q_e \le q_{e.\max} \cdot \min\left(\frac{E}{E+K_e}, \frac{N}{N+K_n}\right) \cdot L_{t,eth} = q_{e,\lim} \tag{33}$$

may be lower as $q_{e,lim}$, if the remaining oxidative capacity is lower than necessary for full oxidation of ethanol. In each case, specific uptake rates for the two C-sources glucose and ethanol are divided into partial fluxes related to maintenance or growth. Figure 9 illustrates the division of substrate flow applied in the Black-Box model. The specific glucose uptake rate q_s is divided into specific rates for maintenance $q_{s,main}$ and growth $q_{s,gr}$. For growth on glucose a further subdivision in substrate uptake related to oxidative and fermentative growth (I,II) or maintenance (IV,V) is established. Similarly, the specific ethanol uptake rate q_e is divided into $q_{e,main}$ (VI) or $q_{e,gr}$ (III).

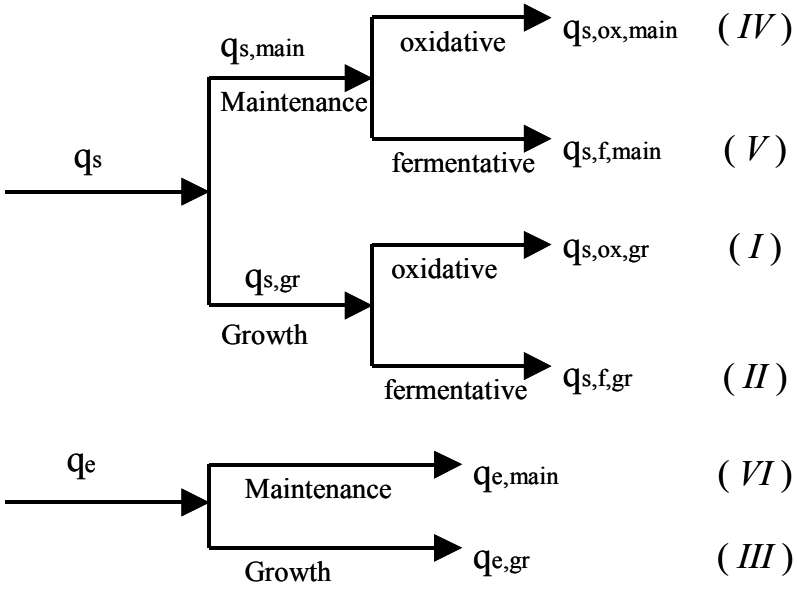

Figure 9: Division of the substrate uptake flux in the Black-Box model. The uptake rates (flux) are divided into portions for growth and maintenance for each substrate. Roman figures indicate relations to biochemical reaction described in Table 3.

The specific uptake rate for glucose q_s and the limits of specific uptake rates for oxygen and ethanol $q_{o2,lim}$ and $q_{e,lim}$ are determined by the above mentioned kinetic equations dependent on substrate conditions. Flux of substrates is first used for maintenance of the yeast cell. For maintenance energy a constant value $m_{ATP} = 0.013$ mol ATP/C-mol biomass and hour is applied here according to Heijnen [63]. Glucose is assumed to be the preferred substrate. Thus, in this approach energy for maintenance is produced using different pathways in the order oxidative degradation of glucose, fermentative degradation of glucose, and, if glucose concentration is low and oxidative capacity is left, oxidative degradation of ethanol. This order is followed until the demanded maintenance energy is reached. Computation of specific substrate uptake rates is illustrated in Table 5.

Table 5: Division and calculation of specific substrate uptake rates in the Black-Box model.

1	$q_{s,ox,main} = min\left(\frac{m_{ATP}}{ATP_{ox}}, \frac{q_{O2,lim}}{6}, q_s\right)$
2	$q_{O2,main} = q_{s,ox,main} \cdot 6$
3	$q_{s,f,main} = min\left(\frac{m_{ATP} - ATP_{ox} \cdot q_{s,ox,main}}{ATP_f}, q_s - q_{s,ox,main}\right)$
4	$q_{s,main} = q_{s,ox,main} + q_{s,f,main}$
5	$q_{s,gr} = \left(q_s - q_{s,main}\right)$
6	$q_{s,ox,gr} = \min\left(\frac{q_{O2,\lim} - q_{O2,main}}{a}, q_{s,gr}\right)$
7	$q_{O2,gr} = q_{s,ox,gr} \cdot a$
8	$q_{s,f,gr} = q_{s,gr} - q_{s,ox,gr}$
9	$q_{O2,e} \le q_{O2,\lim} - q_{O2,main} - q_{O2,gr} = q_{O2,e,\lim}$
10	$q_{e,main} = \min\left(\frac{m_{ATP} - ATP_{ox} \cdot q_{s,ox,main} - ATP_f \cdot q_{s,f,main}}{ATP_{eth}}, \frac{q_{O2,e,\lim}}{3}, q_{e,\lim}\right)$
11	$q_{O2,e,main} = q_{e,main} \cdot 3$
12	$q_{O2,e,gr} = q_{O2,e,\lim} - q_{O2,e,main}$
13	$q_{e,gr} = \min\left(\frac{q_{O2,e,gr}}{k}, \left(q_{e,\lim} - q_{e,main}\right)\right)$
14	$q_e = q_{e,main} + q_{e,gr}$

The specific substrate uptake rate for oxidative maintenance $q_{s,ox,main}$ is limited either by the achievable specific oxygen uptake rate $q_{O2,lim}$, or the demanded maintenance energy, or the specific glucose uptake rate q_s (1). Hence, the specific oxygen uptake rate for maintenance $q_{O2,main}$ can be calculated (2). If not enough oxygen is available for oxidative energy production on glucose, the remaining energy demand is produced using the fermentative pathway. The specific glucose uptake rate for fermentative maintenance $q_{s,f,main}$ is limited by the demanded maintenance energy or the remaining part of the substrate uptake rate q_s (3). So, the specific glucose uptake rate for maintenance $q_{s,main}$ can be computed (4). The residual portion of the specific glucose uptake rate $q_{s,gr} = q_s - q_{s,main}$ can be used for growth (5). In the case of growth, also the oxidative pathway is preferred. If the specific glucose uptake rate is exceeding the oxidative capacity, the remaining glucose is degraded following the fermentative pathway. The specific substrate uptake rate for oxidative growth $q_{s,ox,gr}$ is limited by the remaining respirative capacity or the remaining portion of the specific glucose uptake rate (6). This allows the calculation of the growth related specific oxygen uptake rate $q_{O2,gr}$ (7). The remaining part of the growth related glucose uptake rate $q_{s,f,gr} = q_{s,gr} - q_{s,ox,gr}$ is used

fermentatively (8). Ethanol uptake is only possible, if glucose concentration is very low and oxidative capacity is left. Computation of the remaining oxidative capacity $q_{O2,e,lim}$ is now possible (9). The specific ethanol uptake rate for maintenance $q_{e,main}$ is limited either by either the remaining part of the demanded maintenance energy or remaining oxygen or ethanol.(10). So, the specific oxygen uptake for maintenance on ethanol $q_{O2,e,main}$ can be determined (11). The remaining part of the specific oxygen uptake rate $q_{O2,e,gr} = q_{O2,e,lim} - q_{O2,e,main}$ can be used for growth on ethanol (12). The ethanol uptake rate for growth is limited by the remaining oxygen or ethanol (13). This allows the calculation of the specific ethanol uptake rate $q_e = q_{e,main} - q_{e,gr}$ (14).

Specific growth rates can be computed from the specific uptake rates for oxidative and fermentative growth on glucose or growth on ethanol, respectively, and the yield coefficients:

$$\mu_{s,ox} = q_{s,ox,gr} \cdot Y_{X/Sox} \tag{34}$$

$$\mu_{s,f} = q_{s,f,gr} \cdot Y_{X/Sf} \tag{35}$$

$$\mu_{eth} = q_{e,gr} \cdot Y_{X/e}. \tag{36}$$

The entire specific growth rate μ is calculated as the sum of single growth rates:

$$\mu = \mu_{s,ox} + \mu_{s,f} + \mu_e. \tag{37}$$

Hence, the reaction rate r for each reaction shown in Table 3 is defined and the turnover rates for all relevant substances can be calculated. Turnover rates are computed from the specific rates multiplied with the biomass concentration X. Table 6 presents an overview of all processes of the modelling approach. Each row represents a single process. The columns show the stoichiometric coefficients for each substance and the belonging turnover rate for each process. The turnover of the considered substances (Figure 8) can be computed by summarising the stoichiometric turnover of the different reactions (columns in Table 6).

Table 6: Turnover rates and stoichiometric coefficients for the different processes of the Black-Box modelling approach.

Process	**Substance**						**Rates r**
	X	N	S	O	E	CO_2	
Oxidative growth on glucose	1	-NX	-1/b	-a/b		c/b	$\mu_{s,ox} * X$
Fermentative growth on glucose	1	-NX	-1/g		j/g	h/g	$\mu_{s,f} * X$
Growth on ethanol	1	-NX		-k/l	-1/l	m/l	$\mu_e * X$
Oxidative maintenance on glucose			-1	-6		6	$q_{s,ox,main} * X$
Fermentative maintenance on glucose			-1		2	2	$q_{s,f,main} * X$
Maintenance on ethanol				-3	-1	2	$q_{e,main} * X$

Parameters, finally applied for model based simulations, are summarised in chapter 3.2.

3.1.4 Metabolic modelling approach

Additionally to the Black-Box approach, in this work a metabolic modelling approach is introduced, that describes the states of metabolism dependent on the surrounding medium, following the approaches of Heijnen [65], van Gulik et al. [131] and Krzystek et al. [86].

Similar to the Black-Box approach, the metabolic modelling approach includes the different metabolic states for growth on glucose and ethanol. Limitation effects are considered for glucose, ethanol, nitrogen and oxygen. Also inhibition effects by ethanol are taken into account. The Crabtree effect is integrated by fixing the specific uptake rate for oxygen (oxidative capacity) to a maximum value. Additionally, the model is completed by the consideration of energy demand for maintenance, temperature dependency and lag-phases for growth on glucose and ethanol. In the Black-Box modelling approach only extra cellular substances, which are interacting with the surrounding growth medium, are considered. The metabolic model, however, considers a reaction network, which includes further intracellular reactions and product synthesis. Similar to the Black-Box modelling approach, the metabolic model is based on several assumptions. The latter are identical with the assumptions listed in chapter 3.1.3, except for following alterations or extensions:

- Specific oxygen uptake rate is limited to a maximum value (Crabtree effect). The latter is different for growth on ethanol and glucose.
- Reduction equivalents $NADH/H^+$ and ATP, the energy reservoir, are considered as intracellular substances. A pool of these substances with fixed concentrations is assumed.

A scheme of the model is shown in Figure 10.

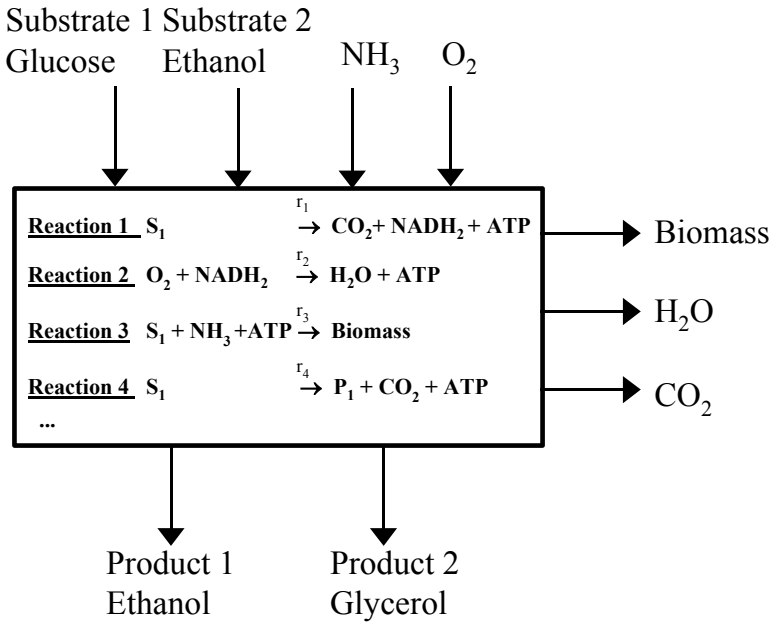

Figure 10: Scheme of the metabolic modelling approach. In addition to extracellular substances, which are interacting with the surrounding media, intracellular substances and reactions are considered.

3.1.4.1 Stoichiometry

Considered substances and rates for this modelling approach are shown in Table 7. For each substance a rate of metabolic turnover r_i is defined. Biomass composition $CH_{HX}O_{OX}N_{NX}$ is adopted from Sonnleitner and Käppeli [127] with HX = 1.79, OX = 0.57 and NX = 0.15.

When the metabolic pathways are known, stoichiometric relationships can be formulated with eight reactions as shown in Table 8. The oxidative degradation of glucose is following the glycolysis, an oxidative decarboxylation step and the Tricarboxylic Acid Cycle. Glucose is fully oxidised to carbon dioxide and 12 $NADH/H^+$ are formed (r_1). In the Respiratory Chain (r_2), δ ATP are formed out of $NADH/H^+$ by oxidative phosphorylation. This relation $ATP/NADH/H^+$ is named P/O-Relation [65, 86, 131]. Biomass synthesis (r_3) from glucose yields c = 0.095 - 0.22 mol CO_2/C-mol biomass [86, 131]. The other stoichiometric coefficients are computed from the balance of the single elements, similar to Table 4.

Table 7: Considered substances and rates.

Substance	Formula	Rate r_i
Glucose	$C_6H_{12}O_6$	r_s
Biomass	$CH_{HX}O_{OX}N_{NX}$	r_x
Nitrogen source	NH_3	r_n
Dissolved oxygen	O_2	r_o
Carbon dioxide	CO_2	r_c
Water	H_2O	r_w
Ethanol	C_2H_5OH	r_e
Glycerol	$C_3H_8O_3$	r_{gly}
$NADH/H^+$	$NADH_2$	r_{NADH2}
ATP	ATP	r_{ATP}

The coefficient K characterises the demanded amount of ATP for biomass synthesis. In (r_4) NAD^+ is regenerated by the hydrogenisation of pyruvate. Under fully anaerobic conditions an additional regeneration of NAD^+ is necessary (r_5), because $NADH/H^+$ is formed during the biomass synthesis. The reduction-equivalent is transferred to glycerol-phosphate and finally to glycerol [68, 86,146]. ATP is needed for the maintenance of the yeast cells (r_6). For non-growth associated maintenance a quantity of m_{ATP} = 0.013 mol ATP per C-mol biomass and hour is applied according to literature [63, 66]. Under aerobic conditions, ethanol can be degraded (r_7), if the glucose concentration in the medium is very low. In this case, ethanol is transformed to acetaldehyde, acetate and acetyl-CoA. The latter is used in the citric acid cycle. Biomass formation from ethanol (r_8) works analogous to (r_3). Here c_e = 0.266 (-0.285 mol) CO_2/C-mol biomass are formed [64, 86] and K_e ATP/C-mol biomass are demanded.

Table 8. Description of the relevant metabolic pathways for the yeast propagation process.

(1)	**Oxidative degradation of glucose r_1** $C_6H_{12}O_6 + 6\ H_2O \rightarrow 6\ CO_2 + 12\ NADH_2 + 2\ ATP$
(2)	**Respiratory chain r_2** $NADH_2 + ½\ O_2 \rightarrow \delta\ ATP + H_2O$
(3)	**Formation of biomass of glucose r_3** $g\ C_6H_{12}O_6 + 0{,}15\ NH_3 + K\ ATP \rightarrow CH_{1{,}79}O_{0{,}57}N_{0{,}15} + c\ CO_2 + n\ NADH_2 + w\ H_2O$
(4)	**Formation of ethanol of glucose r_4** $C_6H_{12}O_6 \rightarrow 2\ C_2H_5OH + 2\ CO_2 + 2\ ATP$
(5)	**Formation of glycerol of glucose r_5** $C_6H_{12}O_6 + 2\ NADH_2 + 2\ ATP \rightarrow 2\ C_3H_8O_3$
(6)	**Maintenance r_6** $ATP \rightarrow ADP$
(7)	**Oxidative degradation of ethanol r_7** $C_2H_5OH + 3\ H_2O \rightarrow 2\ CO_2 + 6\ NADH_2$
(8)	**Biomass formation of ethanol r_8** $e\ C_2H_5OH + 0{,}15\ NH_3 + K_e\ ATP + w_e\ H_2O \rightarrow CH_{1{,}79}O_{0{,}57}N_{0{,}15} + c_e\ CO_2 + n_e\ NADH_2$

The rate of the metabolic turnover of one substance can be formulated as the sum of the turnover in the single reactions. So, it is possible to define linear equations systems for the relation between the turnover of all substances and the rates of all reactions with r representing the vector for the turnover of the single substances (see Table 7), A the matrix of stoichiometry and v the vector for reaction rates (see Table 8).

$$r = \begin{bmatrix} r_s \\ r_x \\ r_n \\ r_o \\ r_c \\ r_w \\ r_e \\ r_{gly} \\ r_{NAHDH2} \\ r_{ATP} \end{bmatrix} \quad A = \begin{bmatrix} -1 & 0 & -g & -1 & -1 & 0 & 0 & 0 \\ 0 & 0 & 1 & 0 & 0 & 0 & 0 & 1 \\ 0 & 0 & -0{,}15 & 0 & 0 & 0 & 0 & -0{,}15 \\ 0 & -0{,}5 & 0 & 0 & 0 & 0 & 0 & 0 \\ 6 & 0 & c & 2 & 0 & 0 & 2 & c_e \\ -6 & 1 & w & 0 & 0 & 0 & -3 & -w_e \\ 0 & 0 & 0 & 2 & 0 & 0 & -1 & -e \\ 0 & 0 & 0 & 0 & 2 & 0 & 0 & 0 \\ 12 & -1 & n & 0 & -2 & 0 & 6 & n_e \\ 2 & \delta & -K & 2 & -2 & -1 & 0 & -K_e \end{bmatrix} \quad v = \begin{bmatrix} r_1 \\ r_2 \\ r_3 \\ r_4 \\ r_5 \\ r_6 \\ r_7 \\ r_8 \end{bmatrix} \tag{38}$$

It is assumed, that $NADH/H^+$ and ATP are neither accumulated in the cell nor excreted ($r_{NADH2} = 0$ and $r_{ATP} = 0$). Therefore, in this modelling approach a linear equation system with 10 equations and 16 rates to be determined (r_s, r_x, r_n, r_o, r_c, r_w, r_e, r_{gly}, r_1, r_2, r_3, r_4, r_5, r_6, r_7, r_8) can be formulated.

The coefficients δ, K and K_e are calculated using the known yield coefficients for purely aerobic growth on glucose, purely anaerobic growth on glucose and aerobic growth on ethanol (see Table 9).

Table 9: Calculation of the stoichiometric parameters δ, K und K_e for different growth conditions.

Aerobic growth on glucose	Anaerobic growth on glucose	Growth on ethanol
$Y_{X/Sox}$ = 3,527 mol BM/ mol glucose [127]	$Y_{X/Sf}$ = 0,72 mol BM/ mol glucose [127]	$Y_{X/E}$ = 1,12 mol BM/ mol ethanol [127]
Ethanol formation rate $r_e = 0$	Oxygen uptake rate $r_o = 0$	
Glycerol formation rate $r_{gly} = 0$	Aerobic glucose consumption $r_1 = 0$	No glucose is consumed $r_1 = 0$, $r_3 = 0$, $r_5 = 0$
Yield coefficient $Y_{X/Sox}$ is defined without maintenance $r_6 = 0$	Yield coefficient $Y_{X/Sf}$ is defined without maintenance $r_6 = 0$	Yield coefficient $Y_{X/E}$ is defined without maintenance $r_6 = 0$
No ethanol is consumed $r_7 = 0$, $r_8 = 0$	No ethanol is consumed $r_7 = 0$, $r_8 = 0$	
Result: $Y_{X/Sox} = \frac{12\delta + 2}{(12g - n)\delta + K + 2g}$	**Result:** $Y_{X/Sf} = \frac{2}{K + 2(g + n)}$	**Result:** $Y_{X/E} = \frac{6\delta}{K_e - n_e\delta + 6e\delta}$

Combining the given equations, numerical values of δ = 1.5 mol ATP/mol $NADH/H^+$, K = 2.2 and K_e = 5.1 mol ATP/C-mol biomass result. Coefficients in the same order of magnitude are presented in literature [65, 86].

In order to solve the equation system (see equation 38) six rates have to be determined first. Kinetic equations for the characterisation of the different metabolic states have to be taken into account. Table 10 summarises known rates for the four different metabolic states and known conditions for each state.

Rates are assumed as known for oxidative growth OG ($r_e = r_{gly} = r_7 = r_8 = 0$), oxidoreductive growth ORG ($r_{gly} = r_7 = r_8 = 0$) and fermentative growth FG ($r_O = r_1 = r_7 = r_8 = 0$) on sugar as well as for oxidative growth on ethanol OGE ($r_1 = r_3 = r_4 = r_5 = 0$) (comp. chapter 2.2.1). For all metabolic states, merely four different rates remain unknown including r_S, r_6, r_O (for oxidative growth on glucose) and r_O (for oxidative growth on ethanol). These rates, for OG (r_S, r_6), ORG (r_S, r_O, r_6), FG (r_S, r_6) and OGE (r_S, r_6), must be calculated for the different metabolic states using kinetic equations describing rates for substrate uptake and maintenance. Principally the same equations and kinetic parameters were applied as in the Black-Box-Model (see equations 29-33 in chapter 3.1.3.2), except for the maintenance rate $r_6 = m_{ATP}*X$ and an additional inhibition constant for glucose inhibition of ethanol degradation $K_{i,s}$ = 0.55 or 2.8 mmol/L [108, 127].

Table 10: Known rates and kinetic equations for the different metabolic states.

Oxidative growth on glucose OG	
$r_S = q_{S,\max} \cdot \min\left(\frac{S}{S+K_s}, \frac{N}{N+K_n}\right) \cdot \frac{K_{i,eth}}{K_{i,eth}+E} \cdot f_{temp} \cdot L_t \cdot X$	$r_{gly} = 0$
$r_6 = m_{ATP} \cdot X$	$r_7 = 0$
$r_e = 0$	$r_8 = 0$
Oxido-reductive growth on glucose ORG	
$r_S = q_{S,\max} \cdot \min\left(\frac{S}{S+K_s}, \frac{N}{N+K_n}\right) \cdot \frac{K_{i,eth}}{K_{i,eth}+E} \cdot f_{temp} \cdot L_t \cdot X$	$r_{gly} = 0$
$r_6 = m_{ATP} \cdot X$	$r_7 = 0$
$r_O = q_{O2,\max} \frac{O}{O+K_O} \cdot \frac{K_{i,eth,o}}{K_{i,eth,o}+E} \cdot X$	$r_8 = 0$
Fermentative growth on glucose FG	
$r_S = q_{S,\max} \cdot \min\left(\frac{S}{S+K_s}, \frac{N}{N+K_n}\right) \cdot \frac{K_{i,eth}}{K_{i,eth}+E} \cdot f_{temp} \cdot L_t \cdot X$	$r_1 = 0$
$r_6 = m_{ATP} \cdot X$	$r_7 = 0$
$r_O = q_{O2,\max} \frac{O}{O+K_O} \cdot \frac{K_{i,eth,o}}{K_{i,eth,o}+E} \cdot X$	$r_8 = 0$
Oxidative growth on ethanol OGE	
$r_O = q_{O2,e,\max}\left(\frac{O}{O+K_O}, \frac{E}{E+K_e}, \frac{N}{N+K_n}\right) \cdot \frac{K_{i,eth,o}}{K_{i,eth,o}+E} \cdot \frac{K_{i,S}}{K_{i,S}+S} \cdot L_{t,eth} \cdot X$	
$r_6 = m_{ATP} \cdot X$	$r_4 = 0$
$r_1 = 0$	$r_5 = 0$
$r_3 = 0$	

The kinetic is herewith determined for each metabolic state. Reaction rates r_i are calculated by means of $r_i = q_i * X_i$.

Switches between the different metabolic states are realised at critical specific substrate uptake rates for oxidative, oxidoreductive and fermentative metabolism, respectively. These rates are calculated by combining conditions of two states and solving the equations for r_s. With the combination of conditions of two states the transition point can be found. Table 11 exemplarily shows the conditions for calculation of critical rates for the switch between oxidative and oxidoreductive or oxidoreductive and reductive metabolism. In the first case, the switch between oxidative and oxidoreductive metabolism, r_s is eliminated from the known rates of oxidative metabolism (see Table 10) and replaced by r_O from the known rates from oxidoreductive metabolism. So, the equation system can be solved for r_s. The latter results from combined conditions and therefore is the critical rate $r_{s,c1}$. This critical rate is compared to r_s calculated in Table 10. The rate $r_{s,c1}$ corresponds with the amount of glucose, which can

be fully oxidised (see chapter 2.2.1.3 Crabtree effect). If r_s is exceeding $r_{s,c1}$, oxidoreductive (overflow) metabolism is occurring.

In the second case, in which the change from oxidoreductive to fermentative metabolism is studied, the proceeding is similar, r_s is eliminated and replaced by r_1 from reductive metabolism. Here, the switch is realised, if $NADH/H^+$ can not be regenerated without formation of glycerol (comp. chapter 2.2.1). The change to growth on ethanol is realised with a Monod term for glucose inhibition of ethanol degradation (comp. Table 10).

Table 11: Calculation of critical rates for determination of switch points between different metabolic states.

Critical rate oxidative-oxidoreductive $r_{s,c1}$	
$r_e = 0$	$r_{gly} = 0$
$r_6 = m_{ATP} \cdot X$	$r_7 = 0$
$r_O = q_{O2,\max} \frac{O}{O + K_O} \cdot \frac{K_{i,eth,o}}{K_{i,eth,o} + E} \cdot X$	$r_8 = 0$
Critical rate oxidoreductive-reductive $r_{s,c2}$	
$r_{gly} = 0$	$r_1 = 0$
$r_6 = m_{ATP} \cdot X$	$r_7 = 0$
$r_O = q_{O2,\max} \frac{O}{O + K_O} \cdot \frac{K_{i,eth,o}}{K_{i,eth,o} + E} \cdot X$	$r_8 = 0$

Applied parameters of the modelling approach are given in chapter 3.2.

3.2 Validation of simulations of yeast propagations

Aim of the model validation is to investigate, whether model based simulations were able to describe progressions of relevant quantities as biomass, glucose and ethanol during growth on glucose or ethanol. The modelling approaches are validated twofold, with experimental data and by the use of sensitivity analysis. In a first step validity of the developed modelling approaches was verified with literature data from baker's yeast batch propagations (see chapter 3.2.1). During model development, for the regarded propagations yield coefficients, maximum specific oxygen uptake rates $q_{O2,max}$ and $q_{O2e,max}$, temperature coefficient f_{temp} and lag-times t_{lag} and $t_{lag,eth}$ were identified as parameters with a high influence on concentrations of the consisted components in a sensitivity analysis (see chapter 3.2.6). Hence, in this work, only the latter five parameters were intended for parameter estimation procedures in order to fit model based simulation runs on experimental data. On the other hand, yield coefficients and parameters with low sensitivity were assumed to be constant for all experiments. Table 12 summarises applied parameters for the validation. The applied values are presented with their references in literature.

Table 12: Parameters of the Black-Box Model and the Metabolic Model applied for validation of both approaches. Parameters with units, applied values and references are presented. Parameters marked with * are either determined in a parameter estimation procedure or are given in literature data used for validation of the model based simulation.

Black-Box-Model				Metabolic Model			
Parameter	**Value**	**Unit**	**Source**	**Parameter**	**Value**	**Unit**	**Source**
Stoichiometric parameters							
$Y_{X/Sox}$	3,527	mol/mol	[108,127]	$Y_{X/Sox}$	3,527	mol/mol	[108,127]
$Y_{X/Sf}$	0,72	mol/mol	[65]	$Y_{X/Sf}$	0,72	mol/mol	[65]
$Y_{X/E}$	1,12	mol/mol	[65]	$Y_{X/E}$	1,12	mol/mol	[65]
HX	1,79	mol/mol	[127]	HX	1,79	mol/mol	[127]
OX	0,57	mol/mol	[127]	OX	0,57	mol/mol	[127]
NX	0,15	mol/mol	[127]	NX	0,15	mol/mol	[127]
δ	1,2	mol/mol	[65]				
				c	0,095	mol/mol	[65]
				ce	0,266	mol/mol	[65]
Kinetic parameters							
$q_{s,max}$	0,486	mol/mol/h	[127]	$q_{s,max}$	0,486	mol/mol/h	[127]
$q_{O2,max}$		mol/mol/h	*	$q_{O2,max}$		mol/mol/h	*
				$q_{O2,e,max}$		mol/mol/h	*
$q_{e,max}$	0,128	mol/mol/h	[128]				
m_{ATP}	0,013	mol/mol/h	[65]	m_{ATP}	0,013	mol/mol/h	[65]
K_s	2,8	mmol/L	[127]	K_s	2,8	mmol/L	[127]
K_o	0,00121	mmol/L	[61]	K_o	0,00121	mmol/L	[61]
K_e	2,2	mmol/L	[108, 127]	K_e	2,2	mmol/L	[108, 127]
K_n	2	mmol/L	[26]	K_n	2	mmol/L	[26]
$K_{i,eth}$	500	mmol/L	[71]	$K_{i,eth}$	500	mmol/L	[71]
$K_{i,eth,o}$	217,39	mmol/L	[108]	$K_{i,eth,o}$	217,39	mmol/L	[108]
	-		-	$K_{i,s}$	0,55	mmol/L	[127]
t_{lag}		h	*	t_{lag}		h	*
$t_{lag,eth}$		h	*	$t_{lag,eth}$		h	*
f_{temp}		-	*	f_{temp}		-	*

Validity for brewers' yeast propagations was examined in different experiments, which are illustrated in chapters 3.2.2-3.2.5 for experiments A and B (bottom fermenting yeast in propagation system 1), C (top fermenting yeast in propagation system 1) and D (bottom fermenting yeast in propagation system 2).

3.2.1 Validation using literature data

Both models were tested using data from literature. Batch propagation data from Sonnleitner and Käppeli [127], Barford (1981) [14] and Barford (1990) [13] were quoted.

Sonnleitner and Käppeli: Oxidative or oxidoreductive growth on glucose with ethanol formation and subsequent growth on ethanol. Measurement values were available for concentrations of glucose, ethanol and biomass.

Barford (1990) and Barford (1981): Oxidative or oxidoreductive growth on glucose with ethanol formation. In addition to concentrations of glucose, ethanol and biomass, the specific oxygen uptake rate q_{O2} was measured as well.

Results using data from Sonnleitner et al. are given in Figure 11 a) for the Black Box approach and d) for the metabolic model. Parameters $f_{temp} = 0.8396$, $q_{O2,max} = 0.1754$ mmol/(mmol*h), $t_{lag} = 0$ h and $t_{lag,eth} = 0$ h as well as $f_{temp} = 0.8209$, $q_{O2,max} = 0.1575$ mmol/(mmol*h), $t_{lag} = 0$ h and $t_{lag,eth} = 4.68$ h, were determined by parameter estimation (see chapter 5.5.1) for the Black Box model or the metabolic model (see Table 13).

Table 13: Estimated parameters during model validation of the Black Box model and the metabolic model with literature data. The maximum specific oxygen uptake rates $q_{O2,max}$ and $q_{O2,e,max}$, the temperature coefficient for temperature dependency of the substrate uptake rate f_{temp}, and the lag times t_{lag} and $t_{lag,eth}$ are listed.

	Black Box Model			Metabolic Model		
Parameter	Sonnleitner / Käppeli	Barford 1990	Barford 1981	Sonnleitner / Käppeli	Barford 1990	Barford 1981
$q_{O2,max}$ [mmol/mmol/h]	0,1754	0,15∗	0,15∗	0,1575	0,15∗	0,15∗
$q_{O2,e,max}$ [mmol/mmol/h]	-	-	-	0,2456	-	0,25∗
f_{temp}	0,8396	0,8352	0,96	0,7931	0,8209	1.05
t_{lag} [h]	0	0	0	0	0	0.95
$t_{lag,eth}$ [h]	0	-	12	4.68	-	12.14

∗Measured values for the particular data set. The other parameters were determined in a parameter estimation procedure.

For growth on glucose, simulation results matched the measurement values for biomass, glucose and ethanol very well. However, during growth on ethanol simulation runs of the Black Box model showed deviations concerning biomass concentration. As can be seen in Figure 11 d) simulations of the metabolic model fitted the measurement values for both, growth on glucose and growth on ethanol. In addition to the parameters f_{temp}, $q_{O2,max}$, t_{lag} and $t_{lag,eth}$, the specific oxygen uptake rate for growth on ethanol $q_{O2,e,max}$ could be determined for the metabolic model. The parameters f_{temp} and t_{lag} resulted in the same order of magnitude for both approaches and the diauxic lag phase $t_{lag,eth}$ was determined with a higher value for the metabolic modelling approach. For growth on ethanol with the additional parameter $q_{O2,e,max} = 0.2456$ mmol/(mmol*h) a higher specific oxygen uptake rate could be set than for growth on glucose ($q_{O2,max} = 0.1575$ mmol/(mmol*h)). According to Sonnleitner and Käppeli [127], a constant specific oxygen uptake rate $q_{O2,max} = 0.1754$ mmol/(mmol*h) is assumed in the Black Box model. Therefore, in the second growth phase, higher biomass concentrations could be reached by the metabolic approach and measurement values could be fitted better. Mean deviations between measurement values and simulation and their standard deviations

were lower for the metabolic model, especially concerning biomass concentration (see Table 14).

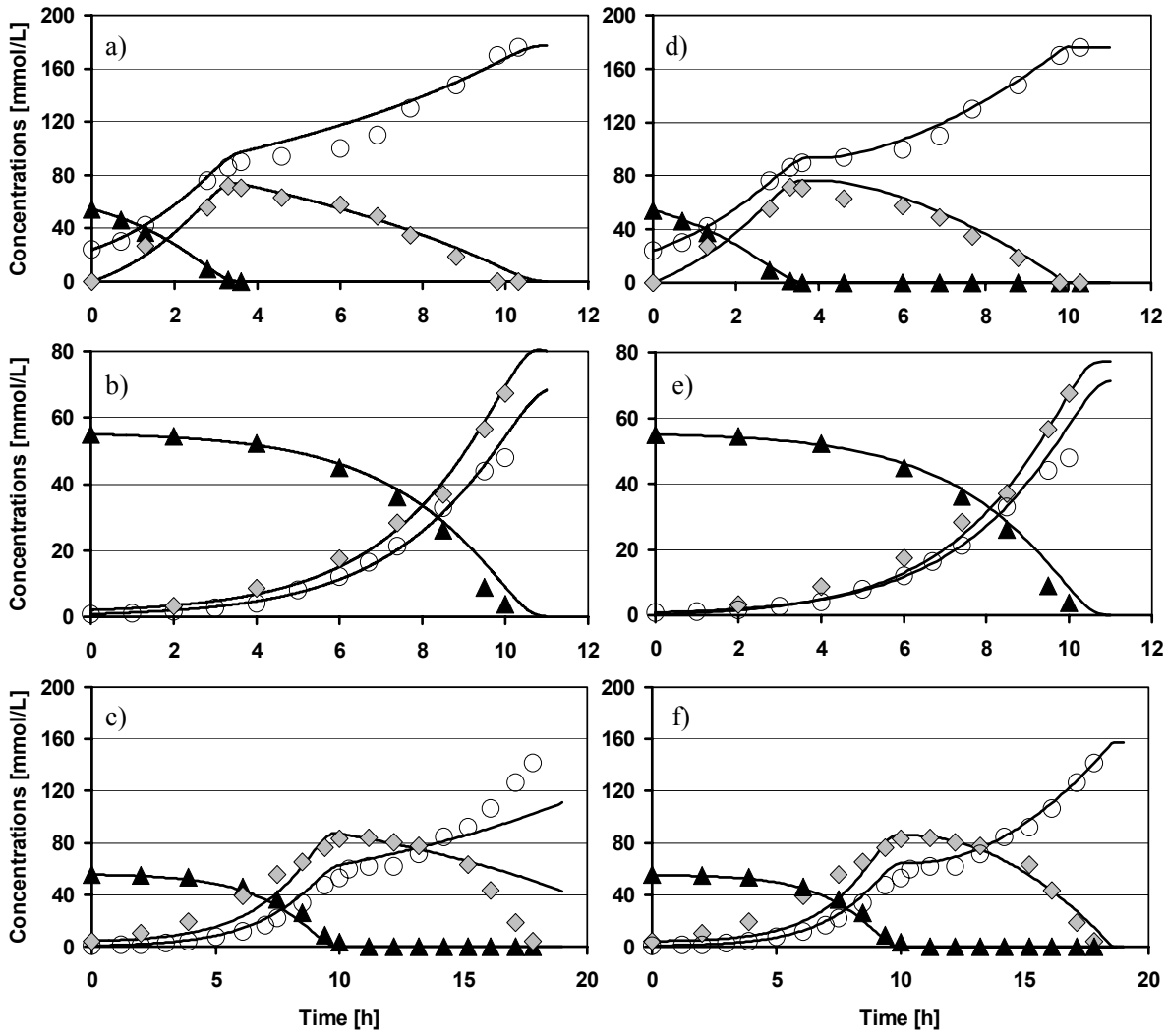

Figure 11: Measurement data compared with model based simulation runs for the Black Box model (left) and the metabolic model (right). Literature data from Sonnleitner et al. (a,d), Barford 1990 (b,e) and Barford 1981 (c,f) were applied for validation of the modelling approaches. Propagation data for biomass (o), glucose (▲) and ethanol (◊) are compared with the model based simulation runs (lines).

Only growth on glucose is comprised in the data from Barford 1990. Fitted were the parameters $f_{temp} = 0.8396$ and 0.8209 for the Black Box model and the metabolic model, respectively, as well as $t_{lag} = 0$ h for both models (see Table 13). Simulation results compared to measurement values are demonstrated in Figure 11 b) and e). Both models represented the data very well with mean deviations about 2 mmol/L for concentrations of biomass, glucose and ethanol (see Table 14). It should be noticed that nearly the same parameters and accuracy of the models resulted for growth on glucose concerning mean deviation and their standard deviations.

Figure 11 c) and f) show measurement values from Barford 1981 and the according simulation runs of the Black Box model or the metabolic model. During these experiments the specific oxygen uptake rates for growth on both, glucose and ethanol were measured (q_{O2} = 0,15 mmol/(mmol*h), $q_{O2,e}$ = 0,25 mmol/(mmol*h)). Parameters were estimated with f_{temp} = 0.96, t_{lag} = 0 h and $t_{lag,eth}$ = 12 h for the Black Box model and f_{temp} = 1.05, t_{lag} = 0.95 h and $t_{lag,eth}$ = 12.14 h for the metabolic model. During growth on glucose, both models described very well the measurement values for biomass and glucose, however, ethanol was not represented with a high accuracy. This could be substantiated by the application of a constant value for q_{O2}. Barford [14] showed in his data that at the beginning of the propagation the oxygen uptake rate is still increasing. Yet, in this work the measured maximum value was applied. Therefore, in the first growth phase too much oxygen was consumed and less ethanol was produced. For growth on ethanol, simulations fitted only for the metabolic model. Similar to data from Sonnleitner and Käppeli [127], the measured specific oxygen uptake rate for growth on ethanol was higher than for growth on glucose. This could not be taken into account for the Black Box model, as the kinetic for oxygen uptake was not dependent on the substrate (see Table 5). Accuracy concerning biomass and ethanol concentration, therefore, was much better for the metabolic model with 50 % of mean deviations and standard deviations compared to the Black Box model (see Table 14).

Table 14: Mean values and standard deviations of the deviation between model based simulations and reference values for literature data from Sonnleitner and Käppeli [124] and Barford, 1981 and 1990 [12, 14].

	Mean Value of deviations [mmol/L]			**Standard deviation [mmol/L]**		
	Substrate	Biomass	Ethanol	Substrate	Biomass	Ethanol
			Black Box Model			
Sonnleitner	1.09	6.29	4.38	1.105	5.62	3.19
Barford 1990	2.42	1.23	2.03	2.60	1.67	1.05
Barford 1981	1.75	7.49	10.99	2.63	9.78	13.66
			Metabolic Model			
Sonnleitner	0.73	2.5	4.56	1.16	2.62	3.26
Barford 1990	1.91	1.54	2.29	2.35	2.94	1.85
Barford 1981	1.34	3.23	6.67	1.99	3.33	6.20

The validity testing for literature data showed that the Black Box model was qualified for model based simulations of the yeast growth on glucose but not for the subsequent growth on ethanol. The metabolic model described both phases with a high accuracy.

3.2.2 Simulations of experiments A

Experiments A comprised 38 isothermal brewery propagations with temperatures between 5 and 35°C. Experiments were carried out with propagation system A and the bottom fermenting yeast *S. cerevisiae uvarum var. carlsbergensis* W34/70 inoculated in a wheat beer wort (see chapter 5.1). Oxygen concentration was kept constant at 0.5 ppm for all

experiments. In order to illustrate the validity of the modelling approaches for brewers' yeast propagations, five experiments were chosen. In Figure 12 a) and b), measurement values of brewery propagations with temperatures of 5, 10, 15, 20 and 30°C are presented. The progressions are compared with the model based simulations of the Black Box model (a) and the metabolic model (b). For simulation, parameters listed in Table 12 were applied. Variable parameters f_{temp}, $q_{O2,max}$ and t_{lag} were determined in a parameter estimation procedure (see Table 22). Parameters relevant for ethanol degradation were not considered as only growth on sugars occurred.

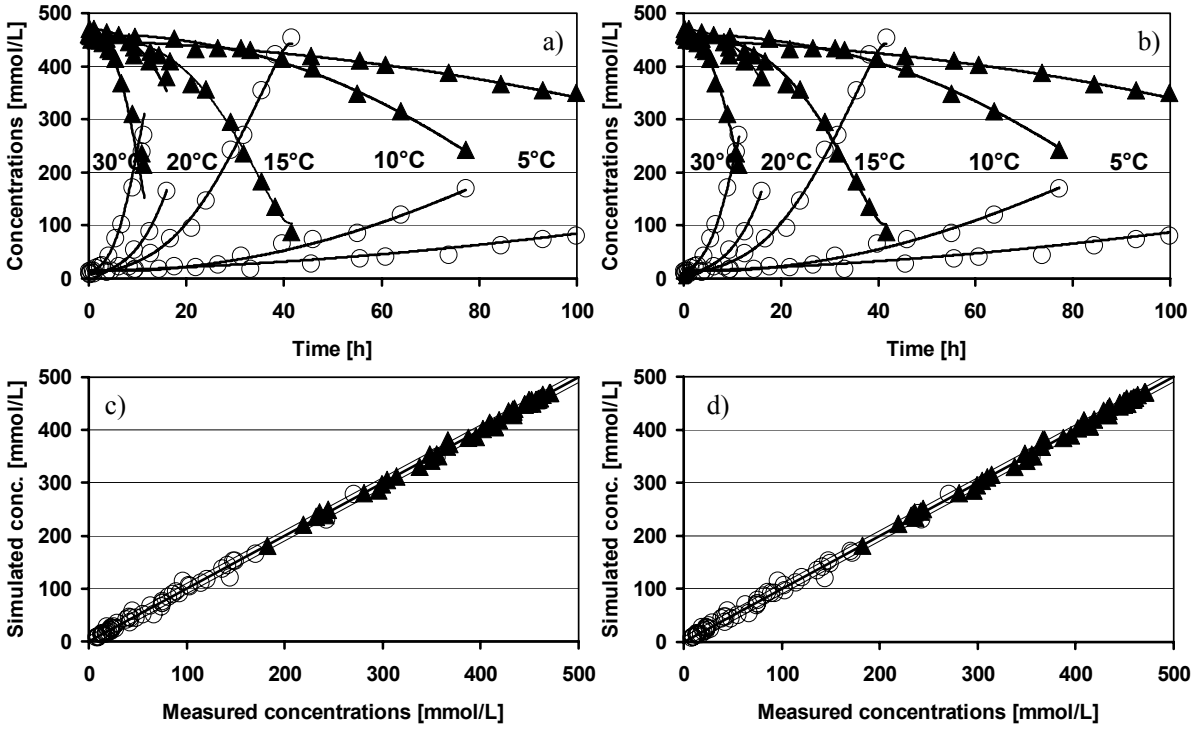

Figure 12: Simulation runs (lines) and experimental data (dotted) of propagations at 10, 15, 20 and 25°C. Plotted are the progressions of substrate (▲) and biomass (o) concentrations. Experiments were made with a 150 L propagator with continuous aeration with a dissolved oxygen concentration of 0.5 ppm.

The accuracy of the simulation concerning biomass and glucose concentrations was validated with the deviation between simulation and reference values. Table 23 (appendix) lists mean values of deviations between measurement and simulation and their standard deviation. In the range of 10 to 20°C mean deviations of 3.79 to 6.58 mmol/L glucose and 2.41 to 7.7 mmol/L biomass could be calculated for the Black Box model. Standard deviations of these results were computed in order to characterise the distribution of these results and detect outliers. Here, standard deviations in the range of the mean values occurred, which showed that no relevant outliers in measurement values were present. Experiments near the limits of yeast growth at 5°C and 30°C, however, resulted in mean deviations between measurement and simulation of 6.04 to 14.82 mmol/L for glucose and 9.92 to 11.27 mmol/L

for biomass. At the same time standard deviations were much higher than mean values, which indicated outliers. A total mean deviation between measured and simulated data of all 38 experiments was calculated with 6.5 mmol/L for glucose (0.12% GG) and 8.50 mmol/L for biomass ($5.31*10^6$ cells/mL). High total standard deviations for glucose and biomass concentrations of 10.41 mmol/L (0.15% GG) and 14.26 mmo/L ($8.91*10^6$ cells/mL) again proved outliers.

Similar tendencies could be found for the metabolic model (see Table 23), but total mean deviations of 5.84 mmol/L and 6.69 mmol/L for sugar and biomass and standard deviations of 6.18 mmol/L (0.09% GG) and 9.72 mmol/L ($6.62*10^6$ cells/mL) kept on a lower level. Also for the metabolic model, experiments with 5°C or 30 °C showed maximum deviations.

Outliers were identified as caused by engineering problems in propagation system A. Many cells could be recovered in the foam, especially at very high and very low temperatures and therefore took no longer part in substrate degradation. So, simulations were calculated with too high biomass concentrations and too low substrate concentrations, respectively. At the end of several yeast propagations, biomass concentration in different levels of the applied propagation system and in the foam was determined, in order to calculate a mean biomass concentration (results not shown). If these errors were corrected, mean deviations and standard deviations marked with * in Table 23 were resulting. Especially, standard deviations, as measures for outliers, could be reduced drastically, e.g. from 15.32 mmol/L ($10.4*10^6$ cells/mL) to 1.08 mmol/L ($0.74 *10^6$ cells/mL) for biomass in the Black Box model. For both modelling approaches parity plots for measured and simulated concentrations of biomass are given in Figure 12 c) and d), which show the accuracy of the modelling approach. A parity line and two lines representing concentrations of ± 10 mmol/L or ± $6.25*10^6$ cells/mL and 0.15% w/w gravity are given. Most of the simulated values fitted very well in this tolerance after correction of engineering problems.

Summarising, it could be stated that model based simulations of both modelling approaches could represent the measurement data of brewers' yeast propagations (experiments A) with a high accuracy and validity for the regarded brewery application could be proved. However, mean deviations of simulations based on the metabolic model were smaller than of the Black Box model. Sensitivity analysis for these experiments are given in chapter 3.2.6.

3.2.3 Simulations of experiments B

Experiments B were carried out with propagation plant A and a bottom fermenting yeast strain *Saccharomyces cerevisiae uvarum var. carlsbergensis* (Yeast strain not further characterised due to secrecy). Ten isothermal yeast propagations with dissolved oxygen concentrations of 0.5 ppm were realised. An adjunct of malt germs were added to the barley

malt wort in five experiments. Figure 13 a) and b) shows measured concentrations of isothermal propagations at four different temperatures and the belonging model based simulation runs (lines). For these experiments the metabolic modelling approach was used exclusively. It can be seen that for both cases, a) without adjuncts and b) with adjuncts, the simulations fitted the offline measured concentrations of biomass and substrate very well.

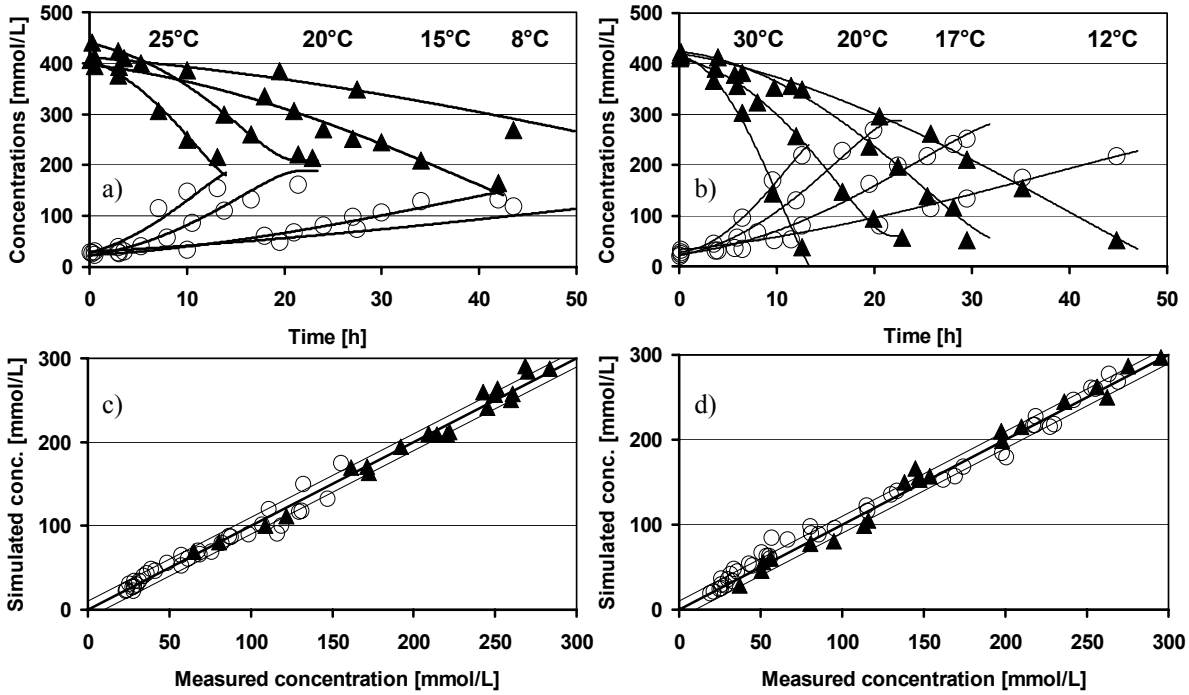

Figure 13: Simulation runs (lines) and experimental data (dotted) of propagations at 8, 15, 20 and 25°C without adjuncts as well as 12, 17, 20 and 30°C with adjuncts. Plotted are the progressions of substrate (▲) and biomass (o) concentrations (a and b) and belonging parity plots (c and d). Experiments were made in a 150 L propagator with continuous aeration with a dissolved oxygen concentration of 0.5 ppm. A bottom fermenting yeast was inoculated.

In order to fit the simulation runs on reference data the parameters f_{temp}, $q_{O2,max}$ and t_{lag} were determined in a parameter estimation procedure. Other parameters listed in Table 12 were kept constant. Results of the parameter estimation procedure are shown in Table 24. Results for the parameter $q_{O2,max}$ were very low compared to results of experiments A and especially for propagations with adjuncts this parameter reached the given boundary of the estimation procedure (zero) for low and high temperatures. Therefore, the anaerobic yield $Y_{X/Sf}$ was adopted from 0.1g biomass/g substrate to 0.07 g biomass/g substrate (0.72 mol/mol to 0.5 mol/mol) according to boundaries given in Table 12. For both yield coefficients an increasing value for f_{temp} resulted with increasing temperatures. Also $q_{O2,max}$ showed a characteristic maximum at temperatures between 20°C and 25°C. However, it can be generally noticed that levels of $q_{O2,max}$ were lower than in experiments A (see chapter 3.3.1).

The accuracy of the model based simulations is illustrated by Figure 13 c) and d). Given is a parity plot of calculated and measured concentrations of biomass and substrate. Most values range in between lines, which represent a tolerance of ± 10 mmol/L or ± 6.25*10^6 cells/mL and 0.15% w/w gravity. For both yield coefficients most values are found inside the allowance. Additionally, Table 25 gives deviations and their standard deviation between measured and simulated concentrations. Deviations marked with * are results from simulations with an applied fermentative yield of 0.5 mol/mol (see appendix).

The accuracy of simulation runs of propagations with or without adjuncts showed no significant differences in the total amount of all belonging propagation runs. Deviations were detected between 3.66 mmol/L (0.08% w/w) and 15.07 mmol/L (0.27% w/w) for substrate and between 2.23 mmol/L (1.7*10^6 cells/mL) and 20.3 mmol/L (13.78*10^6 cells/mL) for biomass. Standard deviations were between 3.07 mmol/L (0.06% w/w) and 13.03 mmol/L (0.24% w/w) for substrate or between 2.33 mmol/L (1.58*10^6 cells/mL) and 20.24 mmol/L (13.74*10^6 cells/mL) for biomass. However, total standard deviations of simulations based on a fermentative yield of 0.5 mol/mol were lower than for simulations applying 0.72 mol/mol especially for propagations with adjuncts. Also, a yield of 0.5 mol/mol resulted in a more homogenous standard deviation and therefore simulations were assumed to give a more representative description of the measurement values. As in chapter 3.2.2 deviations were increasing for experiments at more extreme temperatures.

Summarising, it could be stated that the modelling approaches are valid for different species of bottom fermenting yeast *Sacharomyces cerevisiae uvarum var. carlsbergensis*. However, differences in biomass yields must be considered and will be of interest in further research (see chapter 4).

3.2.4 Simulations of experiments C

Experiments C consisted of five isothermal propagation runs with temperatures between 8°C and 32°C. These trials were carried out with propagation plant A at a dissolved oxygen concentration of 0.5 ppm. A top fermenting brewers‘ yeast *S. cerevisiae* (W68) and a wheat beer wort were applied. In contrast to other experiments, the propagations were not started at the same initial concentrations and additionally were stopped very early in progression. Both models, the Black Box and the metabolic approach, were used for simulation. Figure 14 a) and b) shows simulations of the experiments and belonging reference values for the Black Box model or the metabolic model.

Data of the whole temperature range could be described with a high accuracy, which can be proved by parity plots for simulated and measured concentration during the regarded propagation runs (Figure 14 c/d). Again, most values lie inside the given allowance of ± 10 mmol/L or ± 6.25*10^6 cells/mL or 0.15% w/w gravity.

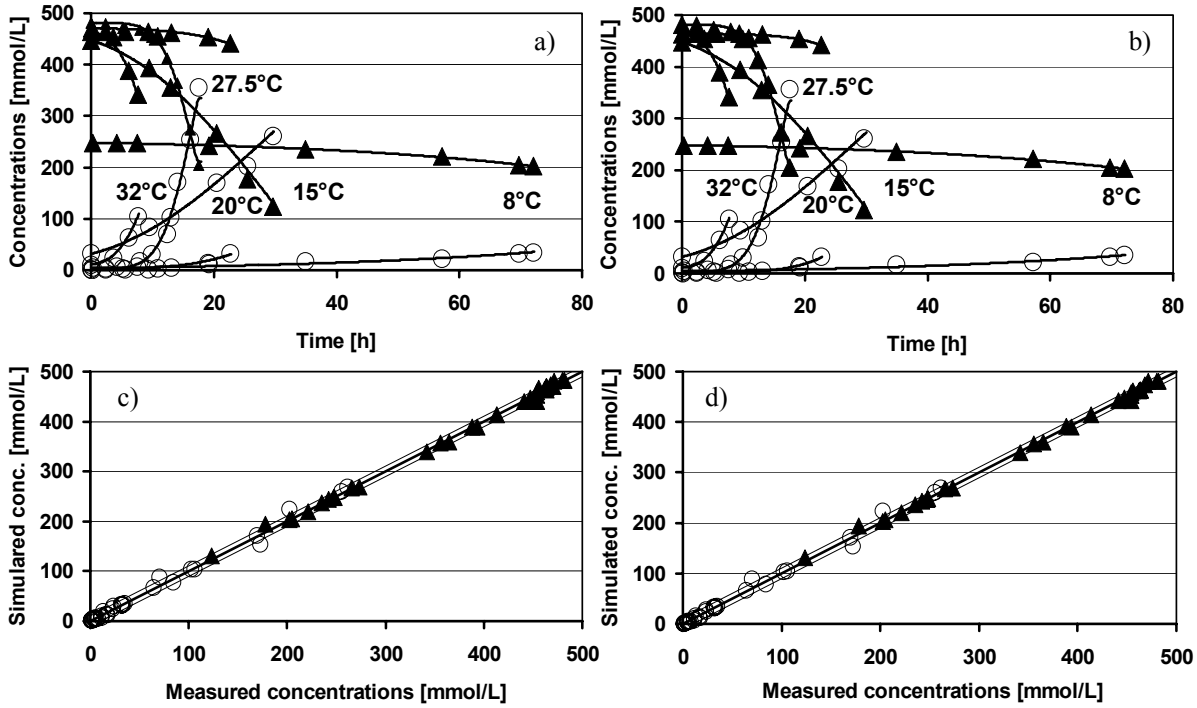

Figure 14: Simulation runs (lines) based on the Black box model (left) and the metabolic model (right) and experimental data (dotted) of top fermenting yeast propagations at 8, 15, 20 and 27.5 and 32°C. Plotted are the progressions of substrate (▲) and biomass (o) concentrations (a and b) and belonging parity plots (c and d). Experiments were made with a 150 L propagator with continuous aeration with a dissolved oxygen concentration of 0.5 ppm.

Estimated parameters f_{temp}, $q_{O2,max}$ and t_{lag} are listed in Table 26 (appendix). Mean deviations between measured and simulated concentrations and standard deviations further illustrate the accuracy of simulation runs. For both models very low mean deviations could be achieved with a total mean deviation of 3.4 mmol/L (0.06% w/w) for substrate and 3.67 mmol/L ($2.5*10^6$ cells/mL) for biomass concerning the Black Box model and 2.87 mmol/L (0.05% w/w) or 3.3 mmol/L ($2.24*10^6$ cells/mL) for the metabolic approach, respectively. Standard deviations occurred in the same range as mean values. Hence, both models show a high accuracy, however, the metabolic approach appeared to be more accurate than the Black Box model. The highest intensity of growth could be achieved for propagations at 27.5°C. Also, here the highest inaccuracies were occurring. A detailed listing of accuracies is given in the appendix (Table 27).

The validity of the regarded modelling approaches for top fermenting yeasts could be proved with experiments C. Estimated model parameters out of the range of 27.5°C come along with above mentioned parameters out of experiments with bakers' yeast (see chapter 3.2.1).

3.2.5 Simulations of experiments D

Experiments D were carried out with propagation plant B. A barley wort was inoculated with a bottom fermenting yeast *Saccharomyces cerevisiae uvarum var. carlsbergensis* (W34/70). A dissolved oxygen concentration of effectively 0.1 ppm was achieved by pulsed aeration. Figure 15 a) and b) show progressions of model based simulations and belonging reference values for substrate, biomass and ethanol concentrations of four experiments with temperatures between 9°C and 30°C. It can be seen that for both modelling approaches, a) Black Box model and b) metabolic model, reference values are represented very well by simulation runs (lines). In this case also ethanol concentrations were determined in order to prove model validity for another important product of yeast metabolism. Estimated parameters are summarised in Table 28 (appendix). Also here, the accuracy is evaluated with a parity plot of simulated and measured concentrations of biomass and substrate (see Figure 15 c and d). Most of the values lie inside the allowance of ± 10 mmol/L or ± 6.25*10^6 cells/mL and 0.18% w/w gravity, respectively.

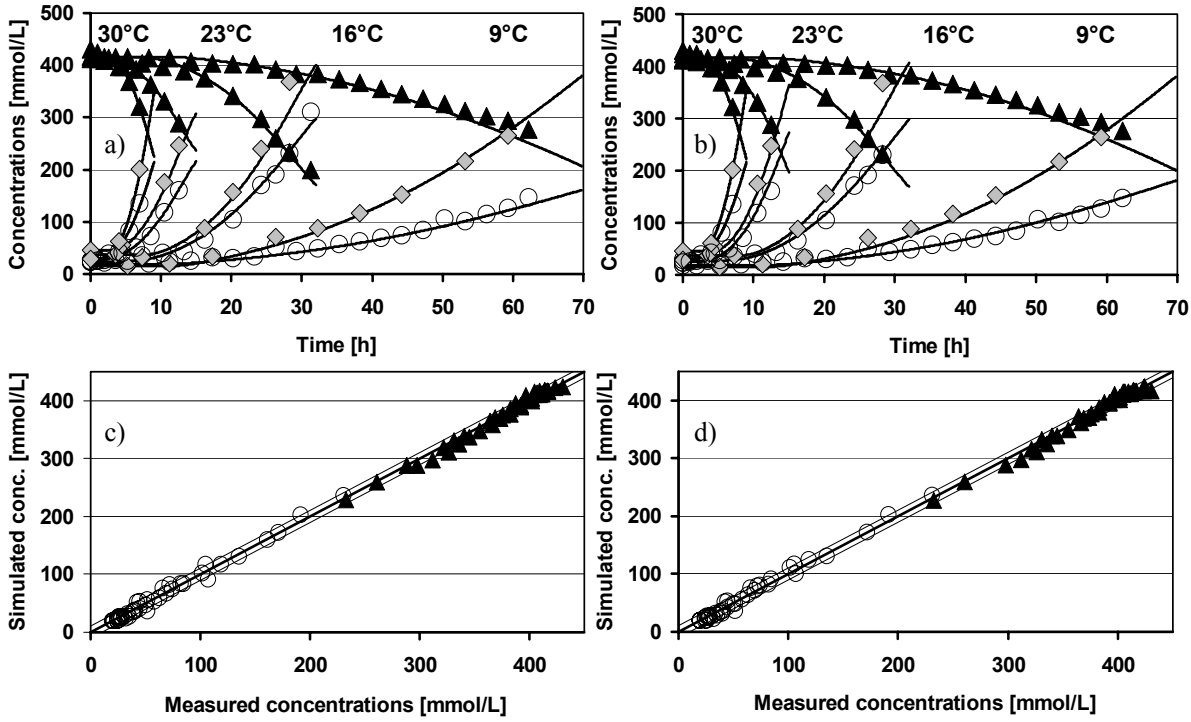

Figure 15: Simulation runs (lines) based on the Black box model (left) and the metabolic model (right) and experimental data (dotted) of propagations at 9, 16, 23 and 30°C. Plotted are the progressions of substrate (▲) and biomass (o) concentrations (a and b) and belonging parity plots (c and d). Experiments were made with a 100 L propagator with pulsed aeration with an effective dissolved oxygen concentration of 0.1 ppm.

Concerning the accuracy of both models, no significant differences could be identified. Table 29 gives an impression of occurring deviations between measured and simulated values and their standard deviations. A total mean deviation between measured and simulated

concentration of 5.68 mmol/L (0.1% w/w) for substrate, 4.78 mmol/L ($3.24*10^6$ cells/mL) for biomass and 7.9 mmol/L (0.04% w/w) for ethanol could be achieved for the Black Box model. Results in the same range occurred for the metabolic model. Due to pulsed aeration foaming could be reduced and therefore deviations between measurement values and simulations or their standard deviations were not increasing at higher temperatures.

With these experiments it was proven that the modelling approaches could also be applied for different propagation plants and different propagation strategies concerning aeration (pulsed versus continuous aeration).

A comparison of the estimated parameters for all experiments and a further interpretation is provided in chapter 3.3.

3.2.6 Sensitivity Analysis

In order to determine the influence of kinetic and stoichiometric parameters, a sensitivity analysis was carried out. Here, simulations were run for every parameter in the course of which in each case one parameter was varied by dp. Absolut sensitivity functions according to equation 39 were applied for single parameters.

$$\delta_{y,p}^{a,r} = p \cdot \frac{dy}{dp} \tag{39}$$

These functions indicate the resulting absolute change of the quantity y (e.g. substrate, biomass or ethanol) caused by a 100% change of the individual parameter (see chapter 5.5.1). The higher the value of the sensitivity function the better a parameter can be fitted in a parameter estimation procedure [117]. These type of sensitivity functions were used in order to show typical progressions of the sensitivity of biomass and substrate on different parameters along the propagation process. In order to show whether the modelling approach is applicable for bakers' yeast and brewers' yeast propagations examples are given for literature data (Barford 1981) with ethanol formation and degradation (Figure 16) and one brewery propagation without ethanol degradation (Figure 17). For all parameters a standard deviation of 10% of the applied value was assumed. The graphs illustrate the change of biomass and substrate concentrations for each hour of the propagation process. Sensitivity functions are only given for the metabolic model, but for the Black Box model similar results were achieved.

The course of the bakers' yeast propagation is divided into a first stage of sugar consumption (left half of each subdivision in Figure 16) and a second stage of ethanol degradation (right half of each subdivision). It is indicated that parameters influencing the results of simulations for biomass and substrate concentrations mainly were the oxidative and fermentative yield coefficients $Y_{X/Sox}$ and $Y_{X/Sf}$, the temperature coefficient of the specific substrate uptake rate f_{temp} and the specific oxygen uptake rate for growth on sugar $q_{O2,max}$. In

the second stage of yeast growth on ethanol the specific oxygen uptake rate for growth on ethanol $q_{O2,e,max}$ and the lag time coefficient $t_{lag,eth}$ became relevant. Initial concentrations of biomass x_{ini} and substrate s_{ini} possessed also a certain influence. Less influence was detected for half saturation constants and inhibition constants, stoichiometric parameters and for the maintenance energy m_{ATP}. Analogue results could be found for the sensitivity functions for ethanol (not shown).

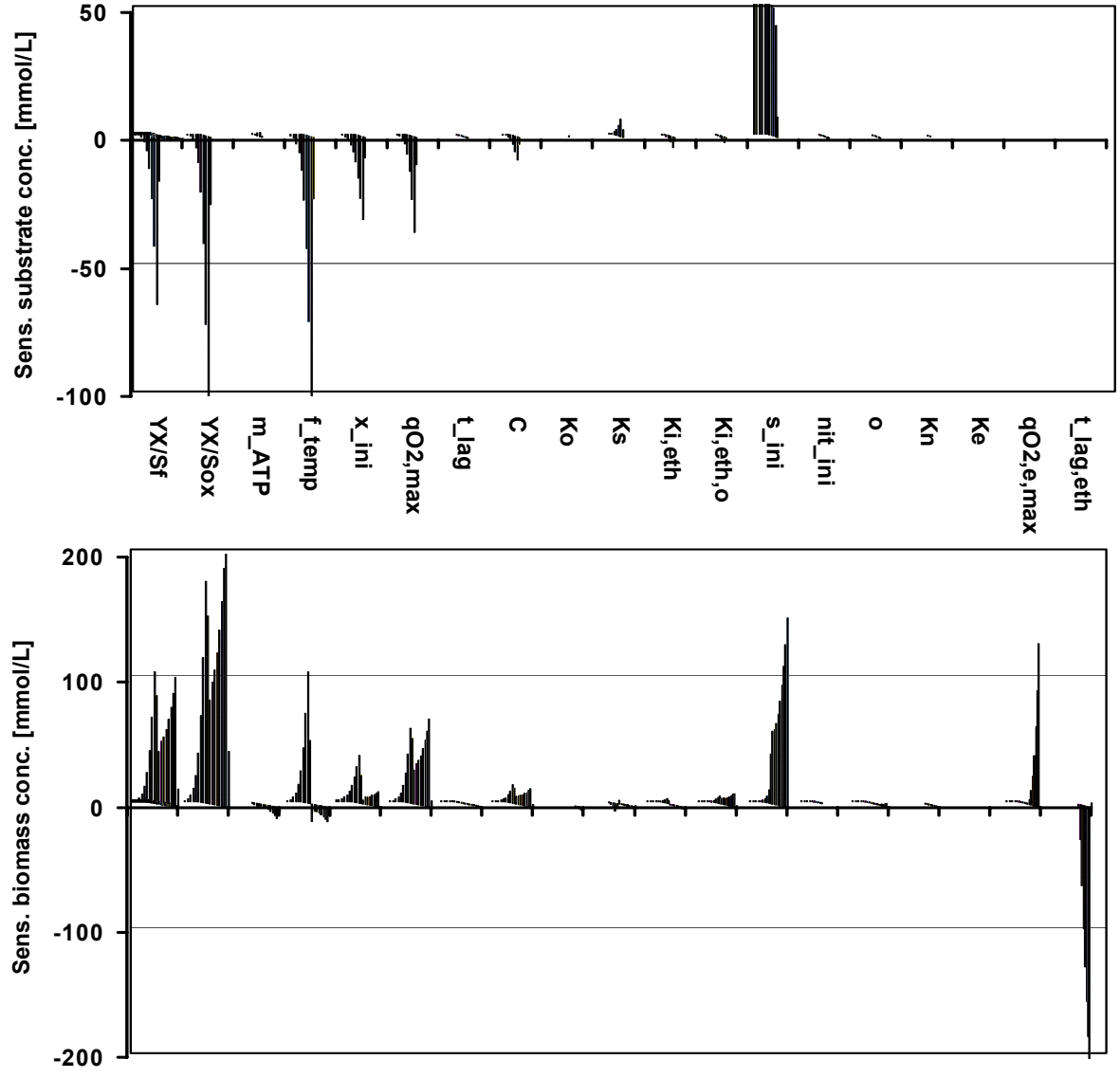

Figure 16: Absolute sensitivity functions for an isothermal yeast propagation (Barford, 1981 [14]) for substrate concentration (above) and biomass concentration (below). Sensitivities are shown for all relevant parameters along the propagation run after each hour for a 100% change of each parameter. Parameters YX/Sf, YX/Sox, m_ATP, (qO2,max), t_lag, f_temp, Ko, Ks, (Ki,eth), (Ki,eth,o), Kn, Ke and (qO2,e,max) correspond to parameters $Y_{X/Sf}$, $Y_{X/Sox}$, m_{ATP}, $q_{O2,max}$, t_{lag}, f_{temp}, K_o, K_s, $K_{i,eth}$, $K_{i,eth,o}$, K_n, K_e and $q_{O2,e,max}$ in Table 12. x_ini (x_{ini}), s_ini (s_{ini}) and nit_ini (nit_{ini}) represent initial concentrations of biomass, substrate and nitrogen.

In order to characterise the influence of the single parameters also for the field of brewing yeast propagation, a sensitivity analysis for this application was realised as well (see Figure 17). As for brewing yeast propagation only growth on sugar is practicable, only this stage of growth was considered for all further considerations.

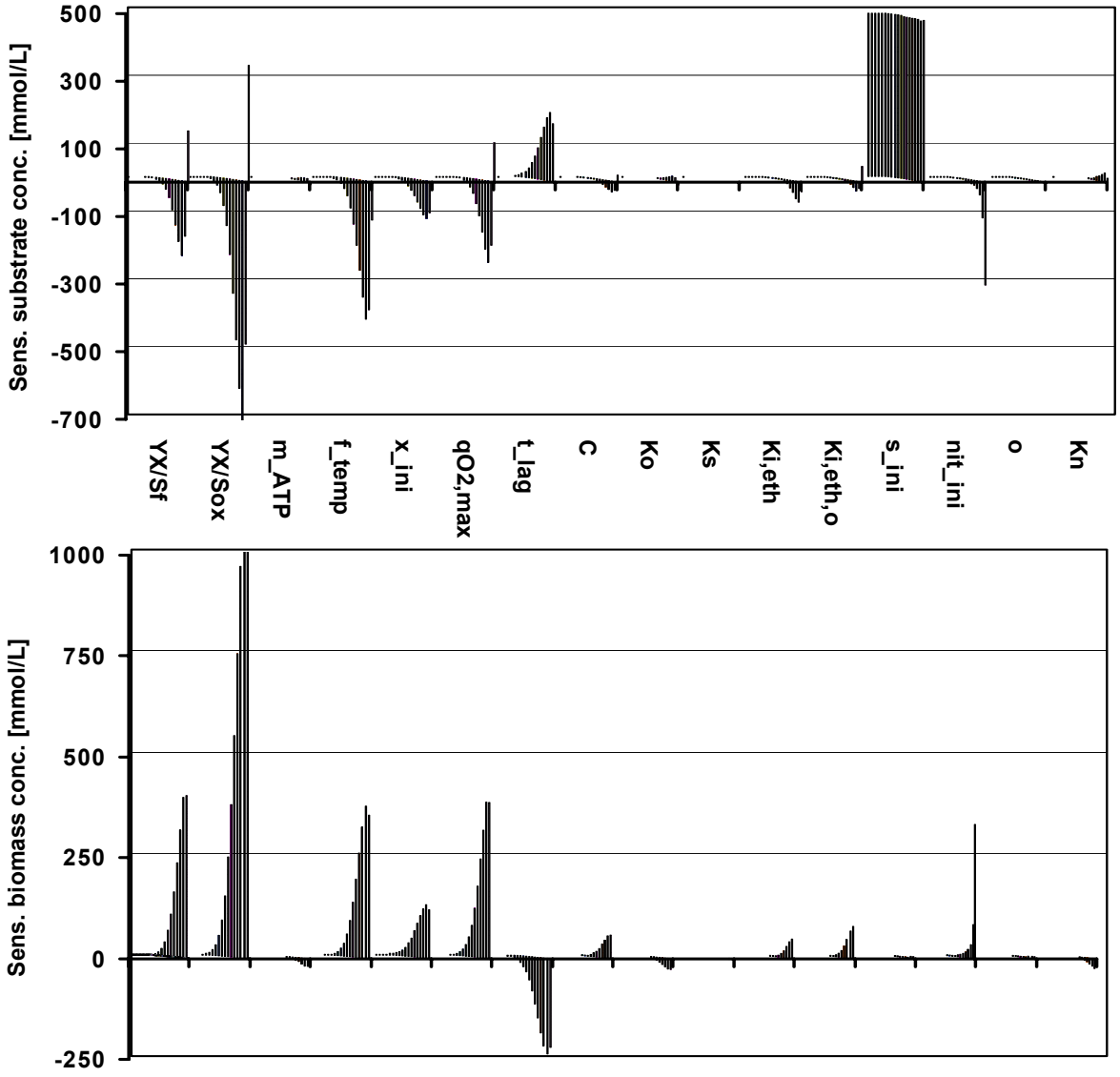

Figure 17: Absolute sensitivity functions for an isothermal yeast propagation (experiments B) at 25°C and 0.5ppm dissolved oxygen concentration for substrate concentration (above) and biomass concentration (below). Sensitivities are shown for all relevant parameters along the propagation run for a 100% change of each parameter. Parameters YX/Sf, YX/Sox, m_ATP, f_temp, (qO2,max), t_lag, Ko, Ks, (Ki,eth) and Kn correspond to parameters $Y_{X/Sf}$, $Y_{X/Sox}$, m_{ATP}, f_{temp}, $q_{O2,max}$, t_{lag}, K_o, K_s, $K_{i,eth}$, $K_{i,eth,o}$, and K_n in Table 12. x_ini (x_{ini}), s_ini (s_{ini}) and nit_ini (nit_{ini}) represent initial concentrations of biomass, substrate and nitrogen.

Here, also the yield coefficients $Y_{X/Sox}$ and $Y_{X/Sf}$, the temperature coefficient of substrate uptake rate f_{temp} and the maximum specific oxygen uptake rate $q_{O2,max}$ were the parameters with the highest influence on substrate and biomass concentrations. The initial concentrations

of biomass x_{ini} had influence on both concentrations, whereas s_{ini} took no effect on biomass concentration. In the second part of the propagation the initial concentration of nitrogen source became more important as the regarded propagation run (experiments B, 25°C, 0.5 ppm dissolved oxygen) was limited by lacking nitrogen sources. This came along with a gaining sensitivity on the half saturation constant K_n. However, the sensitivity was still not in the range of other parameters, because K_n was set on a very small value. It should be noticed, that due to higher ethanol concentrations during brewery propagations the inhibition constants $K_{i,eth}$ and $K_{i,eth,o}$ also showed a remarkable influence on both concentrations. Half saturation constants as K_o or K_s showed no influence for the regarded cases. But, if no nitrogen limitation occurred, the total substrate would have been degraded and K_s would have gained influence at the end of the process. Similarly, concentrations would have beeen sensitiv on K_o, if less oxygen was supplied. Same results were achieved for the Black Box model. However, results of sensitivity analysis always have to be interpreted with care, as they are only valid for the specific simulated experiment.

The presentation of sensitivity functions for all regarded cases of bakers' yeast and brewery yeast propagations is not ingenious for this work. Therefore, another representation of sensitivity data was chosen. Every parameter p was changed by 1/1000 and the relative sensitivity was calculated by dividing the maximal deviation *max(∂y)* during the simulation run (compared to the unchanged parameter) by the maxium value *max(y)* of substrate or biomass concentration and scaling with *p*:.

$$\delta = \frac{\max(\partial y)}{\partial p} \cdot \frac{p}{\max(y)} \text{ , with } \partial p = \frac{p}{1000}. \tag{40}$$

Equation 40 can be interpreted as the relative change of y per 100 % change of the parameter p (assuming linearity). The following tables show all parameters with sensitivities to biomass and substrate more than 10 % in the simulations of literature data (Table 15), experiments A (Table 16), experiments B (Table 17), experiments C (Table 18) and experiments D (Table 19). Also sensitivity analysis for oxygen experiments are presented (Table 20). The latter experiments are described in chapter 3.3.3.

Table 15: Sensitivity analysis. Relative sensitivity of the parameters in respect to the concentrations of substrate (s) and biomass (x) in simulations for yeast batch propagations. <u>All</u> parameters with <u>sensitivities > 0.1</u> are shown. Literature data from Sonnleitner (1), Barford 1990 (2) and Barford 1981 (3) are used (see Figure 11).

	Black Box Model						Metabolic Model					
Parameter	s(1)	s(2)	s(3)	x(1)	x(2)	x(3)	s(1)	s(2)	s(3)	x(1)	x(2)	x(3)
$Y_{XS,ox}$	-0,66	-2,35	-1,99	1,0	3,24	1,62	-0,56	-2,46	-2,13	1,02	3,54	2,04
$Y_{XS,f}$	-0,24	-1,09	-1,25	0,59	1,51	0,95	-0,28	-1,16	-1,27	0,38	1,65	1,02
m_{ATP}	-	-	-	-	-	-	-	-	-	-	-	-
K_o	-	-	-	-	-	-	-	-	-	-	-	-
K_s	-	0,14	0,15	-	0,11	-	-	0,14	0,15	-	-0,11	-
K_n	-	-	-	-	-	-	-	-	-	-	-	-
$K_{i,eth}$	-	-	-	-	-	-	-	-	-	-	-	-
$K_{i,eth,o}$	-	-	-	0,15	0,1	0,24	-	-	-	-	-	0,1
K_e	-	-	-	-	-	-	-	-	-	-	-	-
C							-	-0,16	-0,17	-	0,23	0,14
nit_ini	-	-	-	-	-	-	-	-	-	0,84	0,91	1,35
x_ini	-0,64	-0,57	-0,56	0,19	0,56	0,3	-0,63	-0,6	-0,6	0,37	0,61	0,35
s_ini	1	1	1	0,37	0,7	0,6	1	1	1	-	-	-
$q_{e,max}$	-	-	-	-	-	-	-					
$q_{O2,max}$	-0,25	-0,86	-0,73	0,79	1,18	1,27	-0,19	-0,84	-0,72	0,32	1,20	0,64
$q_{O2,e,max}$	-	-	-	-	-	-	-	-	-	0,64	-	1,24
f_{temp}	-0,9	-1,87	-2	0,57	1,49	0,91	-0,93	-1,91	-1,98	0,24	1,61	0,97
t_{lag}	-0,22	-	-0,4	0,13	-	0,21	-	-	-	-	-	-
$t_{lag,eth}$	-	-	-	-	-	-	-	-	-	-0,51	-	-1,97

Table 16: Sensitivity analysis. Relative sensitivity of the parameters in respect to the concentrations of substrate (s) and biomass (x) in simulations. All sensitivities > 0.1 are shown. Bottom fermenting yeast propagations of experiments A are analysed (see Figure 12).

Parameter	s(5°C)	s(10°C)	s(15°C)	s(20°C)	s(25°C)	s(30°C)	x(5°C)	x(10°C)	x(15°C)	x(20°C)	x(25°C)	x(30°C)
Black Box Model												
$Y_{XS,ox}$	-	-	-1,39	-0,69	-0,98	-0,76	-	0,14	2,69	3,85	2,47	1,76
$Y_{XS,f}$	-0,96	-0,56	-0,41	-0,17	0,33	-0,46	1,55	1,9	0,92	1,03	0,85	1,28
m_{ATP}	0,32	-	-	-	-	-	-0,67	-0,32	-0,15	-	-	-
K_o	-	-	0,1	-	-	-	-	-	-0,19	0,24	-0,16	-0,11
K_s	-	-	-	-	-	-	-	-	-	-	-	-
K_n	-	-	-	-	-	-	-	-	-	-	-	-
$K_{i,eth}$	-0,43	-0,16	-0,19	-	-0,14	-0,2	0,42	0,3	0,12	-	0,11	0,21
$K_{i,eth,o}$	-	-	0,2	-	0,13	-	0,12	-	0,32	0,23	0,26	0,19
nit_ini	-0,14	-	-0,89	-	-0,73	-0,21	0,14	-	0,96	-	0,92	0,22
x_ini	-0,32	-0,28	-0,29	-0,18	-0,28	-0,29	0,32	0,58	0,36	0,71	0,44	0,45
s_ini	1	1	1	1	1	1	0,65	-	-	-	-	-
$q_{O2,max}$	-0,18	-0,11	-0,57	-0,26	-0,38	-0,29	0,29	0,31	1,12	1,48	0,95	0,68
f_{temp}	-1,41	-0,84	-0,79	-0,39	-0,65	-0,83	1,27	1,52	0,55	0,94	0,55	0,92
t_{lag}	-	0,14	-	-	-	-		-0,25	-	-	-	-0,1
Metabolic Model												
$Y_{XS,ox}$	-1,3	-0,4	-1,55	-0,7	-0,98	-0,7	2,06	1,28	3,06	4,7	2,49	1,72
$Y_{XS,f}$	-0,53	-0,48	-0,39	-0,12	-0,33	-0,5	0,7	1,61	0,84	0,81	0,91	1,31
m_{ATP}	0,51	0,13	-	-	-	-	-0,94	-0,44	-0,17	-	-	-
K_o	-	-	-	-	-	-	-	-	-	-0,11	-	-
K_s	-	-	-	-	-	-	-	-	-	-	-	-
K_n	-	-	-	-	-	-	-	-	-	0,11	-	-
$K_{i,eth}$	-0,44	-0,17	-0,2	-	-0,14	-0,16	0,38	0,32	0,14	-	0,12	0,19
$K_{i,eth,o}$	-0,1	-	0,18	-	0,12	-	0,19	-	0,3	0,19	0,23	0,16
C	-	-	-	-	-	-	0,1	0,2	0,12	0,11	0,12	0,18
nit_ini	-0,13	-	-0,87	-	-0,72	-0,1	0,11	-	0,92	-	0,92	0,11
x_ini	-0,29	-0,27	-0,29	-0,16	-0,28	-0,28	0,28	0,55	0,35	0,73	0,44	0,44
s_ini	1	1	1	1	1	1	0,2	-	-	-	-	-
$q_{O2,max}$	-0,29	-0,1	-0,54	0,24	-0,35	-0,24	0,41	0,29	1,04	1,6	0,87	0,58
f_{temp}	-1,38	-0,87	-0,84	-0,33	-0,68	-0,82	1,06	1,6	0,64	0,88	0,63	0,98
t_{lag}	-	0,15	-	-	-	-	-	-0,26	-	-	-	-

Table 17: Sensitivity analysis. Relative sensitivity of the parameters in respect to the concentrations of substrate (s) and biomass (x) in simulations for yeast propagations of experiments B. All sensitivities > 0.1 are shown. Experiments are shown in Figure 13.

Parameter	s(8°C)	s(15°C)	s(20°C)	s(25°C)	s(30°C)	x(8°C)	x(15°C)	x(20°C)	x(25°C)	x(30°C)
Metabolic Model without adjuncts										
$Y_{XS,ox}$	-0,41	0,28	0,39	0,52	0,21	-3,79	0,68	0,67	0,82	0,30
$Y_{XS,f}$	-0,32	0,30	0,37	0,42	0,57	-2,04	0,76	0,74	0,73	0,92
m_{ATP}	0,1	-	-	-	-	1,61	-0,1	-	-	-
K_o	-	-	-	-	-	-	-	-	-	-
K_s	-	-	-	-	-	-0,43	-	-	-	-
K_n	0,11	-	-	-	-	-0,78	-0,11	-0,1	-	-0,12
$K_{i,eth}$	-0,28	-0,15	-0,12	-0,14	-0,17	1,4	0,19	0,16	0,14	0,22
$K_{i,eth,o}$	-	-	-	-	-	-0,7	-	-	0,12	-
C	-	-	-	-	-	0,2	-	-	-	-
nit_ini	-0,57	-0,54	-0,53	-0,64	-0,63	5,82	0,67	0,81	0,82	0,83
x_ini	-0,34	-0,26	-0,22	-0,27	-0,27	1,49	0,52	0,53	0,53	0,52
s_ini	1	1	1	1	1	-5,09	-	-	-	-
$q_{O2,max}$	-0,12	-	0,12	0,17	-	-1,05	0,21	0,22	0,28	0,95
f_{temp}	-0,86	-0,53	-0,44	-0,52	-0,57	3,38	0,67	0,61	0,55	0,75
t_{lag}	-	0,13	-	-	-	-	-0,19	-	-	-
Parameter	**s(12°C)**	**s(17°C)**	**s(20°C)**	**s(25°C)**	**s(30°C)**	**x(12°C)**	**x(17°C)**	**x(20°C)**	**x(25°C)**	**x(30°C)**
Metabolic Model with adjuncts										
$Y_{XS,ox}$	-0,35	0,87	0,78	0,92	0,46	-0,89	1,49	1,29	1,47	0,59
$Y_{XS,f}$	-0,41-	0,45	0,54	0,56	0,83	1,08	0,8	0,91	0,86	1,05
m_{ATP}	-	-	-	-	-	-0,18	-	-	-	-
K_o	-	-	-	-	-	-	-	-	-	-
K_s	-	-	-	-	-	-	-	-	-	-
K_n	-	-	-	-	0,10	-	-	-	-	-
$K_{i,eth}$	-0,31	-0,20	-0,22	-0,24	-0,31	0,29	0,16	0,18	0,17	0,25
$K_{i,eth,o}$	-	0,15	0,14	0,16	-	0,12	0,21	0,18	0,20	-
C	-	-	-	-	-	0,1	-	-	-	0,1
nit_ini	-0,20	-0,82	-0,86	-0,95	-0,98	0,19	0,90	0,90	0,91	0,89
x_ini	-0,37	-0,3	-0,31	-0,34	-0,38	0,51	0,45	0,43	0,44	0,45
s_ini	1	1	1	1	1	-	-	-	-	-
$q_{O2,max}$	-0,11	0,29	0,26	0,31	0,15	0,26	0,52	0,45	0,52	0,20
f_{temp}	-0,91	-0,67	-0,75	-0,77	-0,92	0,84	0,57	0,64	0,57	0,75
t_{lag}	-	-	-	-	0,13	-	-	-	-	-0,11

Table 18: Sensitivity analysis. Relative sensitivity of the parameters in respect to the concentrations of substrate (s) and biomass (x) in simulations for top fermenting yeast propagations of experiments C. All parameters with sensitivities > 0.1 are shown. Experiments are illustrated in Figure 14.

Parameter	s(8°C)	s(15°C)	s(20°C)	s(27.5°C)	s(32°C)	x(8°C)	x(15°C)	x(20°C)	x(27.5°C)	x(32°C)
Black Box Model										
$Y_{XS,ox}$	-	-0,15	-0,12	-1,5	-	-	0,3	2,29	3,58	0,36
$Y_{XS,f}$	-0,24	-0,58	-0,1	-0,42	-0,33	1,9	1,5	1,94	1,15	1,9
m_{ATP}	-	-	-	-	-	-0,3	-0,15	-0,13	-	-
K_o	-	-	-	-	-	-	-	-0,15	-0,22	-
K_s	-	-	-	-	-	-	-	-	-	-
K_n	-	-	-	-	-	-	-	-	-	-
$K_{i,eth}$	-	-0,26	-	-0,12	-	-	0,3	-	0,12	0,21
$K_{i,eth,o}$	-	-	-	0,11	-	-	-	-	0,26	-
nit_ini	-	-0,11	-	-0,63	-	-	0,12	-	0,98	-
x_ini	-0,16	-0,35	-	-0,22	-0,2	0,83	0,53	0,83	0,38	0,74
s_ini	1	1	1	1	1	-	-	-	-	-
$q_{O2,max}$	-	-0,11	-	-0,53	-	0,21	0,25	0,93	1,29	0,17
f_{temp}	-0,41	-0,95	-0,17	-0,82	-0,54	1,86	1,07	2,03	1,03	1,65
t_{lag}	-	-	-	0,44	-	-	-	-	-0,73	-0,15
Metabolic Model										
$Y_{XS,ox}$	-0,16	-0,26	-0,21	-1,48	-	1,24	0,66	5,35	3,57	0,26
$Y_{XS,f}$	-0,2	-0,59	-	-0,46	-0,34	1,62	1,51	1,25	1,26	1,93
m_{ATP}	-	-	-	-	-	-0,49	-0,18	-0,15	-	-
K_o	-	-	-	-	-	-	-	-0,12	-	-
K_s	-	-	-	-	-	-	-	-	-	-
K_n	-	-	-	-	-	-	-	-	-	-
$K_{i,eth}$	-	-0,27	-	-0,13	-	0,1	0,33	-	0,14	0,2
$K_{i,eth,o}$	-	-	-	0,1	-	-	-	-	0,24	-
C	-	-	-	-	-	0,22	0,2	0,17	0,17	-
nit_ini	-	-	-	-0,63	-	-	0,13	-	0,98	-
x_ini	-0,16	-0,35	-	-0,22	-0,2	0,81	0,52	0,87	0,39	0,74
s_ini	1	1	1	1	1	-	-	-	-	-
$q_{O2,max}$	-	-0,1	-	-0,5	-	0,26	0,17	1,71	1,2	0,14
f_{temp}	-0,43	-1	-0,12	-0,86	-0,53	1,98	1,17	1,81	1,14	1,64
t_{lag}	-	-	-	0,42	-	-	-	-0,82	-0,71	-0,28

Table 19: Sensitivity analysis. Relative sensitivity of the parameters in respect to the concentrations of substrate (s) and biomass (x) in simulations for yeast propagations of experiments D. All parameters with sensitivities > 0.1 are shown. Experiments are illustrated in Figure 15.

Parameter	s(9°C)	s(16°C)	s(23°C)	s(30°C)	x(9°C)	x(16°C)	x(23°C)	x(30°C)
Black Box Model								
$Y_{XS,ox}$	-	-0,6	-0,34	-0,5	-	1,77	1,48	1,52
$Y_{XS,f}$	-0,71	-0,25	-0,14	-0,3	1,84	0,88	0,75	1,15
m_{ATP}	0,1	-	-	-	-0,28	-0,12	-	-
K_o	-	0,12	-	-	-	-0,37	-0,28	-0,14
K_s	-	-	-	-	-	-	-	-
K_n	-	-	-	-	-	-	-	-
$K_{i,eth}$	-0,27	-0,16	-	-0,14	0,38	0,16	0,14	0,21
$K_{i,eth,o}$	-	-	-	-	-	0,27	0,18	0,16
nit_ini	-	-0,2	-0,28	-	0,13	0,2	0,39	-
x_ini	-0,35	-0,3	-0,22	-0,3	0,55	0,55	0,6	0,68
s_ini	1	1	1	1	-	-	-	-
$q_{O2,max}$	-0,1	-0,25	-0,13	-0,19	0,17	0,75	0,57	0,58
f_{temp}	-1,08	-0,64	-0,45	-0,65	1,47	0,65	0,67	0,95
t_{lag}	0,2	0,3	0,2	0,29	-0,26	-0,43	-0,4	-0,48
Metabolic Model								
$Y_{XS,ox}$	-0,57	-0,66	-0,70	-0,47	1,52	2,02	2,85	1,41
$Y_{XS,f}$	-0,46	-0,24	-0,25	-0,35	1,34	0,86	1,21	1,34
m_{ATP}	0,14	-	-	-	-0,4	-0,12	-	-
K_o	-	-	-	-	-0,11	-0,18	-0,26	-
K_s	-	-	-	-	-	-	-	-
K_n	-	-	-	-	0,11	0,18	0,26	-
$K_{i,eth}$	-0,21	-0,17	-0,16	-0,15	0,31	0,18	0,24	0,24
$K_{i,eth,o}$	-	-	-	-	0,13	0,24	0,32	0,13
C	-	-	-	-	0,18	0,12	0,17	0,18
nit_ini	-	-0,20	-0,13	-	-	-	-	-
x_ini	-0,32	-0,29	-0,29	-0,31	0,53	0,54	0,78	0,68
s_ini	1	1	1	1	0,12	0,21	0,19	0,1
$q_{O2,max}$	-0,15	-0,22	-0,23	-0,16	0,38	0,66	0,94	0,47
f_{temp}	-0,93	-0,66	-0,67	-0,69	1,33	0,74	1,06	1,07
t_{lag}	0,23	0,36	0,41	0,28	-0,33	-0,54	-0,86	-0,47

Table 20: Sensitivity analysis. Relative sensitivity of the parameters in respect to the concentrations of substrate (s) and biomass (x) in simulations for propagations of experiments A and B (oxygen experiments). All parameters with sensitivities > 0.1 are shown. Experiments are illustrated in Figure 33.

Parameter	s(0.02ppm)	s(0ppm)	s(0ppm)	x(0.02ppm)	x(0ppm)	x(0ppm)
Black Box Model						
$Y_{XS,ox}$	-0,64	-0,75	-0,66	2,04	1,98	2,02
$Y_{XS,f}$	-0,34	-0,38	-	1,18	1,16	-
m_{ATP}	-	-	-	-0,15	-0,16	-0,16
K_o	0,10	0,13	0,11	-0,32	-0,34	-0,34
K_s	-	-	-	-	-	-
K_n	-	-	-	-	-	-
$K_{i,eth}$	-0,13	-0,17	-0,13	0,16	0,17	0,16
$K_{i,eth,o}$	-	-	-	0,25	0,25	0,23
nit_ini	-	-0,14	-	-	0,15	0,1
x_ini	-0,27	-0,28	-0,28	0,55	0,47	0,56
s_ini	1	1	1	-	-	-
o	-0,1	-	-	0,32	-	-
t_{lag}	-	-	0,32	-	-	-0,53
Metabolic Model						
$Y_{XS,ox}$	-0,74	-0,88	-0,81	2,46	2,50	2,48
$Y_{XS,f}$	-0,33	-0,36	-	1,13	1,12	-
m_{ATP}	-	-	-	-0,17	-0,19	-
K_o	-	-	-	-0,22	-0,25	-0,25
K_s	-	-	-	-	-	-
K_n	-	-	-	-	-	-
$K_{i,eth}$	-0,13	-0,16	-0,14	0,18	0,19	0,19
$K_{i,eth,o}$	-	-	-	0,23	0,23	0,22
C	-	-	-	0,15	0,15	0,14
nit_ini	-	-0,11	-	0,10	0,13	0,10
x_ini	-0,27	-0,28	-0,28	0,54	0,50	0,56
s_ini	1	1	1	-	-	-
o	-	-	-	0,22	0,25	0,24
t_{lag}	-	-	0,33	-	-0,14	-0,56

For all referenced experiments the yield coefficients $Y_{X/Sox}$ and $Y_{X/Sf}$ as well as the temperature coefficient of the substrate uptake rate f_{temp} appeared to be parameters with the most relevant influence on the simulation results. Maximum specific oxygen uptake rate $q_{O2,max}$ and the lag-time t_{lag} showed a lower but still relevant influence on biomass and substrate concentrations. However, simulation runs reacted sensitively on the latter parameter only if yeast in a poor physiological condition was used as inoculum. As shown, in most cases no relevant lag phase occurred and the system was not sensitive to the parameter t_{lag}. Other parameters were negligible at least during the growth phase on glucose. If ethanol reached high concentrations, additional inhibition constants for substrate uptake $K_{i,eth}$ and oxygen uptake $K_{i,eth,o}$ were important. Besides, in the case of occurring limitations due a lack of glucose or nitrogen the system became sensitive on half saturation constants K_s and especially on K_n for brewing yeast propagations.

The main contribution to simulation inaccuracy is generally due to parameters which were not exactly known and at the same time sensitivity function took high values. In the referenced cases the parameters were $q_{O2,max}$, f_{temp}. and t_{lag} as yield coefficients were known and assumed to be constant. For ethanol degradation $t_{lag,eth}$ and $q_{O2,e,max}$ also had to be considered. The mentioned parameters were strongly dependent on temperature. However, they possessed a strong effect on simulation results, therefore, the mentioned parameters are intended to be estimated in a parameter estimation procedure for all experiments concerning bakers' yeast or brewing yeast propagations.

Parameters with a great influence could be estimated very well, if reliable experimental data was available. It was not possible to determine parameters with poor influence. For example the maintenance energy m_{ATP} is known only inexactly and is dependent on temperature. The sensitivity function of such parameters, however took only small values and therefore it was not intended to estimate these parameters. A fixed set of such parameters could be applied for all model based simulations.

3.3 Technological and mathematical validation of the influence of manipulated variables

Aiming at the development of a process management tool, which is able to predict and manipulate the propagation process, it was necessary to describe its dependency on the common manipulated variables temperature and dissolved oxygen concentration. This knowledge had to be transferred into the process model by formulating the estimated parameters as functions of the manipulated variables. In this regard, the analysis of the experimental data revealed important specific information about the relationship between temperature and oxygen content during the yeast propagation, substrate uptake and biomass formation, respectively.

3.3.1 Technological validation of the influence of temperature as manipulated variable

In Figure 18 the maximum occurring specific growth rate is plotted versus the absolute temperature. It can be seen that as reported in literature [30, 63, 91, 122] for all referenced experiments the growth rates of all experiments follow an activation and inactivation path with increasing temperature. All applied yeasts featured an exponential increase of the maximum specific growth rate up to a temperature of 25 - 27°C. With higher temperatures the slope was decreasing due to starting thermal inactivation processes. For experiments A (♦) following the principle of a master reaction for the biomass growth, an Arrhenius approach (see equation 2) with an activation energy E_a = 84.801 kJ mol^{-1} could be used to describe the temperature dependency of the specific growth rate in a temperature range between 10 and 25°C. The activation energy E_a was in a reasonable range for microbial specific growth rates [63, 122]. Experimental data of bakers' yeast propagations and industrial trials with bottom fermenting brewing yeasts (W34/70) from Manger et al. [91] and Lehmann [87] showed similar results.

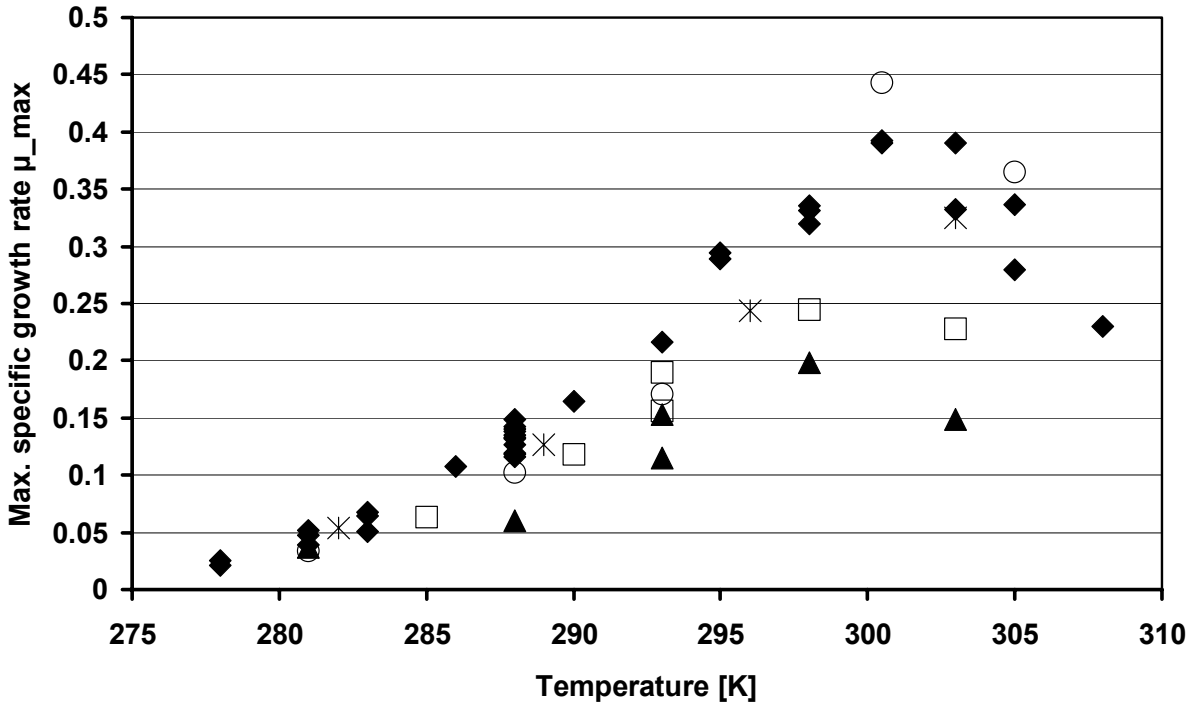

Figure 18: Maximum specific growth rate µ_max versus the temperature. Bottom and top fermenting yeast propagations from experiments A (♦), B (▲ without adjuncts,□ with adjuncts), C (○) and D (ж) are presented.

During experiments B (see Figure 18 ▲ without adjuncts, □ with adjuncts A) another bottom fermenting yeast strain was used and a lower range of specific growth rate compared to Saccharomyces uvarum var carlsbergensis W34/70 was detected. The top fermenting yeast of experiments C (○) showed a low level of specific growth rates at low temperatures but

appeared to possess a high maximum specific growth rate in a temperature range between 25 and 28°C. Since in experiments D (ж) the same yeast was applied as in experiments A, the temperature dependency had a similar result. Here, it should be noticed that the specific growth rate seemed to be dependent only on the yeast type but less on the propagation plant or procedure.

In brewing industry, however, not only the maximum specific growth rate is of interest, but also the appearing yield gravity / biomass. If low yields occurred, too much sugar is degraded and an unacceptable dilution of the initial wort concentration in the inoculated fermentation resulted. Figure 19 illustrates the relation between the mentioned yield (gravity / biomass) and the temperature of the yeast propagation for experiments A (□) and B (♦). All experiments were carried out with a dissolved oxygen concentration of 0.5 ppm. Both experiments resulted yields at the same level. The lowest extract per biomass was needed in a temperature range between 15 and 28°C. At lower temperatures the yield is slightly increasing and more sugar was consumed per biomass. A remarkable increase of the yield, however was regarded especially for higher temperature with an eight-fold increase of the yield between 28°C and 35°C. This result should be associated with examinations of Zepf et al. [144] who found that the quality of the fermentation and the resulting beer increased if propagations were carried out in a temperature range between 16 and 20°C. Aspects of yeast physiology referring to this should be discussed in chapter 4.

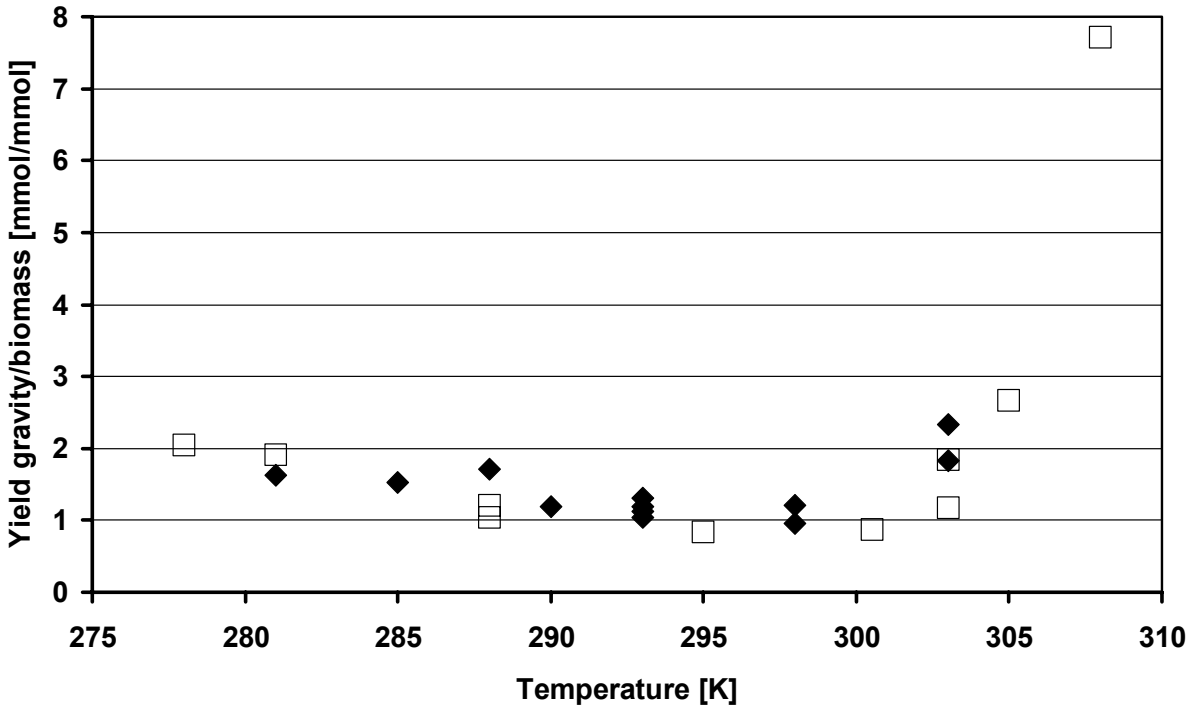

Figure 19: Temperature dependency of the yield gravity / biomass during experiments A (□) and B (♦)

In brewing science much experimental work has been done to find "optimal" process strategies for the yeast propagation. However, the introduced results concerning temperature dependency of specific growth rate and yield (gravity / biomass) indicate a systematic temperature dependency of the *Saccharomyces* yeast metabolism. In inference, as the temperature coefficient of the substrate uptake rate f_{temp} and the maximum specific oxygen uptake rate $q_{O2,max}$ possessed the highest sensitivities on the simulation result, reasons for the behaviour were assumed to be in the substrate and oxygen uptake behaviour of the yeast cells. In Figure 20 the temperature coefficient of the sugar uptake rate f_{temp} is plotted versus the specific growth rate. Data from experiments A (♦), B (▲ without adjuncts,□ with adjuncts), C (○) and D (ж) are considered. For all experiments f_{temp} was increasing quasi exponentially between 5 and 32°C. A single experiment at 35°C resulted in a lower value, which has to be confirmed in further trials. This means, that with increasing temperature the substrate uptake rate of the yeast cell was increasing with the temperature coefficient also. Results of experiments B with adjuncts lied on a higher level. This indicates an improved ability for substrate uptake caused by a better supply of e.g. trace elements or vitamins. Examinations in this regard are still being carried out. Other experiments including different yeast strains and propagation procedures appeared to show no relevant difference in the temperature dependency of the substrate uptake kinetics.

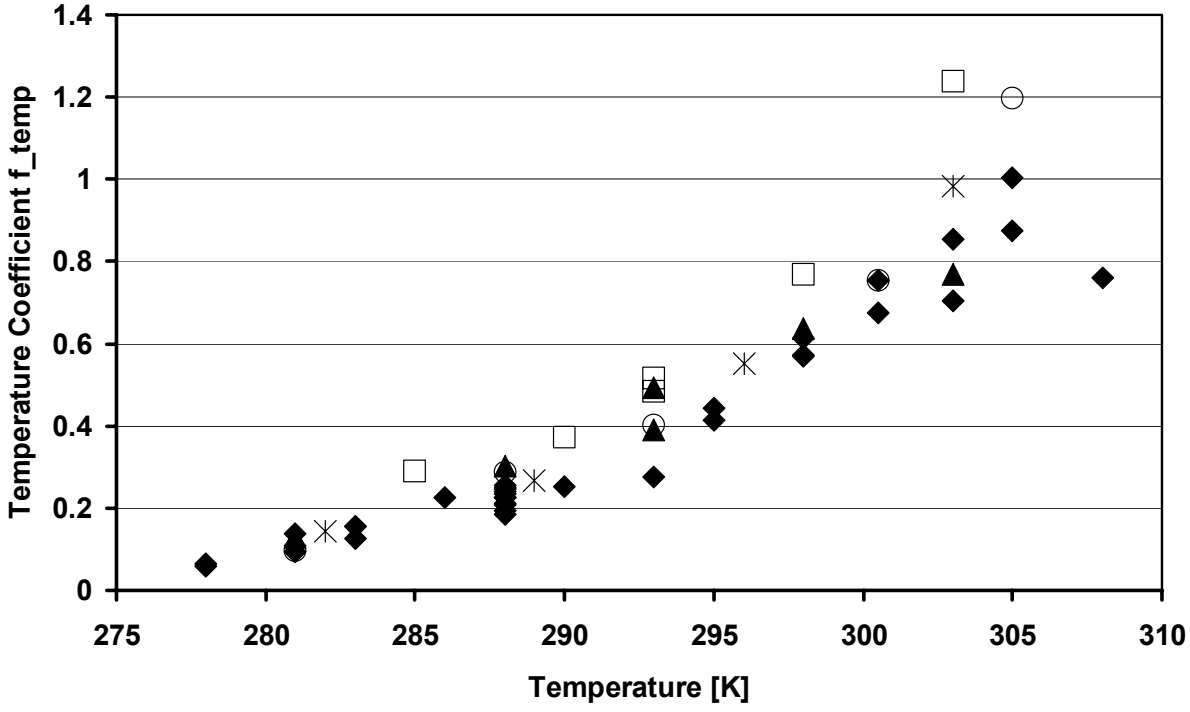

Figure 20: Temperature coefficient f_{temp} versus the temperature. Experiments A (♦), B (□ with adjuncts, ▲ without adjuncts), experiments C (○) and experiments D (∗) are considered.

The maximum specific oxygen uptake rate $q_{O2,max}$ can be interpreted as a measure for the size of the respirative bottleneck (s. Figure 7). Figure 21 summarises the results of the parameter estimation for $q_{O2,max}$ of experiments A (♦), B (▲ without adjuncts, □ with adjuncts), C (○) and D (ж). For all experiments the parameter is increasing exponentially with the temperature in a range of 5 to 22°C. With higher temperatures the slope is decreasing and between 32 and 35°C $q_{O2,max}$ became zero. This confirmed results of Hartmeier [61] who analysed the temperature dependency of the maximum specific oxygen uptake rate for *Saccharomyces cerevisiae*.

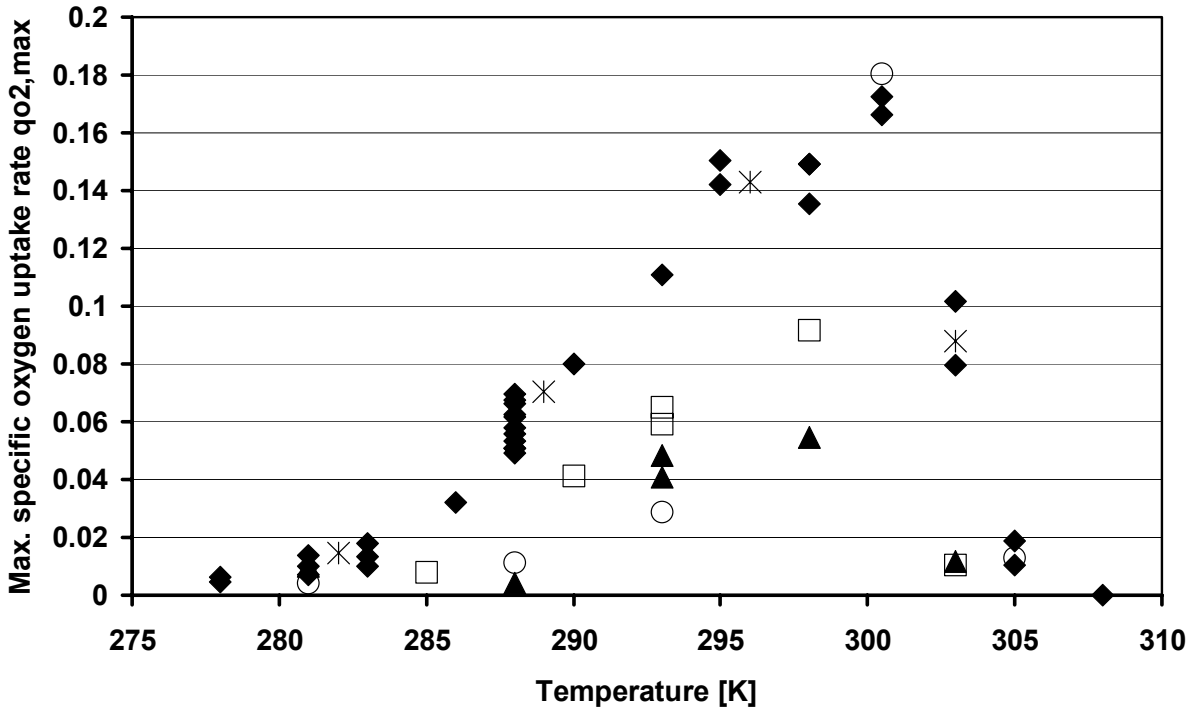

Figure 21: Maximum spec. oxygen uptake rate $q_{O2,max}$ versus the temperature. Regarded are experiments A (♦), B (□ with adjuncts, ▲ without adjuncts), experiments C (○) and experiments D (∗).

Again, it was of interest how different yeast strains performed concerning the oxygen uptake kinetics. Results of the parameter estimation for experiments A (♦) and D (ж), both with *Saccharomyces uvarum var. carlsbergensis* W34/70 were nearly identical. Another bottom fermenting strain of experiments B showed a minor maximum oxygen uptake kinetic with or without adjuncts. Remarkable was the fact that for the top fermenting yeast (W68) a very low oxygen uptake ability occurred at low temperature, but above 20°C the highest value of all regarded yeast appeared.

Summarising, it can be stated that with higher temperatures the uptake rate for sugars is increased up to a maximum temperature of around 32°C. The differences between the uptake kinetics of different yeast strains seemed to be negligible. On the other hand, the oxygen

uptake rate is increasing up to a temperature of 22-25°C. With higher temperatures the oxygen uptake rate is decreasing. In this case the course of the temperature function appeared to be dependent on the yeast strain and the availability of trace elements and nutrients in the growth medium.

So, the phenomena of Figure 18 could be explained. The specific growth rate was increasing due to increasing substrate uptake and oxygen uptake rates. When oxygen uptake rate started to decrease the specific growth rate showed the same effect also, because more substrate was catabolised using the fermentative pathway causing a lower biomass production. In the same way high yield coefficients (gravity / biomass) at higher temperatures were constituted (see Figure 19). Due to overflow metabolism with decreasing size of the respirative bottleneck a rising part of the biomass was built using the fermentative pathway (comp. chapter 2.2.1.3). At colder temperatures the relation substrate uptake and oxygen uptake were divergent only in a minor degree and therefore only little increase in the regarded yield resulted.

With these results important characteristics of the temperature depencency of yeast growth could be extracted and the understanding of yeast metabolism was improved. A main aspect of this work was to create a comprehensive modelling approach for the yeast growth. Therefore, the integration of the temperature dependency of substrate and oxygen uptake kinetics was a prerequisite.

3.3.2 Modelling the temperature dependency of substrate and oxygen uptake kinetics and specific growth rate

In order to describe the temperature dependency of the maximum specific growth rate μ_{max} and the parameters f_{temp} and $q_{O2,max}$ four different modelling approaches were tested, a square-root approach, a potential approach of Bělehrádek, the Schoolfield model and an Arrhenius approach of Mohr and Krawiec.

3.3.2.1 Square-root- model

The square model for the specific growth rate

$$\mu(T) = \left\langle b \cdot (T - T_{min}) \cdot \left\{ 1 - \exp\left[c \cdot (T - T_{max}) \right] \right\} \right\rangle^2 \qquad (41)$$

is given in its quadratic form in order to be compared to other approaches. Similar formulations were applied for $f_{temp}(T)$ and $q_{O2,max}(T)$. In a first step the parameters of the two parameter model (see equation 19) were determined. The figures of chapter 3.3.1 illustrate the suboptimal range for μ_{max} and $q_{O2,max}$ reaching from (5 - 27.5°C). The same range was applied for f_{temp}. Initial values for parameter estimation, error contribution and resulting parameters b and T_{min} are shown in Table 30 in the appendix. Subsequently, all four parameters were

estimated for the whole temperature range. As the value for $q_{O2,max}$ at 308 K is zero this value was excluded (for all models). Beyond that, the progression of the curve in Figure 22 suggests a null at a lower temperature.

Considering the whole temperature range (see Table 31 in the appendix) for f_{temp} an optimal temperature of only slightly below 308 K was resulting. Therefore, the curve plunged down steeply in the superoptimal range (see Figure 22). It was notable that the determined minimum temperatures were all below zero. This confirmed results from Ratkowsky [113, 114], as T_{min} could not be interpreted as a metabolic parameter. Similar considerations had to be made for T_{max}, because maximum temperatures of around 39°C lied out of the range reported in literature [91]. However the predicted optimum temperature for μ_{max} was found in a realistic range [91]. Parameters b and c were simple regression coefficients without any biological impact [67].

3.3.2.2 Bělehrádek-Model

In order to represent the whole temperature range the applied Bělehrádek relation for suboptimal temperature ranges was extended similar to the square root model:

$$\mu(T)=\langle b\cdot(T-T_{min})\cdot\{1-\exp[c\cdot(T-T_{max})]\}\rangle^{\alpha}. \quad (42)$$

In a first step, three parameters were determined for the suboptimal temperature range. As initial values parameters of the square root model were applied. Results are listed in the appendix (Table 32). Subsequently, parameters c and T_{max} of the completed model (equation 42) were estimated. The above determined parameters were set constant for this step. Parameters are listed in Table 33 (appendix).

A biological interpretation of the determined parameters proved to be difficult. For example the minimum temperature T_{min} for f_{temp} was far below the absolute minimum. However, the growth optimum (μ_{max}) could be found in a reasonable range (29.3°C) (see Figure 26) [91]. Bělehrádek interpreted the parameter α as an indicator for the viscosity of the protoplasm during the development of a species [16]. This assumption was founded on an increase of α with increasing age of the population. In this work, however, only single isothermal propagations at different temperature were regarded. None of the applied yeast populations was examined during several propagations. Therefore, this interpretation could not be verified here. Dantigny reused the approach of Bělehrádek, in order to plot dimensionless variables of growth rates versus the temperature: $\mu_{dim} = \mu/\mu_{opt} = T_{dim}^{\alpha} = \{(T-T_{min})/(T_{opt}-T_{min})\}^{\alpha}$ [38]. T_{opt} represented the temperature belonging to a maximum specific growth rate μ_{opt}. Thermophile microorganisms featured a lower value for α as meso- and psychrophile organisms ($\alpha = 0{,}68$ for *Bacillus stearothermophilus* with $T_{opt} = 65$°C; $\alpha = 1{,}21$ for *Acinetobacter* with T_{opt}=29°C) [114]. Similar to this with

$\mu_{max,opt} = 0{,}38\ h^{-1}$ and $T_{opt} = 27{,}9°C$ the parameters T_{min} und α were determined for the transformed values of μ_{max}. A calculated α=1,39 (T_{min}=2,95) confirmed the theory of Dantigny for the mesophile brewers' yeast [122].

3.3.2.3 Schoolfield-Modell

As the objective function for this model (see equation 16) featured different local minima, according to Heitzer et al. [67] it was reasonable to adapt a 4 parameter model in a first step. Therefore, the exponential expression representing the inactivation of the master enzyme at low temperatures, was eliminated. For μ_{max}, $q_{O2,max}$ and f_{temp} the low temperature range was set below 283 K. Medium range was defined between 286 and 300.5 K and high range above 303 K. Results of the parameter determination are given in the appendix (Table 34). Analogue to this modus operandi parameters were determined for the suboptimal temperature range, i.e. low and medium temperatures. (see Table 35). In the following step the remaining parameters were calculated (appendix Table 36).

Heitzer et al. [67] found questionable values for the parameter of this model concerning the biological interpretation, e.g. negative ΔH^0 (not shown). Similar problems occurred for example for $q_{O2,max}$ in Table 36 (appendix). No comparable values could be found in literature. A comparison of calculated enthalpies to activation / inactivation enthalpies of substrate carrier proteins or of enzymes out of the basic pathways of metabolism could be conceivable. The thermodynamic parameters of this model, however, should not be understood as biological parameters, since master reactions are not characterised. They should rather be interpreted as strain specific constants, which are valid for the specific experimental conditions [67]. The predicted growth optimum of $T_{opt} = 27{,}9°C$ ($\mu_{max,opt} = 0{,}38\ h^{-1}$) however was reasonable (see Figure 27). Maximum or minimum temperatures could not be calculated, as the model was approximating the abscissa asymptotically (see Figure 24).

3.3.2.4 Model of Mohr and Krawiec

The model of Mohr and Krawiec was modified by a shift of the temperature axes in order to avoid inaccuracies in the parameter calculation due to extreme preexponential coefficients:

$$\mu(T) = \frac{1}{A_1 \cdot exp\left[\frac{E_{a1}}{R}\cdot\left(\frac{1}{T}-\frac{1}{t}\right)\right] + A_2 \cdot exp\left[\frac{E_{a2}}{R}\cdot\left(\frac{1}{T}-\frac{1}{t}\right)\right]} - B \cdot exp\left[-\frac{E_b}{R}\cdot\left(\frac{1}{T}-\frac{1}{t}\right)\right]. \qquad (43)$$

This model was also fitted on the data in several steps. The parameter t was fixed to 288 K. By elimination of the subtrahend and setting A_2 to zero, an adaptation to the medium temperature range was carried through by calculation of the two remaining parameters (see Table 37 in the appendix). For representation of the sub optimal temperature range, the model was extended to a four parameter model. Initial values and results are given in Table 38

(appendix). Finally, the complete six parameter model was fitted on values of the whole temperature range (see Table 39).

Whereas values for the parameters E_{a1} in Table 37 or E_b in Table 39 were in the same order of magnitude as reported in literature (E_a=118996 J·mol^{-1} und E_b=506990 J·mol^{-1} for the specific growth rate of *Saccharomyces cerevisiae* [25]), the values of E_{a1} did not fit in this range. Solely the parameter E_{a1} of f_{temp} seemed to be biologically reasonable. The biological impact of the parameters of this model has to be interpreted deliberately, similar to the parameters of the Schoolfield approach. The predicted growth optimum was also in a realistic range with 29.3°C (see Figure 27).

3.3.2.5 Comparison and evaluation of the results

Figure 22 to Figure 27 compare the results of all models compared to the data sets of estimated parameters (metabolic model) $q_{O2,max}$, f_{temp} and μ_{max} of experiments A (see Table 41). Based on the calculated sum of squares due to error (SSE) for each temperature model and the mean deviation of model and data, it could be stated that the Schoolfield model described the data best. This could be verified concerning the four parameter model (Table 35) for the suboptimal temperature range (278 - 300.5 K) as well as concerning the six parameter model (Table 36) for the whole temperature range (278 – 308 K in the cases of μ_{max} and f_{temp} or 278 - 305 K in the case of $q_{O2,max}$). In view of the well founded model theory this result could have been expected [125, 126]. On the other hand it was not examined whether other models represent other data sets of other experiments better. In the order of descending accuracy the model of Mohr and Krawiec, the Bělehrádek model and the square root approach were following. The accuracy of the Schoolfield model was nearly reached by the model of Mohr and Krawiec. A weak aspect of the latter approach however is the transition from the sub optimal to the super optimal temperature range for the regarded data sets. The abstraction of two processes in the opposite direction proved to be inadequate in this application.

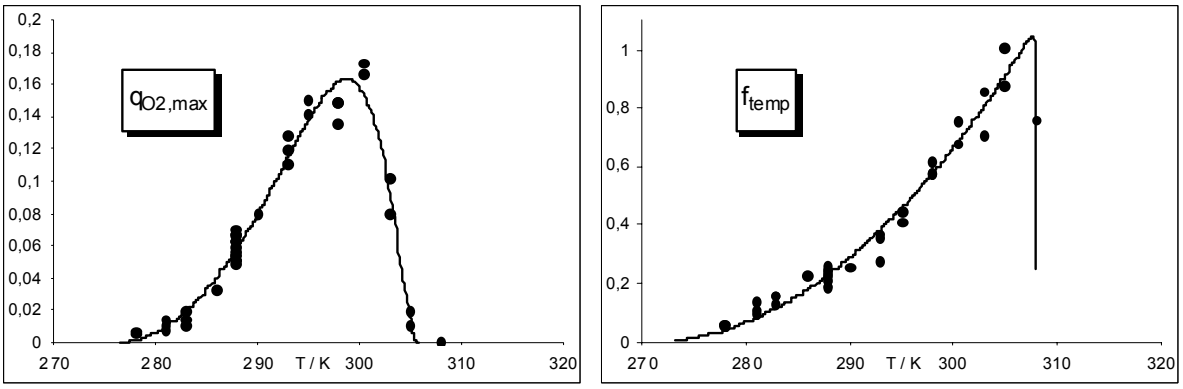

Figure 22: Square root modell fitted on data sets of $q_{O2,max}$ and f_{temp}.

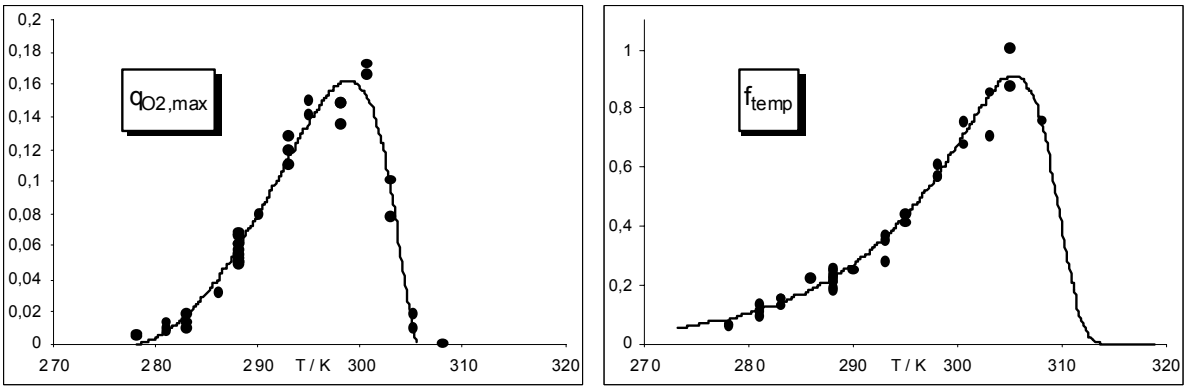

Figure 23: Belehradek Model fitted on data sets of $q_{O2,max}$ and f_{temp}.

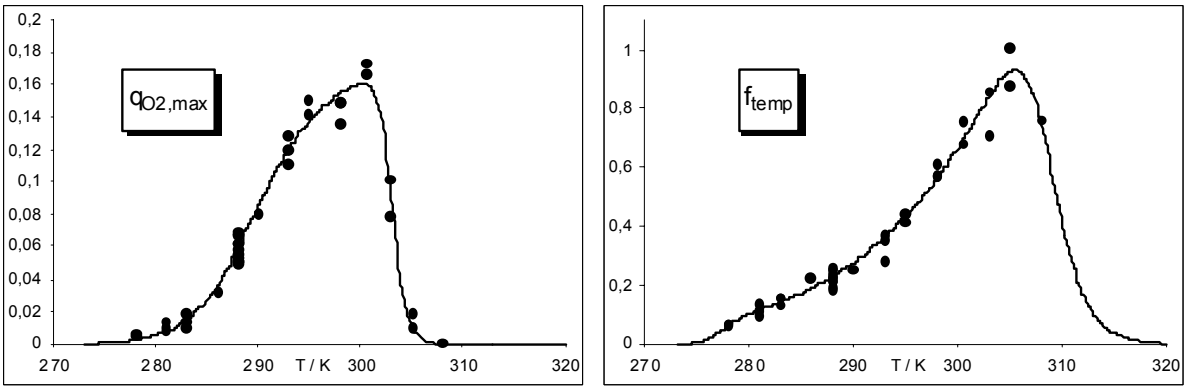

Figure 24: Schoolfield model fitted on data sets of $q_{O2,max}$ and f_{temp}.

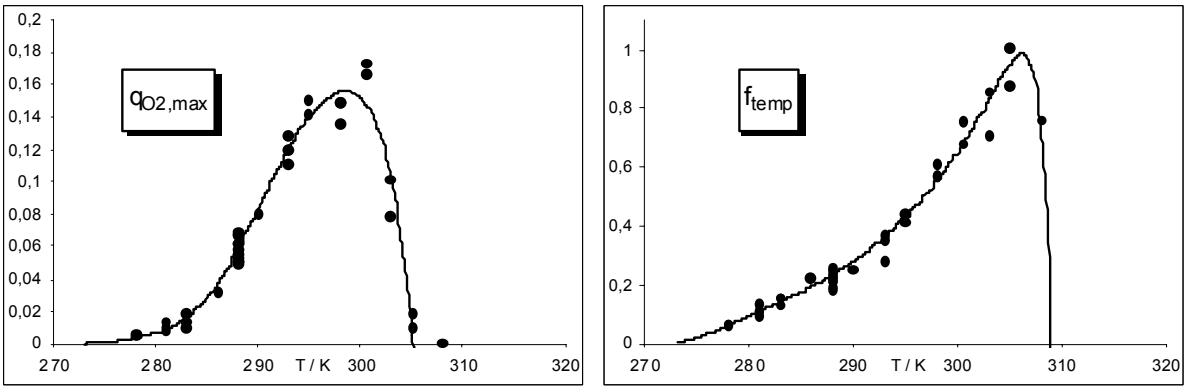

Figure 25: Mohr and Krawiec model fitted on data sets of $q_{O2,max}$ and f_{temp}.

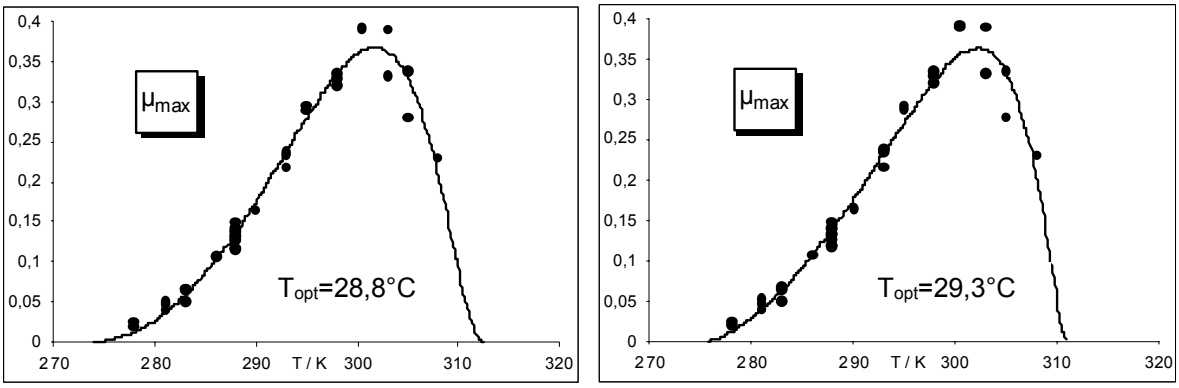

Figure 26: Square root model (left) and Bělehrádek model (right) fitted on data sets for μ_{max}.

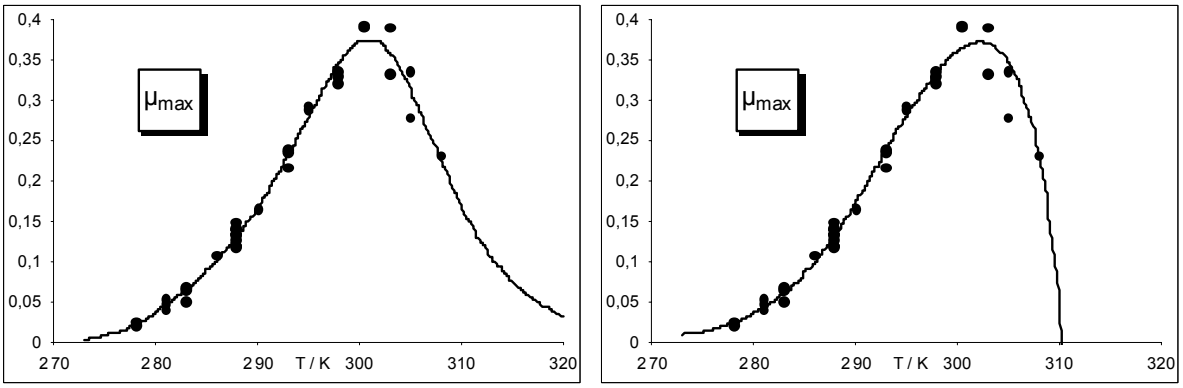

Figure 27: Schoolfield model (left) and Mohr and Krawiec model (right) fitted on data sets for μ_{max}.

The superiority of the Schoolfield model was ascertained before by Adair et al. [1]. Ratkowsky, however, doubted the superiority of the Schoolfield model and accounted wrong stochastic assumptions and data transformation effects for this result [115]. Therefore, the results of this work should be challenged as well, as here similar to the proceeding of Adair et al. the parameter estimation was based on the minimisation of unweighted squares of errors. Typically, in order to include the variance of measurement values, SSE are weighted according to the following equation.

$$\text{Weighted SSE}\left(p_1,\ldots,p_m\right)=\sum_{k=1}^{n}\left(\frac{\left(f\left(x_k;\vec{p}\right)-y_k\right)^2}{\text{Var}\left(y_k\right)}\right) \tag{44}$$

So, the consideration of values with a large variance was prevented. In order to achieve a sufficient regression curve, it was important that the variances of the data points (at each temperature) were nearly constant, especially if unweighted SSE were applied. Prevalent methods for homogenisation of variances are data transformations as $\sqrt{\mu}$ (see square-root-model) or $\ln(\mu)$. Effects of the transformation should be evaluated for each application. In the regarded application for the data sets of experiments A for the temperatures 286, 290 and 308 K only single data points were available. Therefore, the weighted SSE was not applicable

without neglecting these data points. All the more it is of importance that the variances of the other data points were on a low level. Figure 28 to Figure 30 show the calculated variances of μ_{max}, f_{temp} und $q_{O2,max}$ and their transformations (not full scale).

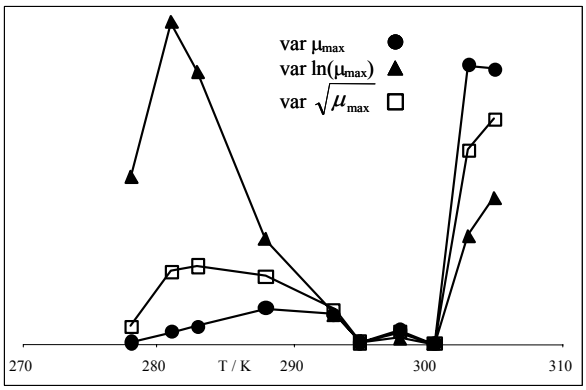

Figure 28: Variances of μ_{max}, $\ln(\mu_{max})$, $\sqrt{\mu_{max}}$.

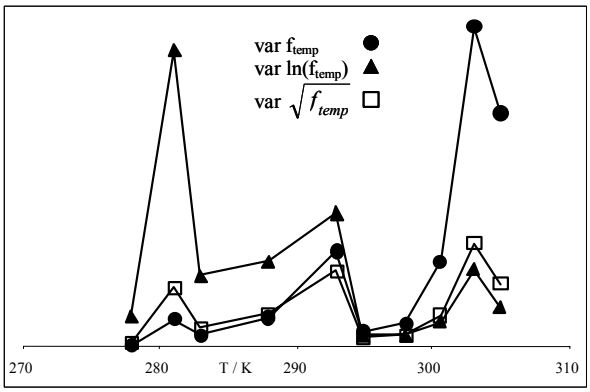

Figure 29: Variances of f_{temp}, $\ln(f_{temp})$, $\sqrt{f_{temp}}$.

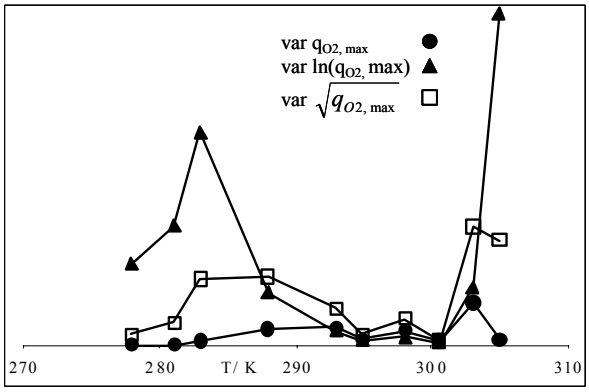

Figure 30: Variances of $q_{O2,max}$, $\ln(q_{O2,max})$, $\sqrt{q_{O2,max}}$.

The progression of the different variances showed that generally a data transformation was not necessary. Large variance occurred only in the cases of μ_{max} and f_{temp} at temperature of 303 and 305 K which were caused by two values. In some cases data transformation caused the opposite effect, for example for $q_{O2,max}$. For μ_{max} no transformation increased the homogeneity significantly. In the case of f_{temp}, a square root transformation could have resulted in a better regression. However, especially for the Schoolfield model, this effect was not expectable due to the quasi linear progression of f_{temp} versus the temperature.

Summarising, the Schoolfield model, after determination of six parameters, described the data sets for $q_{O2,max}$, f_{temp} and μ_{max} very accurate. Hence, the Schoolfield model was ready to be implemented in the Black Box or metabolic modelling approach. Apart from data sets of experiments A, the model was fitted on data sets of experiment B as well (not shown), however, as less data sets were available, a four parameter model was chosen for the sub optimal temperature range. Final parameters referring to these experiments are summarised in the appendix (Table 40). Table 41 and Table 42 present the data sets of parameters f_{temp} and

$q_{O2,max}$ and μ_{max}, respectively, estimated for simulations of propagations of experiments A using the the metabolic or Black Box model. According data sets for experiments B are listed in Table 24.

3.3.3 Validation of the influence of oxygen as manipulated variable

Compared to the temperature, practice relevant concentrations of dissolved oxygen in the regarded range of 0.1 to 0.8 ppm for experiments at 15°C (experiments A) or 20°C (experiments B) possessed a minor influence on the biomass growth. However, lower dissolved oxygen concentrations than 0.1 ppm decreased the specific growth rate due to oxygen limitation effects, e.g. to 70% at 0.05 ppm dissolved oxygen concentration (not shown). This confirmed results of Manger et al. [91] and kinetic experiments of Hartmeier [61] or Cho et al. [31] and is therefore not presented in detail. Figure 31 illustrates the influence of the dissolved oxygen concentration on the yield (gravity / biomass). For isothermal experiments (♦ experiments A at 15°C and ■ experiments B at 20°C) the yield is plotted. Below concentrations of 0.1 ppm the yield is increasing rapidly for both experiments. This could not be substantiated by the size of the oxidative bottleneck, which appeared to be dependent on the temperature (comp. chapter 3.3.1). Rather the oxygen uptake kinetic was limited by the available dissolved oxygen concentration. Transport phenomena appeared to dominate in this case over metabolic regulation effects.

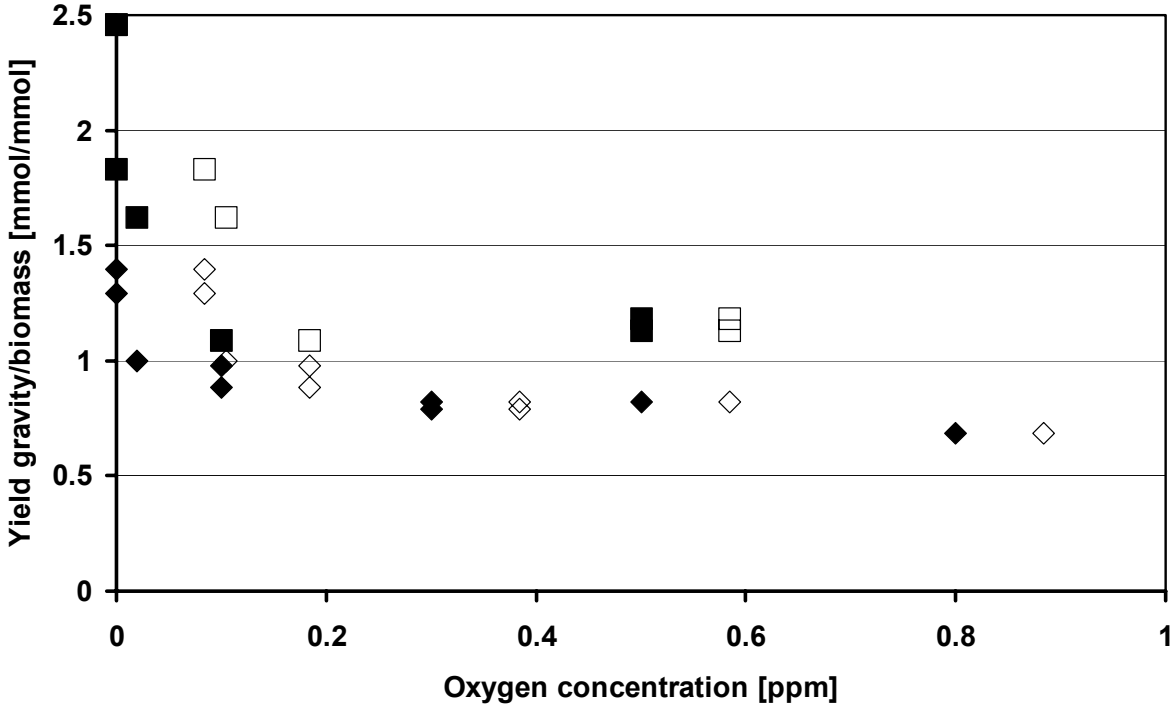

Figure 31: Yield (gravity/biomass) dependent on the dissolved oxygen concentration. Measured: ♦ experiments A at 15°C, ■ experiments B at 20°C; Calculated: ◊ experiments A at 15°C and □ experiments B at 20°C.

During experiments B one propagation was run with 0 ppm dissolved oxygen concentration and one propagation with 0 ppm and evacuation of air before filling. Both yields of both experiments resulted on a different level (left side of Figure 31). Therefore, theoretical oxygen concentrations were calculated using the metabolic modelling approach. For this purpose the temperature dependency of the variable parameters was implemented in the model (Schoolfield model comp. chapter 3.3.2) and the dissolved oxygen concentration was estimated in a parameter estimation procedure. The symbols ◊ and □ indicate calculated dissolved oxygen concentrations for experiments A and B respectively. The calculated concentration could be interpreted as the real oxygen concentration in the propagator without measurement errors due to matrix effects of the sensor device. The difference between the measured value (zero) and the calculated value was added as an offset in further simulations of experiments concerning low oxygen concentrations. A sensitivity analysis based on data of propagations with dissolved oxygen concentration below 0.1 ppm and occurring dissolved oxygen limitation, showed a relevant influence of K_o on the biomass growth (see Table 20). Other parameters were not affected significantly. However, a particular implementation of the dissolved oxygen dependency in the process models was not necessary, because the dependency was represented by the temperature dependent maximum specific oxygen uptake rate $q_{O2,max}$ and the fixed half saturation constant $K_o = 0.00121$ mmol/L [31, 61] without an individual adaptation.

3.4 Process control scenarios for brewing yeast propagations

With the formulation of the variable parameters f_{temp} and $q_{O2,max}$ as $f_{temp}(T)$ and $q_{O2,max}(T)$, respectively, and a fixed set of stoichiometric and kinetic parameters, in particular the half saturation constant K_o for oxygen limitation (see Table 12), a predictive simulation of the yeast propagation process was possible even for the application of temperature and dissolved oxygen profiles. Herewith a prerequisite for the realisation of an active process control and evaluation tool for control strategies was established. In order to show this potential, case scenarios were studied, which for example simulate a delay in a preliminary production step.

For the regarded experiments already adapted yeast, inoculated in an exponential state, was used for the propagation. Less than one hour resulted in most experiments for the lag time by the parameter estimation. Therefore, the parameter t_{lag} was fixed to zero for these scenarios. Experiments with dried yeast (not presented here) yielded a temperature dependency of the lag-time similar to trials described in Wijtzes et al. [142] or Gianuzzi et al. [58]. These results, however, could not be confirmed statistically.

3.4.1 Temperature control scenarios

Figure 32 shows yeast propagations performed with two different temperature profiles. Additionally, a parity plot (simulated concentrations versus measured concentrations) illustrates the accuracy of all realised temperature scenarios in experiments A. For simulation, the Schoolfield temperature functions of experiments A (comp. chapter 3.3.2.) were integrated in the metabolic model for $q_{O2,max}(T)$ and $f_{temp}(T)$.

The first graph demonstrates a temperature decrease from 30°C to 10°C during the propagation run. Simulation results (lines) matched the data points for biomass and substrate very well along the entire temperature range. Mean deviations resulted between simulated and measured concentrations of 8.5 mmol/L ($5.76*10^6$ cells/mL) for biomass and 7.28 mmol/L (0.13% w/w) for substrate.

The second graph represents a typical control scenario with a temperature profile 20°C-10°C-20°C. The potential of an active control could be pointed out with these kind of scenarios, in particular by the deceleration of biomass growth and substrate uptake at a process time of 7.5 h and the acceleration at process time 15 h during the temperature control scenario. With the regarded temperature profile a delay of the yeast propagation process of about 6 hours could be achieved compared to an isothermal 20°C propagation run and the pitching yeast could be harvested out of the exponential state of the propagation. Also, in this case, simulation results fitted the reference data very well. A mean deviation between simulation and measurement of 7.18 mmol/L ($4.87*10^6$ cells/mL) for biomass and of 6.66 mmol/L (0.12% w/w) for substrate concentration was achieved for all temperature scenarios realised in experiments A. Additionally, the third graph demonstrates that deviations between simulated and measured values for both biomass and substrate concentration for most cases were within the allowance of ± 10 mmol/L ($6.78*10^6$ cells/mL or 0.15% w/w). A more detailed statistical evaluation is given in the appendix (Table 43).

Next Page

Figure 32: Temperature scenario metabolic model. Measured concentration of biomass (○) and substrate (▲) are shown. Simulation results are indicated as lines. Temperature in the propagator is plotted as dashed line.

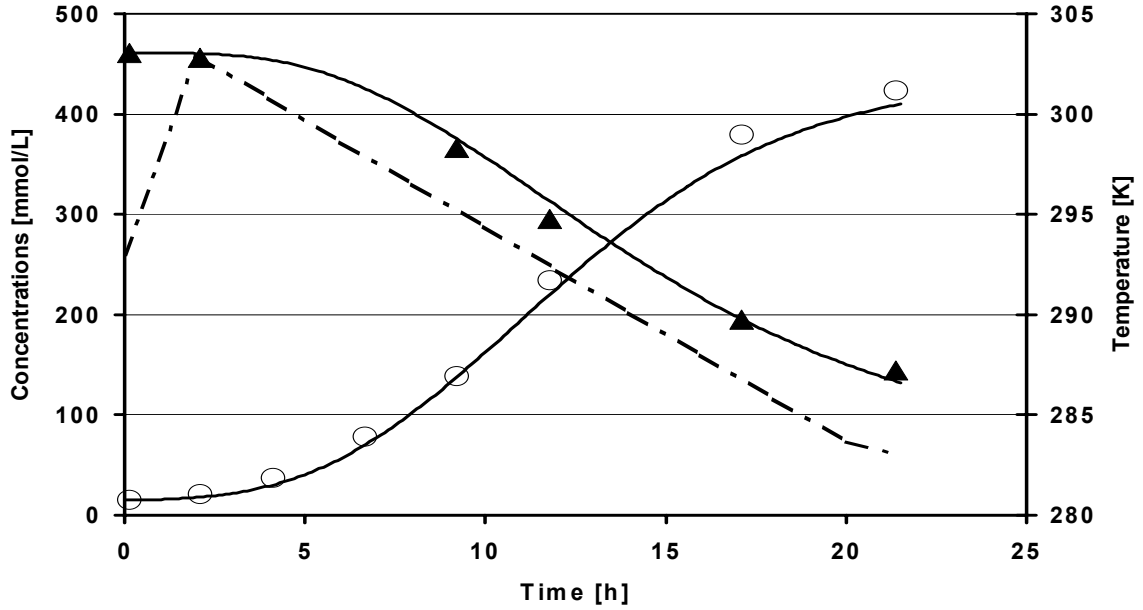
Concentrations [mmol/L]
Temperature [K]
Time [h]
0
100
200
300
400
500
280
285
290
295
300
305
0
5
10
15
20
25

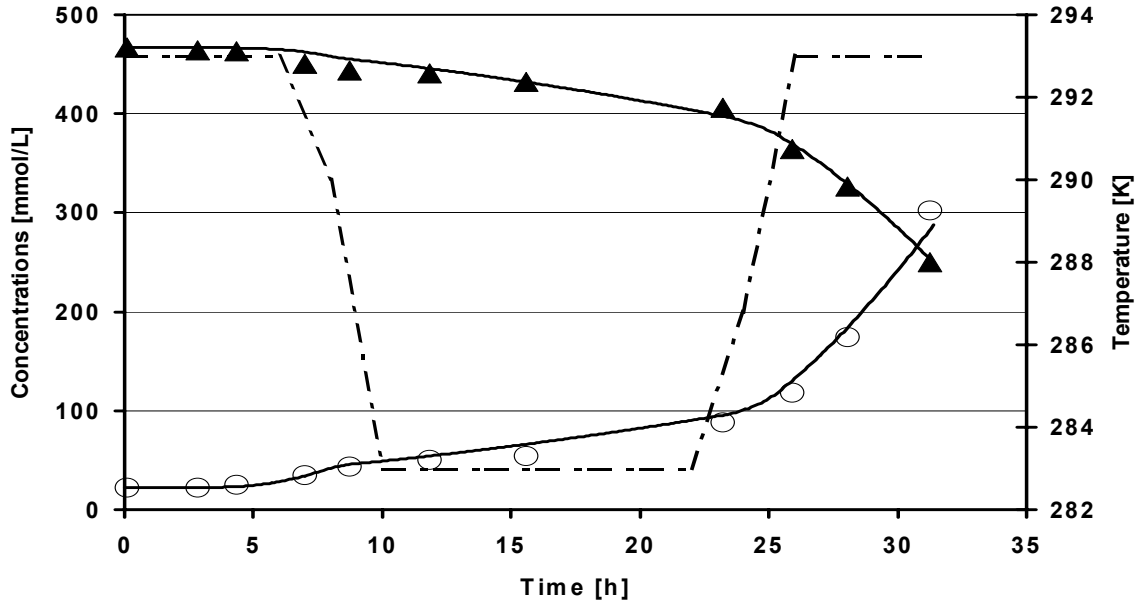
Concentrations [mmol/L]
Temperature [K]
Time [h]
0
100
200
300
400
500
282
284
286
288
290
292
294
0
5
10
15
20
25
30
35

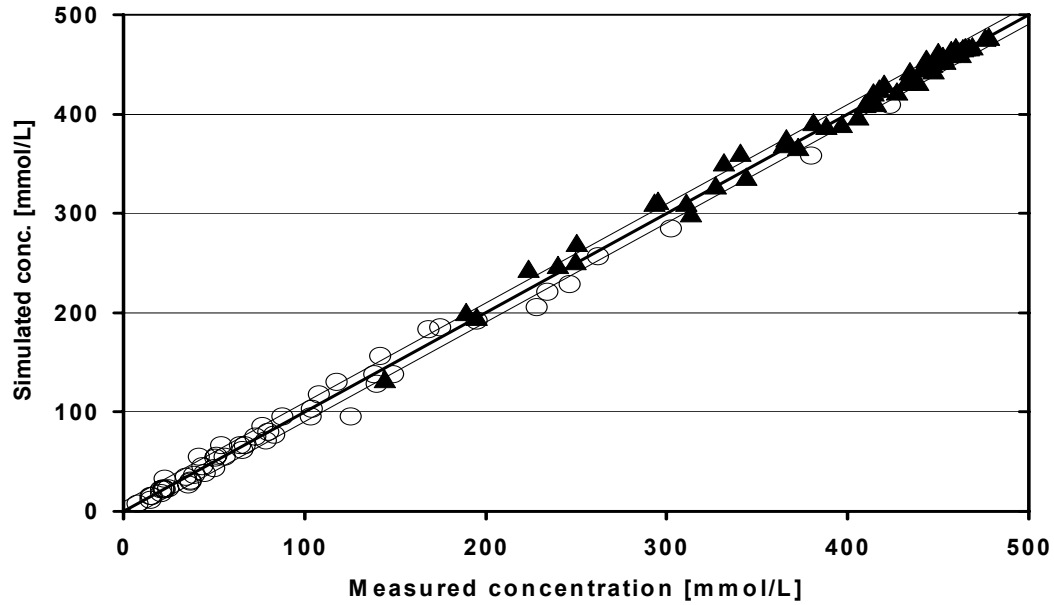
Simulated conc. [mmol/L]
Measured concentration [mmol/L]
0
100
200
300
400
500

The failure of temperature control is a practice relevant disturbance, which allows to prove the validity of the temperature functions in the modelling approach in particular. In such a case it is important to evaluate the effect of the "unplanned" temperature profile on the propagation process in order to create a new propagation strategy. Figure 49 (appendix) shows the progressions of the simulation runs and the reference data for a temperature profile resulting of a simulated failure of the temperature control. After 8 h the temperature was decreasing to 10°C followed by a fast increase to 25°C and finally a temperature of 19°C was reached. The deceleration of the biomass growth within the cooling phases and the acceleration during the heating phases of the scenario is obvious. The process model even represented reactions of the yeast metabolism on very fast changes in temperature.

Model based simulations using the Black Box model resulted in similar results after application of the regarded temperature profiles (see Figure 48 in the appendix). Analogue to temperature scenarios within experiments A, control scenarios were accomplished in experiments B. Temperature functions (Schoolfield model) for experiments B were integrated in the metabolic model for $q_{O2,max}(T)$ and $f_{temp}(T)$. Lag time was set zero for these propagations (previously propagated inoculum). A statistical evaluation of these trials is listed in Table 44.

3.4.2 Dissolved oxygen scenarios

Similar to the latter scenarios, in Figure 33 different profiles of dissolved oxygen concentration were realised in order to examine the influence of dissolved oxygen as manipulated variable and to evaluate the model based simulation as an instrument for an active process control. Scenarios of experiments A are studied. The first graph presents a scenario using a constant aeration rate. Due to increasing oxygen demand during the yeast growth, the oxygen concentration was decreasing continuously. In the interim, the aeration rate was increased for a short time, which can be seen in a short increase of dissolved oxygen concentration. The second graph represents an oxygen control scenario. Dissolved oxygen concentration was decreased from 0.5 ppm to 0.08 ppm. 0.08 ppm represented the calculated dissolved oxygen concentration while 0 ppm was measured (comp. chapter 3.3.3). After a holding time of four hours it was increased back to the initial concentration. These experiments were run at a temperature of 20°C.

Next Page

Figure 33: Oxygen scenario metabolic model. Measured concentration of biomass (○) and substrate (▲) are presented. Simulation results are indicated as lines. Oxygen concentrations in the propagator are plotted as dashed lines.

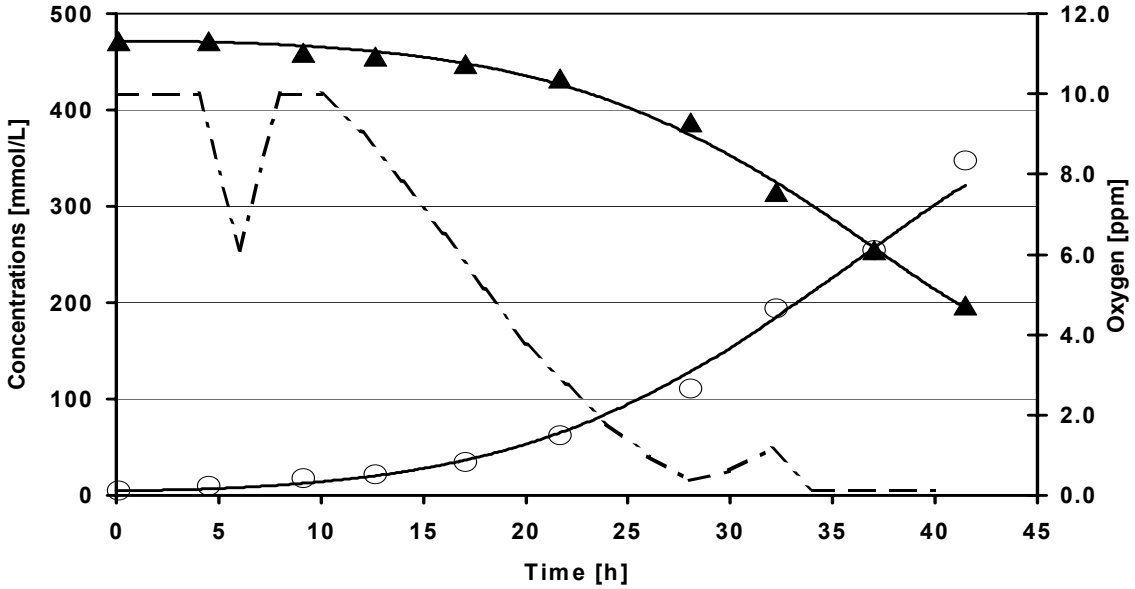
Concentrations [mmol/L]
Oxygen [ppm]
Time [h]
0
100
200
300
400
500
0.0
2.0
4.0
6.0
8.0
10.0
12.0
0
5
10
15
20
25
30
35
40
45

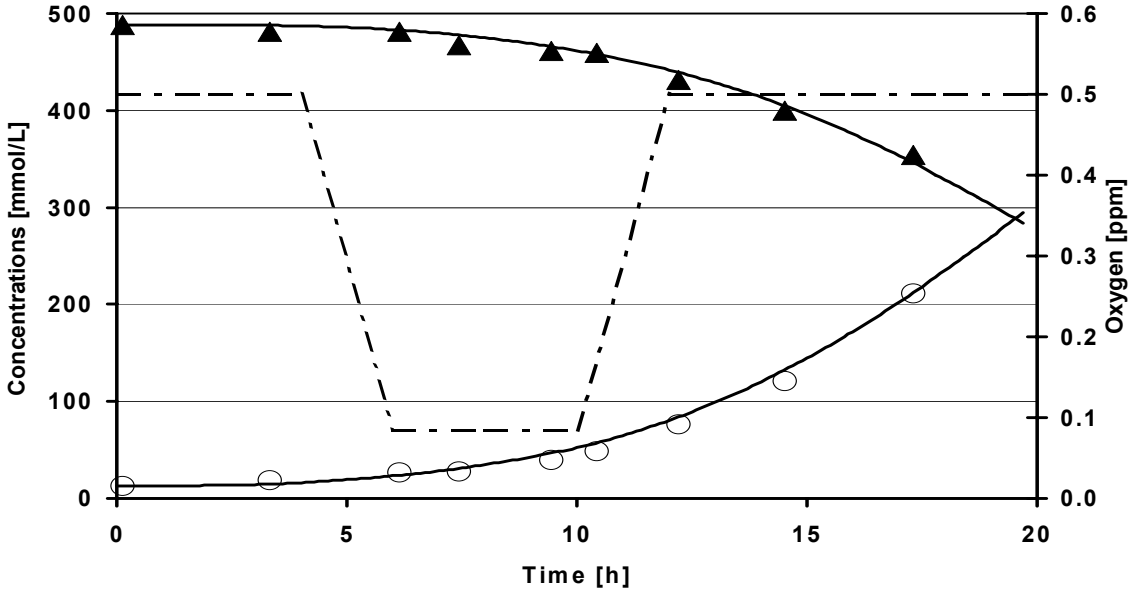
Concentrations [mmol/L]
Oxygen [ppm]
Time [h]
0
100
200
300
400
500
0.0
0.1
0.2
0.3
0.4
0.5
0.6
0
5
10
15
20

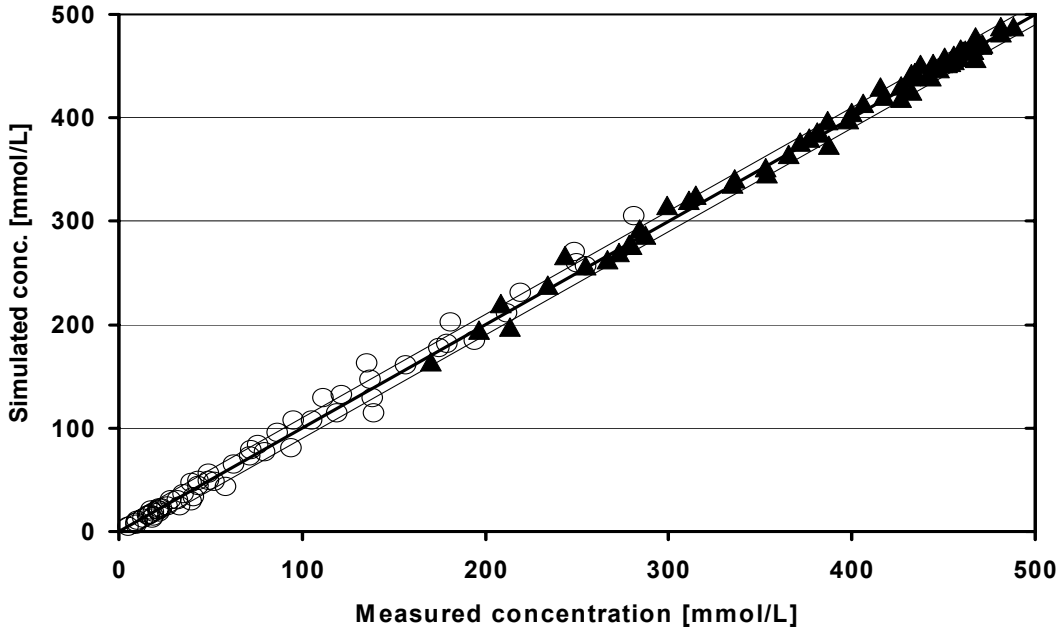
Simulated conc. [mmol/L]
Measured concentration [mmol/L]
0
100
200
300
400
500

With the presented scenario a reduction of the specific growth rate to 70% compared to a propagation with 0.5 ppm dissolved oxygen concentration could be achieved. A further deceleration of the growth rate should be possible using nitrogen or carbon dioxide for aeration. This was realised in experiments B. But the desired deceleration of biomass growth applying an oxygen limitation caused a higher ethanol production and potentially a lower activity during following fermentations (see Figure 31 in chapter 3.3.3). The third graph proves in a parity plot, that deviations between model based simulation and reference values lied in the defined allowance of ± 10 mmol/L ($6.78*10^6$ cells/mL or 0.15% w/w) for concentrations of biomass and substrate. For all dissolved oxygen scenarios a high accuracy of the simulation was reached. Regarding the performance of the metabolic model for experiments A, mean deviations between simulated and measured concentrations were 6.42 mmol/L ($4.35*10^6$ cells/mL) for biomass and 5.34 mmol/L (0.09% w/w) for substrate. The Black Box model performed more inaccurate with mean deviations of 8.87 mmol/L ($6.0*10^6$ cells/mL) and 8.57 mmol/L (0.15% w/w) for biomass and substrate concentrations, respectively. Simulations for experiments B were carried out with the metabolic model only. Here, mean deviations of 7.08 mmol/L ($4.8*10^6$ cells/mL) and 7.55 mmol/L (0.13% w/w) for biomass or substrate concentrations could be achieved. A more detailed statistical evaluation is provided in Table 45 (see appendix).

3.5 Simulations of industrial batch propagations

Model validation under industrial conditions was realised with experiments in four different breweries. The experiments varied in the applied propagation procedures, the volume of the propagation plants, the applied temperatures and in the composition of the growth medium (beer wort) as well as in the inoculated yeast strain. In the following, results are presented especially considering the accuracy of simulations of the experiments in different breweries.

3.5.1 Isothermal propagations

Isothermalc propagations were regarded of experiments E, F and G. Simulations were carried out with the Black Box model only.

3.5.1.1 Results of experiments E

In experiments E a propagation plant for top fermenting yeast was examined (propagation plant 3). Experiments were made at 18°C and 22°C. Figure 34 shows a progression of a yeast propagation at 18°C. Simulated results as well as measured values for biomass, ethanol and substrate concentration are presented. Remarkable were large deviations between the measured and simulated concentration of biomass. However, simulations of ethanol and

substrate concentrations matched very well the measured data. Mean deviations between simulation and measurement and standard deviations are listed in Table 46. The inaccuracies concerning biomass concentration could be recovered also in the statistical evaluation with an unacceptable mean deviation of 33.2 mmol/L ($22.5*10^6$ cells/mL). Partially appearing fluctuations in measured biomass concentrations could not be explained technologically or biologically. A more probable reason lied in non representative sampling methods.

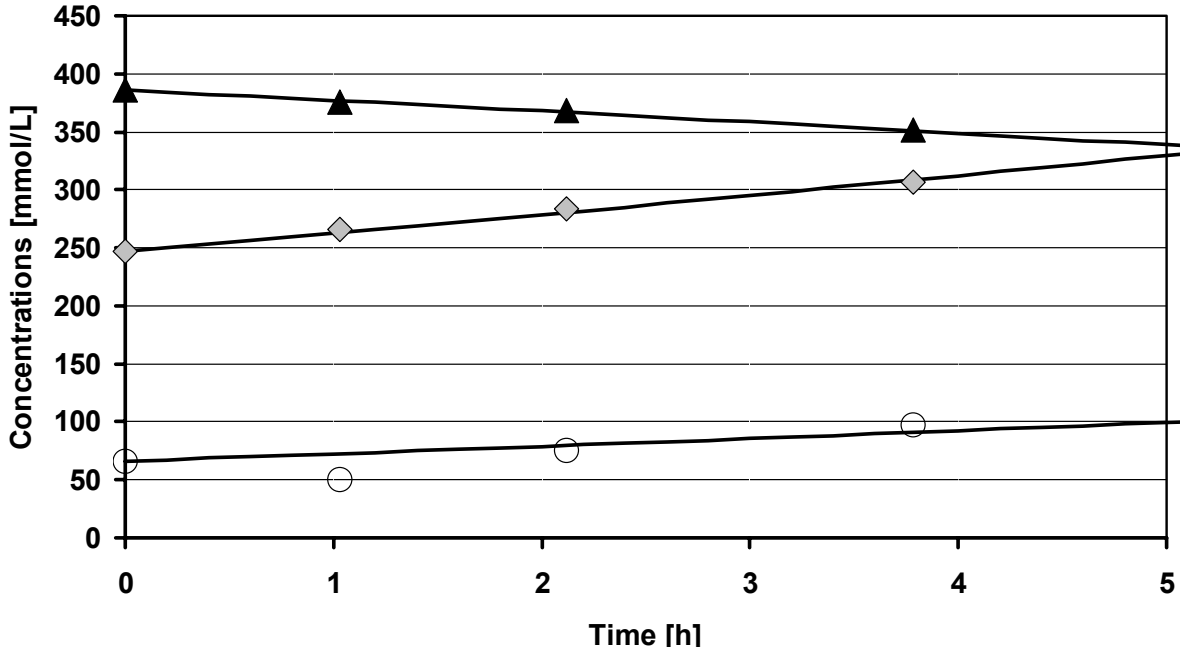

Figure 34: Plot of a growth period of a top fermenting yeast in experiments E at 18°C. Offline measured concentrations of biomass (○), ethanol (◊) and substrate (▲) are plotted. Indicated with lines are results of the model based simulation (Black Box model).

However, deviations concerning concentrations of ethanol or substrate were very low. Mean deviations of 4.4 mmol/L (0.08% w/w) for substrate and 6.5 mmol/L (0.03% w/w) for ethanol concentration anticipated a high accuracy of the simulation. As experiments E were run with a top fermenting yeast *S. cerevisiae* W68, for simulation the parameters f_{temp} and $q_{O2,max}$ of experiments C could be applied. As pulsed aeration was applied for these experiments, an average dissolved oxygen concentration of 0.05 ppm was set for simulations. The lag time coefficient t_{lag} was fitted in a parameter estimation procedure. Simulations of propagation at 18°C or 22°C showed no significant difference in accuracy.

3.5.1.2 Results of experiments F

In experiments F a propagation plant for bottom fermenting yeast was examined (propagation plant 4). Figure 35 exemplarily presents a progression of a yeast propagation at 16°C. Measurement values for concentrations of biomass (○), ethanol (◊) and substrate (▲) are shown. Model based simulations are indicated with lines. For simulation parameters f_{temp},

$q_{O2,max}$ and t_{lag} had to be estimated. Temperature functions for these parameters were not available for the applied yeast strain. Deviations between simulation and measurement values appeared to be very low for ethanol and substrate concentration. However, again slightly larger deviations occurred for the biomass concentration.

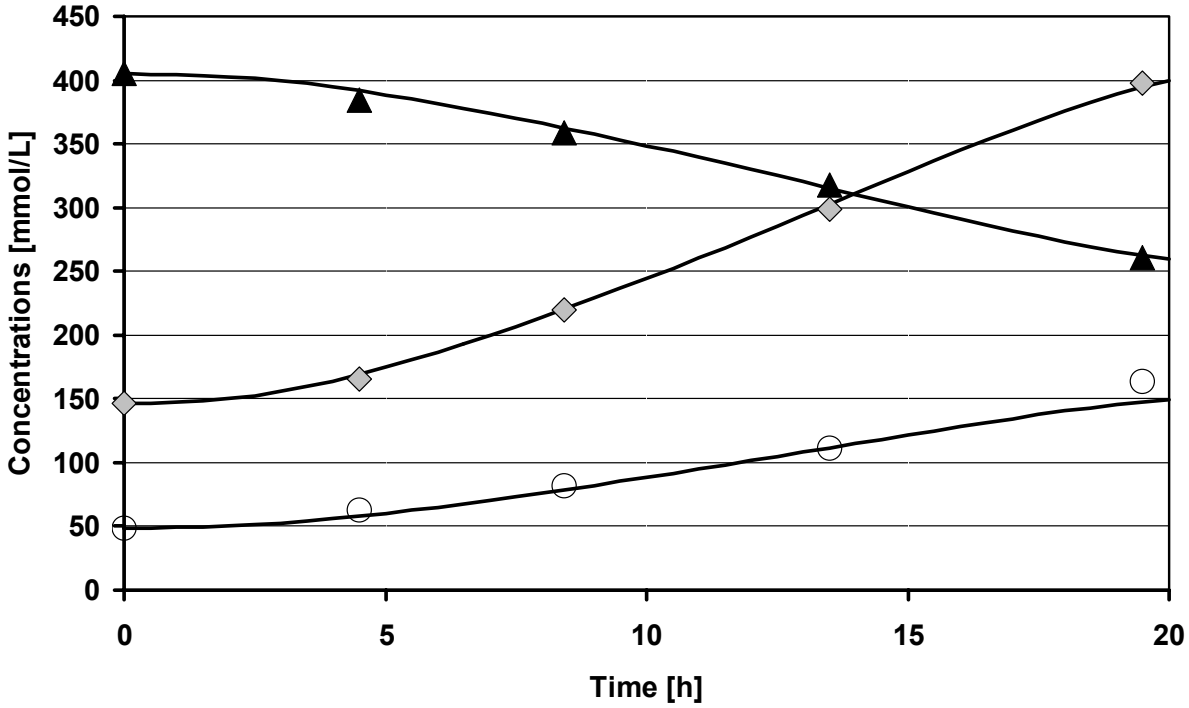

Figure 35*:* Bottom fermenting yeast propagation at 16°C out of experiments F. Offline measured concentrations of biomass (○), ethanol (◊) and substrate (▲) are presented. Results of the model based simulation (metabolic model) are indicated with lines.

Table 46 (appendix) gives a statistical validation of the model based simulations. The mean deviation of the biomass concentration with 7.7 mmol/L or 7.6% ($5.2*10^6$ cells/mL) was slightly over the accuracy of the haemocytometer counting method (Accuracy 5% [54]). Mean deviations of 7.1 mmol/L (0.13% w/w) for substrate concentration again indicated a very high accuracy of the model based simulation. Similarly, the accuracy of the simulation for ethanol concentration was very high (mean deviation 6.6 mmol/L (0.03% w/w). However, in single experiments outliers in measurement decreased the accuracy, which could be proved by higher standard deviations.

3.5.1.3 Results of experiments G

In experiments G a propagation plant for bottom fermenting yeast was examined (propagation plant 5). The yeast was propagated in two steps with 12 and 14°C, respectively. Figure 36 shows exemplarily a propagation run at 14°C. Shown are measurement values for concentrations of biomass (○), ethanol (◊) and substrate (▲). Model based simulations are indicated with lines. As a bottom fermenting yeast strain W34/70 was inoculated, temperature functions of experiments A could be applied for the parameters f_{temp} and $q_{O2,max}$. Lag time was

fitted in a parameter estimation procedure. A statistical examination brought a high accuracy of the model based simulation. The mean deviation of biomass concentration (10.6 mmol/L or 8.8%) only marginally exceeded the assumed accuracy of the haemocytometer cell count method. The lowest deviations were calculated for substrate concentration with 5.93 mmol/L (0.10% w/w). Deviations of about 10.92 mmol/L (0.06% w/w) appeared for the ethanol concentration.

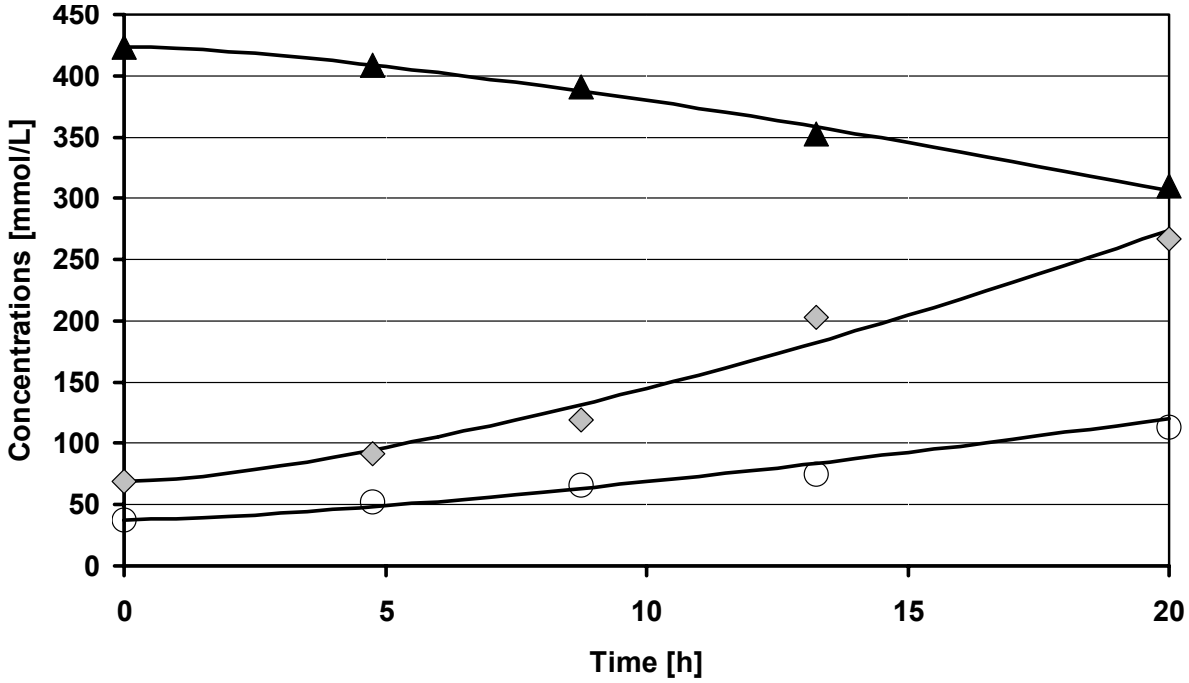

Figure 36: Growth phase in experiments G at a temperature of 14°C. Offline measured concentrations of biomass (○), ethanol (◊) and substrate (▲) are presented. Indicated with lines are results of the model based simulation (metabolic model).

Figure 37 shows a parity plot for measured concentrations of biomass, ethanol and substrate versus simulated data. Regarded were all industrial propagations from experiments E-G. Remarkable was a high deviation between measured and simulated biomass concentrations. On the other hand ethanol and substrate concentration predominantly were within the given allowance of ± 10 mmol/L ($6.25*10^6$ cells/mL or 0.15% w/w).

In comparison to the propagation systems 1 or 2, used for experiments A-D, most of the applied industrial propagation plants were not “ideally” mixed. Especially the system used in experiments E with pulsed circulation resulted in large inhomogeneities for the yeast cells. In experiments F with a continuous circulation and in experiments G with an internal stirrer, increased homogeneities could be achieved compared to the pulsed system. Summarising, total mean deviations for all experiments of 18.5 mmol/L for biomass concentration is calculated in Table 46. Deviation of 5.8 or 7.5 mmol/L for substrate and ethanol concentration lied on a significant lower level. Non representative sampling was as well indicated by a high total standard deviation.

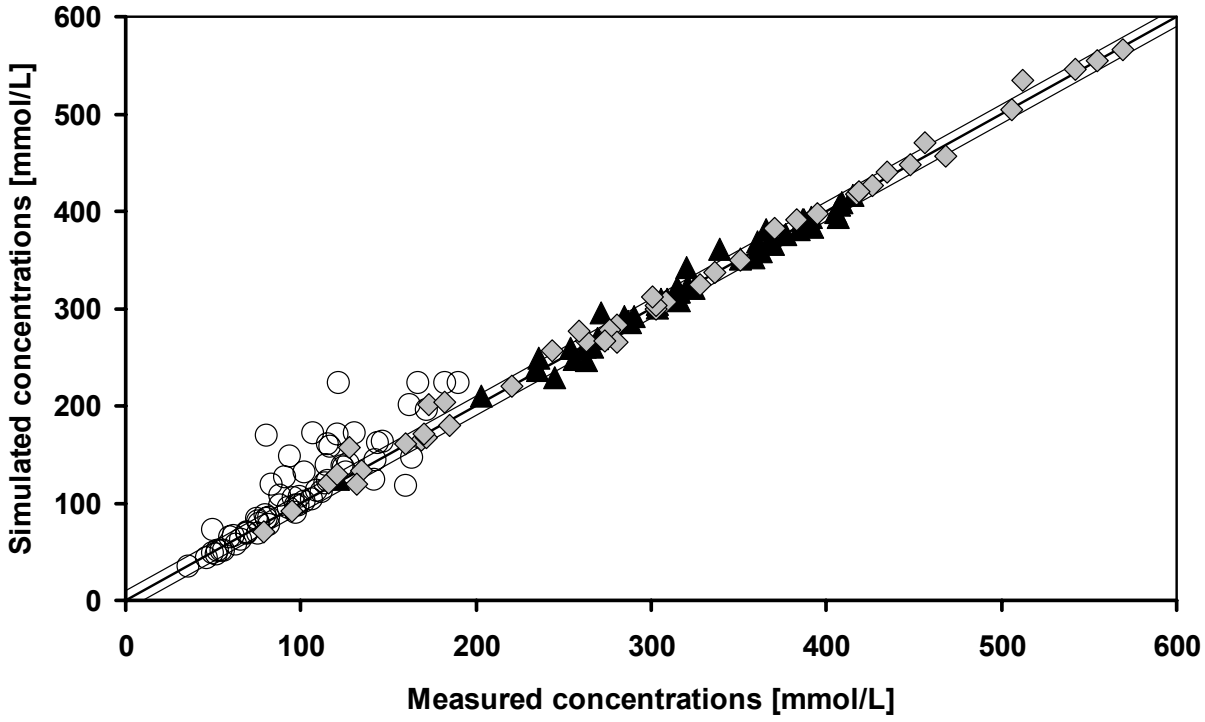

Figure 37: Parity plot of industrial propagations. Data sets from experiments E, F and G were regarded were. concentrations of biomass (○), ethanol (◊) and substrate (▲) are presented.

3.5.2 Sequencing batch propagations

Sequencing batch propagations are common practice in brewing industry. Figure 38 demonstrates an example for this modus operandi. Two subsequent single experiments were coupled and simulated as two steps of one yeast propagation. In this example out of experiments E a top fermenting yeast strain W68 was inoculated, therefore, parameters $q_{O2,max}$ and f_{temp} could be adopted from experiments C. The higher number of measurement values compared to the single experiment (see Figure 34) resulted from samples during pitching and refilling phases. Accuracies achieved by simulation of the single experiments turned out to be not reachable as accuracies decreased by 30%. As main reasons inaccuracies concerning the volume of yeast suspension taken as inoculum for fermentations and the volume of refilled wort were supposed. These procedures were realised manually. Therefore, simulation values lied on a higher level and deviations cumulated for the second phase of the sequencing batch propagation. Nevertheless for practice conditions a sufficient accuracy of the simulation could be reached. Another coupled propagation of experiments E is shown in the appendix (Figure 46). Results were comparable to the above mentioned.

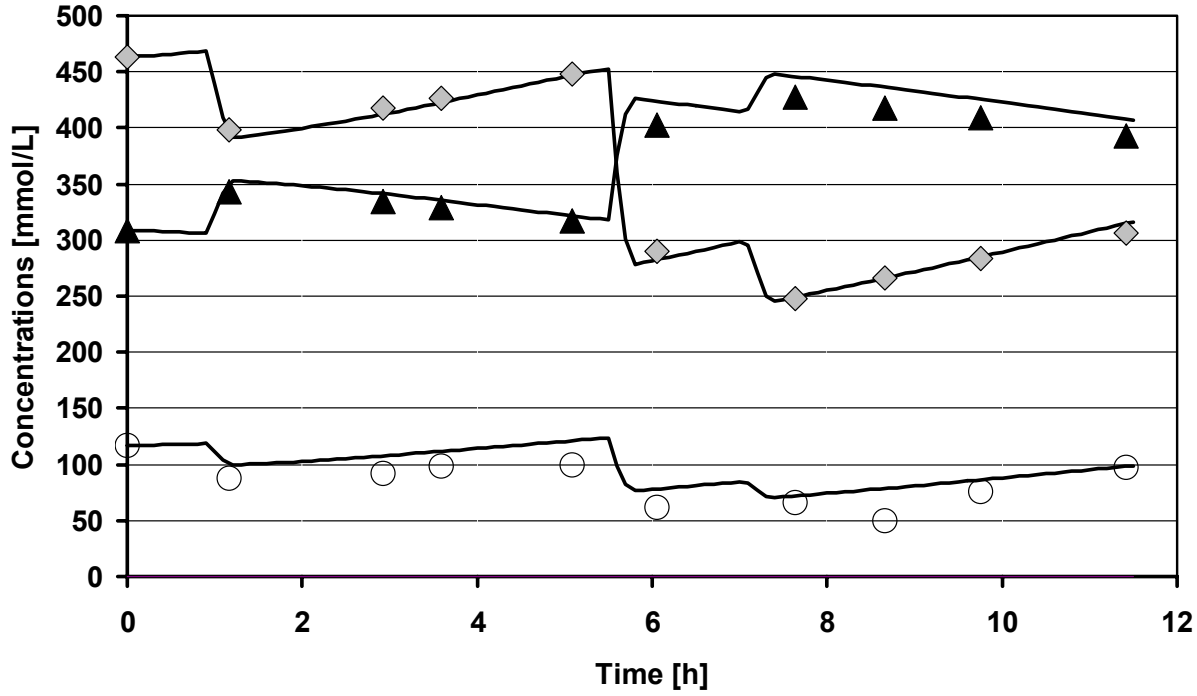

Figure 38: Sequencing batch propagation. Two subsequent growth phases of combined out of two single propagations of experiments E (18°C) are shown. offline measured concentrations of biomass (○), ethanol (◊) and substrate (▲) are presented. Indicated with lines are results of the model based simulation (Black Box model).

Of special interest was the simulation of a coupled bottom fermenting yeast propagation of experiments G (see Figure 47). Here, the propagation was realised in two steps in two different plants at different temperatures. Similar to experiments G for simulation the parameters f_{temp} and $q_{O2,max}$ were adopted from experiments A (Schoolfield model). Accuracies of the belonging simulations were in the same range as in experiments E-G.

3.5.3 Non-isothermal propagations

Experiments H were carried out in a propagation plant similar to propagation plant 1. The yeast suspension was continuously aerated and mixed by an impeller in the bottom of the tank. The same yeast strain as in experiments B was inoculated in the 200 hL fermenter. Different propagation strategies were applied concerning temperature of inoculation and cooling strategy. Figure 39 shows exemplarily a propagation run. The propagation started a 13°C and was not continuously cooled during the process. Presented are concentrations of biomass and substrate. Simulation is indicated by a line. A dotted line represents the temperature progression in the propagation system. Additionally, a parity plot proves that for all experiments made in experiments H the simulated concentrations of biomass and substrate lied in an allowance of of ± 10 mmol/L ($6.78*10^6$ cells/mL or 0.15% w/w) compared to the measured concentrations. Temperature functions of experiments B were implemented for the parameters f_{temp} and $q_{O2,max}$ (Schoolfield model with four parameters). No lag time occurred for the considered experiments. Mean deviations between simulated and measured

concentration are reported in Table 47 in detail. An average value of 5.4 mmol/L ($3.7*10^6$ cells/mL) for biomass and 4.0 mmol/L (0.07% w/w) for substrate concentration indicated a very high accuracy of the simulation runs. Compared to other industrial propagation systems, the applied propagation plant equipped with an internal aeration (comp. Figure 43) and stirrer featured the best homogeneity. Therefore, sampling seemed to be more representative and deviation concerning biomass concentration rested on a low level.

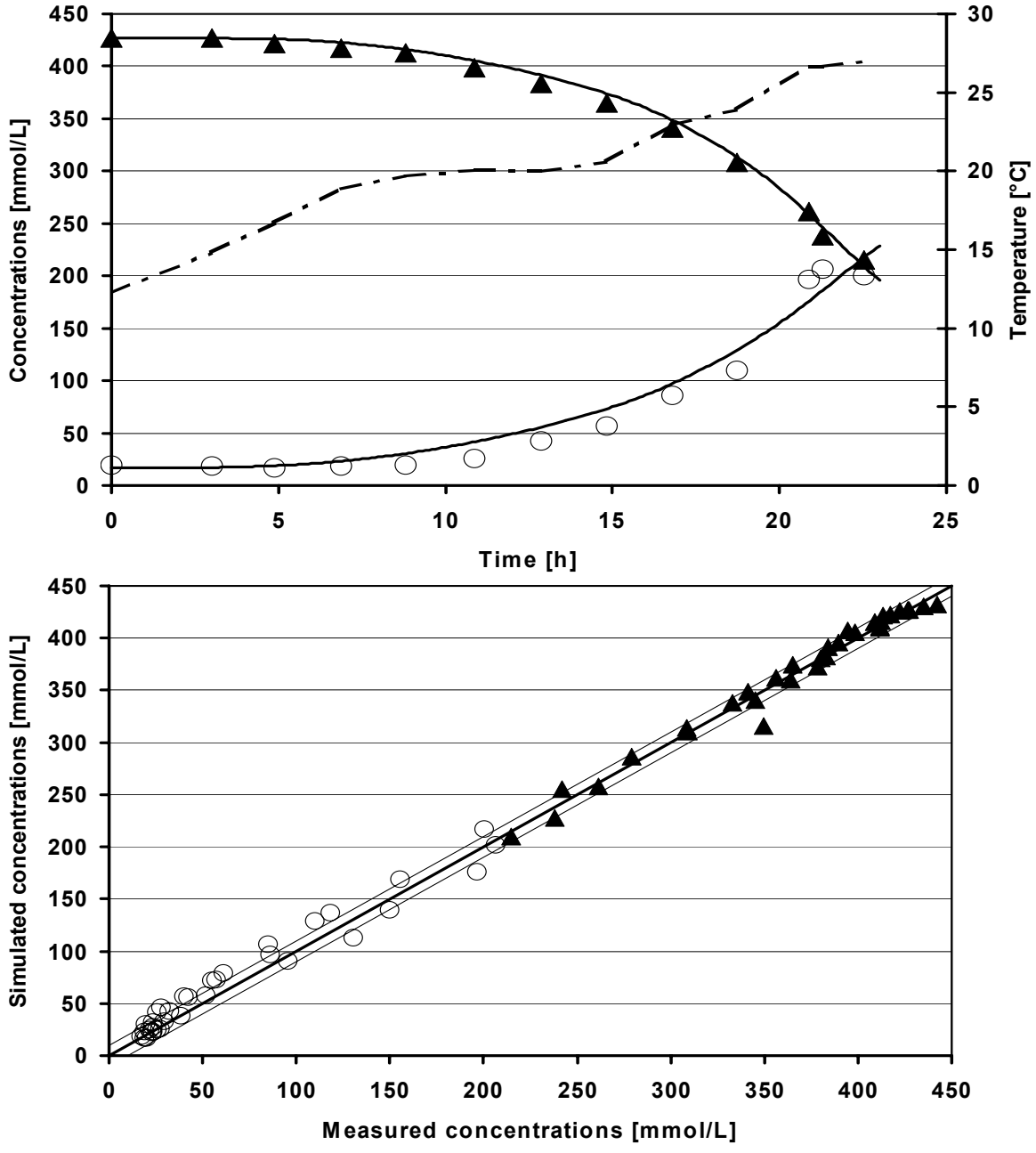

Figure 39: Industrial bottom fermenting yeast propagation (Experiments H). Above progressions of biomass (○) and substrate concentration (▲) during a propagation at increasing temperatures is presented. Results of model based simulation are indicated with lines. A dotted line represents the temperature profile. Below, a parity plot of simulated concentrations of biomass versus the calculated concentrations is shown.

3.6 Simulation of brewing fermentations

Common practice for brewing fermentations is an initial aeration of the beer wort to a dissolved oxygen concentration of about 8.0 ppm. Usually, the oxygen is consumed during the first hours of the fermentation process. During the following phase, the available sugar is metabolised totally anaerobic using the fermentative pathway only. As shown in chapter 3.1, in both modelling approaches a pure fermentative metabolism is implemented. However, at least for bottom fermenting yeast strains, a physiologically reasoned sedimentation during the fermentation is known and desirable, in order to be able to harvest a sufficient amount of yeast for further inoculation in brewing practice.

In industrial cylindroconical fermentation tanks (CCF) this phenomenon is not of practical relevance for simulation as the sedimentation process was too slow and biomass concentration seemed to remain constant after finishing the growth phase. However, in small CCF or in horizontal tanks a decrease in biomass concentration was observed.

Mean values for sizes of yeast cells are known to be around 10 µm [85, 102]. However, cell diameters of a bottom fermenting yeast strain W34/70 were measured to be distributed between 7 and 25 µm (not published results). Cells with a diameter between 7 and 15 µm had 72% of the cell mass. The remaining cells were in a range between 15 and 25 µm. These data allowed to calculate for each yeast diameter the belonging portion of the whole cell population concerning volume or weight. Assuming yeast cells to be globular particles, which are sedimenting in a fluid, bigger particles would sediment faster. If all particles of one size passed the sampling level of a CCF, they were not longer detectable and the concentration of suspended particles decreased. To allow a simulation of the yeast fermentation in small or horizontal tanks, the Black Box modelling approach was extended by a sedimentation model. For this model, several assumptions were made:

- The yeast is suspended ideally at the beginning of the fermentation,
- No convection or mixing occurs,
- Yeast cells can be described as particles with a certain size distribution and
- Density and viscosity of the wort is constant during the fermentation or progression of both quantities can be expressed as function of known quantities (e.g. sugar concentration)

According to Podgornik et al. [110] an incremental method of a suspension model was applied in this work. This method is based on the observation of the progression of the biomass concentration at the sampling level of a CCF.

Experiments were carried out in a 10 hL CCF. The sampling level was 1.5 m below the fluid level. As fermentations were performed with the same yeast applied in experiments B,

the distribution was adapted for this strain. The adjusted distribution was integrated in the sedimentation model after classification in 10 cell size classes (see Table 21).

Table 21: Classes of cell sizes and belonging mass portions for the sedimentation model. Sedimentation velocities and sedimentation times were calculated according to equations (45 and 46. A portion of 3% remains in suspension.

Class	Mass portion [%]	Mean diameter [µm]	Sedimentation velocity [m/s]	Sedimentation time [h]
1	12	25	1.6E-05	24.59
2	7	23	1.4E-05	29.05
3	6	21	1.1E-05	34.85
4	7	19	9.7E-06	42.57
5	8	17	7.8E-06	53.18
6	8	15	6.0E-06	68.31
7	9	13	4.5E-06	90.94
8	21	11	3.2E-06	127.02
9	15	9	2.1E-06	189.75
10	4	7	1.3E-06	313.66

According to Stokes, sedimentation velocity w_f, in the quiescent wort postulated, was calculated as

$$w_f = \frac{(\rho_Y - \rho_F) * g * d^2}{18 * \eta_F} \qquad (45)$$

with ρ_Y = 1080 kg/m^3 (density of the yeast cell) [23, 82], ρ_F = 1005.6 kg/m^3 (density of beer at 20°C [82], g = 9.81 m/s^2 (gravitational acceleration), η_F = 1.556 mPas (dynamic viscosity of beer at 20°C [82]) and d representing each diameter of the cell classes in Table 21.

Sedimentation time t is calculated as

$$t = \frac{h}{w_f} \qquad (46)$$

with h = 1.5 m for the regarded CCF and w_F calculated in equation 45.

After each of these sedimentation times the cell concentration calculated with the Black Box model was reduced by the mass portion of the belonging cell class. Figure 40 presents exemplarily a fermentation run of the regarded 10 hL fermenter. Presented are measurement values for biomass and substrate as well as simulation results including the sedimentation model. For simulation parameters f_{temp} and $q_{O2,max}$ were adopted from experiments B (parameters at 10°C), as the same yeast strain was inoculated. The lag time coefficient t_{lag} was fitted in a parameter estimation procedure. The graph demonstrates, that the biomass concentration was reduced stepwise at the sedimentation times calculated by the sedimentation model for the different cell classes (see Table 21). In between these times

biomass growth and sugar degradation was computed by the Black Box model each time based on a new „initial“ concentration. In this way, the Black Box model was extended by the sedimentation model without influencing the core of the yeast metabolism model. After 125 h the substrate was exhausted. In the following phase of fermentation (maturation) only sedimentation without intermediate biomass growth was detectable. The accuracy of the simulation was not evaluated statistically. However, a splined curve through the measurement values fitted well the simulated data at each time after sedimentation of a cell class. This could be verified in several fermentations for the regarded fermentation tank size and yeast strain (see Figure 50).

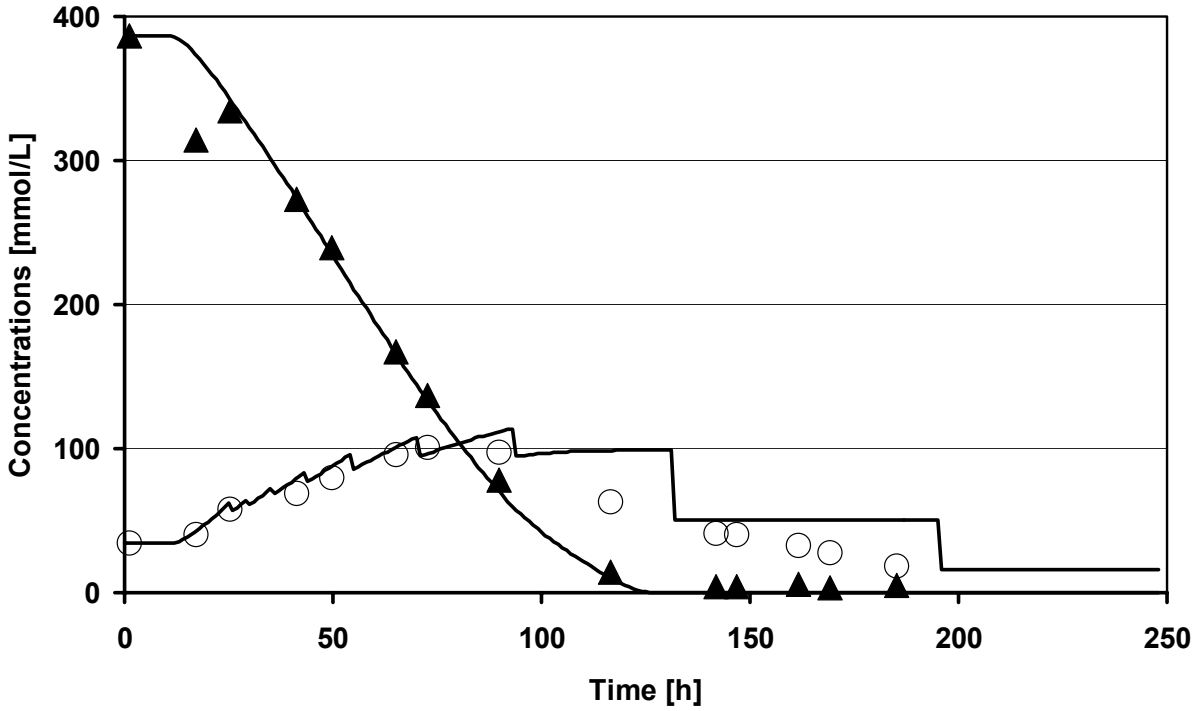

Figure 40: Fermentation run in a 10 hl CCF. Measurement values for biomass (○) and substrate (▲) are presented. Lines indicate simulation results.

Further experiments were made with fermentations in yeast propagation system A and B with a bottom fermenting yeast strain W34/70. Cell size distributions had to be adapted to the characteristics of the yeast strain and the fermenter height had to be implemented. Results of these experiments were similar (not shown). Additionally, the sedimentation model was extended by functions for viscosity and density of the growth medium according to literature data [82, 133]. However, no improvement in performance could be achieved. Further research including measurements of viscosity and density of the growth medium and size distributions of the sedimenting yeast cells are in preparation. A further increase in accuracy could have been reached by an extension of the number of classes or even the implementation of a density function of cell size distribution. The latter was not possible with the applied simulation software. Fluid dynamic aspects as convection and CO_2 bubbles affecting the

sedimentation process were not considered in this work. Certainly, a potential for a better understanding and description of yeast sedimentation processes lies in this field of research (see chapter 4).

In the introduced sedimentation model particle classes, which were totally sedimented below the measurement level were not built newly during biomass growth. This could be seen as the major drawback of the introduced model. Usually, during biomass growth the entire range of cell sizes is detectable in the yeast population due to the normal behaviour in the mitotic cell cycle [74, 102].

Summarising, the sedimentation model in combination with the Black Box modelling approach provides a tool to simulate fermentations with an accuracy sufficient for practice. Especially fermentations in small CCF and horizontal tanks now can be simulated. An additional feature of a sedimentation model lies in the estimation of the amount of sedimented yeast for harvesting in industrial CCF. Besides, with the sedimentation model an important prerequisite for modelling of biochemical substances as diacetyl was created. For example in the implementation of diacetyl formation and degradation kinetics from Engasser [47] or Votruba et al. [137] a great potential was found and further research was initiated (not shown). Alternatively, the model may be implemented in hybride approaches, as e.g. Fellner et al. [53], for a further process optimisation.

4 Conclusions and Outlook

Two deterministic modelling approaches, a Black Box approach and a metabolic model, were developed in order to describe the metabolism of *Saccharomyces sp.* during experiments in research and industrial applications. The models comprised oxidative, fermentative and oxidoreductive metabolism. Especially, limitation and inhibition effects are considered for example caused by high ethanol concentrations during brewing yeast propagations or a lack of nitrogen sources in the industrial growth medium beer wort. Both modelling approaches were validated with literature data of bakers' yeast propagations and experimental data of brewing yeast propagations, particularly designed and performed in the present work.

In a sensitivity analysis three parameters appeared to have a relevant influence on the simulation results concerning calculated concentrations of biomass and substrates. These were the lag time t_{lag}, the maximum specific oxygen uptake rate $q_{O2,max}$ and the temperature coefficient of the specific substrate uptake rate f_{temp}. In order to fit the simulation on reference data, only these parameters were determined in a parameter estimation procedure for each data set. Other parameters were kept constant. Simulations based on the suggested modelling approaches matched experimental data very well for experiments with different yeast strains and propagation strategies.

The temperature dependency of yeast growth was studied by analysis of the estimated parameters of all experiments in a range between 5 and 35°C. The parameter f_{temp} was exponentially increasing with the temperature, whereby the progressions appeared to be similar for all applied yeast strains (bottom and top fermenting) and propagation strategies. The parameter $q_{O2,max}$ was exponentially increasing to a maximum between 20 and 25°C and decreased to zero at about 30 –32°C, however, different progressions appeared. These differences were characteristic for the specific yeast strains but not for propagation strategies applying the same yeast. So, with increasing temperatures an exponentially increasing substrate uptake rate was observed. On the other hand, above temperatures of 20 –25°C the maximum specific oxygen uptake rate, as a measure for the oxidative capacity of the yeast cell, was decreasing. These tendencies in opposite direction explained an increasing yield (substrate per biomass) below and especially above a temperature range of 15 – 28°C observed in brewing yeast propagations. Here, much substrate had to metabolised and only a low oxidative capacity was available. The temperature dependency of the yeast growth and of the estimated parameters could be represented by an Arrhenius type model (Schoolfield model) and so, the formerly estimated parameters were replaced by temperature functions.

An influence of the dissolved oxygen concentration on the yeast growth was found only below 0.1 ppm concerning an ideally mixed propagation system. Below this value, the yield (substrate per biomass) increased and the specific growth rate decreased. This was contrary to

usual recommendations in brewing technology with dissolved oxygen concentrations of above 0.5 ppm [5, 87, 102]. Possible reasons for the recommendation of higher dissolved oxygen concentrations found in an inhomogeneous distribution of oxygen due to non ideally mixed propagation systems. Thus, applying a higher aeration rate, in these propagators an average dissolved oxygen of above 0.1 ppm was achieved. In the modelling approaches, the dependence of biomass growth on the dissolved oxygen concentration was represented by a Monod expression for oxygen limitation.

The implementation of the influence of the manipulated variables temperature and dissolved oxygen concentration in both modelling approaches allowed predictive simulations of the yeast propagation process using non isothermal trajectories. With a precise adjustment of trajectories of both, temperature and dissolved oxygen, the crop time of the inoculum could be varied within a period of several days to maintain high fermentation activity for the subsequent anaerobic fermentation. Thus, a tool was provided, which enabled a more effective planning and evaluation of process control strategies. Especially, the limits of controllability of the yeast propagation were pointed out.

Simulations based on the process models performed well for industrial brewing yeast propagations in not ideally mixed plants also. In this applications, an inhomogeneous distribution of yeast biomass and an insufficient aeration were identified. However, considering these effects an accurate description of substrate degradation and ethanol formation was achieved. The additional implementation of a sedimentation model, taking into account the physiologically reasoned sedimentation of bottom fermenting yeast cells, allowed a comprehensive description of yeast fermentation with a practicable accuracy.

Summarising, the developed process models proved to be valid for propagations and fermentations applying different yeast strains or propagation strategies. Simulations achieved a high accuracy for all regarded applications. Therefore, an automatic adaptation of the model parameters, as it is proposed in other works [52] to reach a higher simulation accuracy, was not indicated in the present work.

Many modelling approaches for the description of yeast growth are available in literature. However, the objective targets were different to this work. Complex, structured models were developed to identify specific intrinsic metabolism regulation effects. Other modelling approaches described only single aspects, as the temperature dependency of microbial growth or the oxygen demand. However, no comprehensive modelling approach for the yeast propagation considering different metabolic states and the influence of the manipulated variables was found in literature. Especially in brewing technology such modelling approaches are not available, which take into account the limiting and inhibiting effects caused by an industrial beer wort as growth medium.

Further examinations are necessary to verify the results for the dependency of yeast growth on temperature and dissolved oxygen concentration. Oxygen balances of the applied propagation system should be measured for propagations at different temperatures, since in own experiments for example the temperature dependency of the maximum oxygen uptake rate differed from results of Hartmeier [61] (comp. Figure 7 and Figure 21).

Further works have to study, whether trace elements as zinc or other quantities have to be taken into account in the modelling approaches to represent limitation and inhibition effects occurring in the industrial practice comprehensively. Also the yeast growth at low temperatures below 10°C should be studied in more detail, as these temperatures are used for yeast storage and to bridge longer interruptions in production. Additionally, examinations on the temperature dependency of the lag time and the inaccuracies caused by the formulation of the substrate as glucose equivalents instead of different sugars featuring different uptake mechanisms have to be carried out, in order to improve the sufficiency of the approach.

A further step of the development of an active process control tool is the integration of information about the yeast vitality in the modelling approach (segregated model comp. chapter 2.1.2.3). In particular, works concerning the actual proliferation state and enzymatic activities of key enzymes of different metabolic pathways are in progress. Planned is a comprehensive examination of intrinsic reactions of the yeast based on measured physiological data (cell cycle, trehalose, proteomics), in order to give an explanation of metabolism regulation effects (Crabtree effect or stress reactions) dependent on the manipulated variables. In this regard, an interpretation of differing biomass yields (comp. [33]) is aimed , as well.

A combination of fluid dynamic aspects with above mentioned biochemical studies potentiates a better understanding of the physiologically reasoned sedimentation of bottom fermenting yeast cells.

The benefit for the engineer, delivered with this work, lies in a gain of process knowledge about both, the influence of manipulated variables and growth medium on the biomass growth as well as the resulting biomass activity. Though, using an industrial growth medium, process control strategies can be simulated and evaluated. The gained knowledge about the process behaviour allows the employment of optimisation algorithms, e.g. genetic algorithms, in order to plan propagation strategies more efficient than before. Mistakes in the process strategies are avoided and active yeast is provided for inoculation even considering scenarios in practice. The applicability of the developed system is principally not limited to the considered case. Conceivable are applications applying other propagation strategies (fed batch or continuous [94]) or in other industrial fermentations, where economical or traditional aspects prohibit the usage of customised growth media, as e.g. the production of vinegar, wine, single cell proteins or secondary metabolites.

5 Materials and Methods

In this chapter materials and methods applied in the yeast propagation and fermentation systems are introduced. Chapter 5.1 describes a yeast propagation system, which was used for most experiments. Additional yeast propagation plants used for verification of the results received from propagation plant A in pilot and industrial scale as well as a fermentation plant are illustrated. Online measurement devices and analytical methods are described in chapters 5.2 and 5.3. Chapter 5.4 illustrates applied microorganisms and media for propagations and fermentations. Finally, in chapter 5.5 computational methods are introduced.

5.1 Yeast propagation system

5.1.1 Yeast propagation system 1

The propagation system consisted of a propagator tank and peripheral equipment including switch cabinet, personal computer, supply and control devices, and a thermostat unit. The plant was used for experiments A, B and C. Substrate (wheat beer wort) and yeast (W34/70) were got from a brewery. Original gravity of the substrate was between 12.5 and 12.7 ww% with a proportion of fermentable sugars of around 70%. Initial pH-value was 5.2. To avoid limitation effects 60 mg Zinc-Chloride $ZnCl_2$ were added. So, an initial Zinc-concentration of 0.2 mg/L could be guaranteed. The mean value of free amino acids in the substrate was at 220 mg/L. Figure 41 demonstrates the installation of the propagation system ” in a brewery.

Figure 41: Installation of the propagation system 1 in experiments A.

5.1.1.1 Experimental Set Up

The volume of the propagator was 0.25 m^3 with 50% (0.125 m^3) usable volume for propagation medium and 50 % for foaming. The diameter was 0.55 m. A sketch of the propagator is shown in Figure 42. The installation scheme of the reactor and peripheral

devices as pipes and valves is presented. Symbols describe applied measurement and control technology, which are described subsequently.

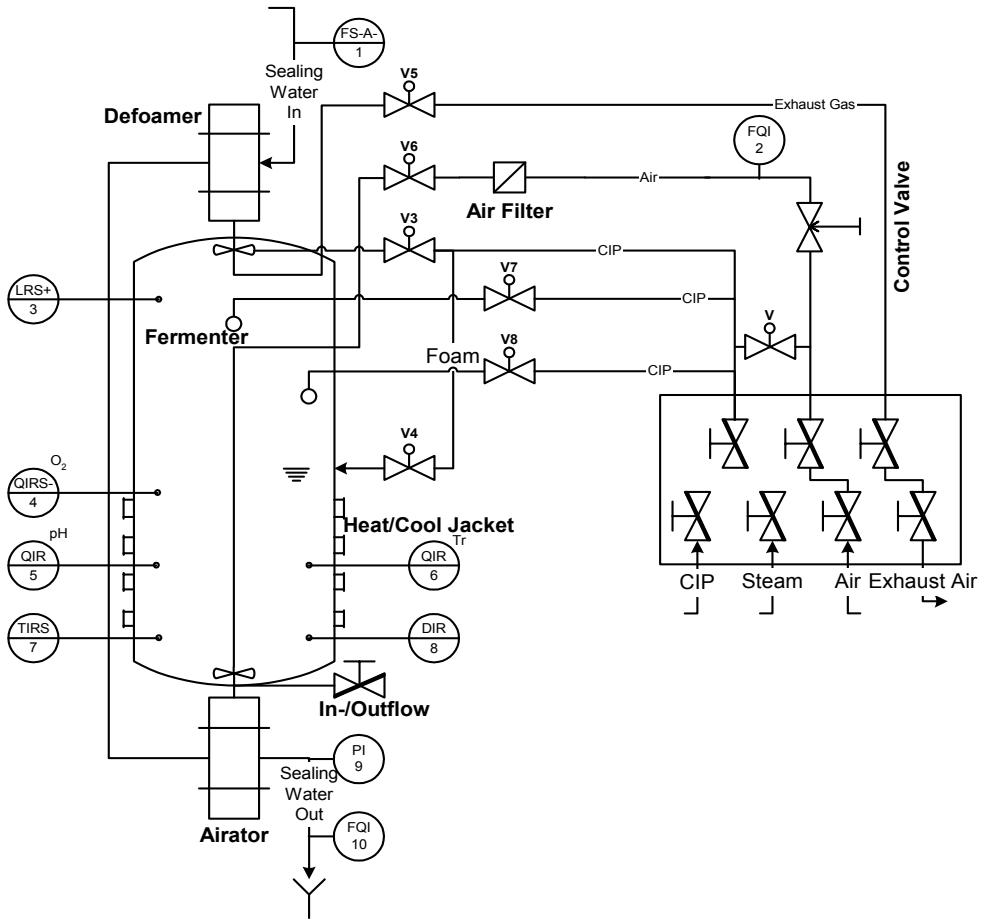

Figure 42: Sketch of the propagation system. For CIP or air supply the panel is used. All valves are operated pneumatically. The dissolved oxygen content inside the fermenter is controlled by the air flow with a control valve. The air passes through a sterile filter. A heat/cool jacket allows efficient temperature control. The defoamer unit works controlled by a foam detector. The foam is degassed and pipelined back into the fermenter. Sealing water is required for the rotating mechanical seal for the defoamer and the aerator unit.

Specific features of the used propagation system were the aerator (Frings TRG) and defoamer units. The aerator unit consists of a self-aspirating frequency controlled rotor-stator-turbine. The rotor pumps the influent medium radial into the stator channels of the turbine. Here, behind the paddles of the rotor an area with negative pressure is existent and sterile filtered air flows in this area. Inside the stator channels the gas is dispersed in the liquid medium in a highly turbulent flow and leaves the stator channels as a turbulent stream. For all experiments the electro motor (1.5 kW at 50 Hz) was run at 25 Hz. The turbine combines homogeneous solution of gases in disperse bubbles and the continuous mixing of the medium in the propagation system (44).

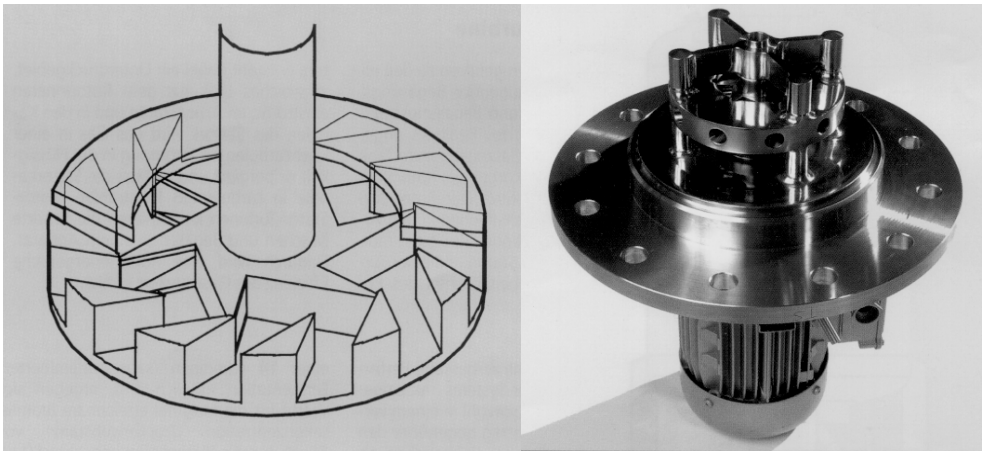

Figure 43: Left: Sketch of a rotor-stator-turbine [46]. Right: Picture of the aerator unit (Frings TRG) with motor, Turbine, flange and mechanical seal.

Usually, foam occurs during yeast propagations as no pressure is applied. Therefore, a mechanical vertical-defoamer unit (0.75 kW at 50 Hz) is installed. A capacitive sensor detects the level of foam and triggers the defoamer unit (runs at 50 Hz), if necessary. The foam is degassed by the centrifugal effect and gas escapes through the exhaust. The liquid fraction is lead back into the fermenter below the filling level.

5.1.1.2 CIP and supply

Interface of the propagation plant for supply of steam, air, and CIP was a panel (see Figure 42). All valves (pneumatic valves) were controlled by the PLC. Piping and valves were made in ID25 cross section. For CIP, a pump (1,5m^3/h) could be integrated in a circle built by the propagator tank, the outflow valve, and the panel. From the latter different pipes could be cleaned individually. Sterilisation of the propagator was possible with steam. After steaming the tank was cooled down with sterile air via the panel. Filling and outlet was realised via the in-/outflow valve with a ID25 tube directly from the cold wort supply of the brewery.

5.1.1.3 Temperature control of the propagation system

The structure of the cooling system (see Figure 44) is described in Hege [62] and was adapted for this application. It allowed a case dependent switch between two separated cycles (aggregate cycle and propagator cycle) or the application of one large cycle. The cycles were separated by a control valve. Due to a throttle in the first bypass on the aggregate side (see Figure 44 left side) and the aggregate pumping against atmospheric pressure, both cycles can be pumped parallel without mixing of medium. If the valve was opened, the cooling jacket of the propagator was supplied directly by the cooling aggregate. A cryostat was used for cooling and heating of the propagation system. The aggregate was modified in order to allow remote control by a PLC. Modifications are described more detailed in Hege [62]. For heating, the waste heat of the cooling system was used. Cooling medium was glycol.

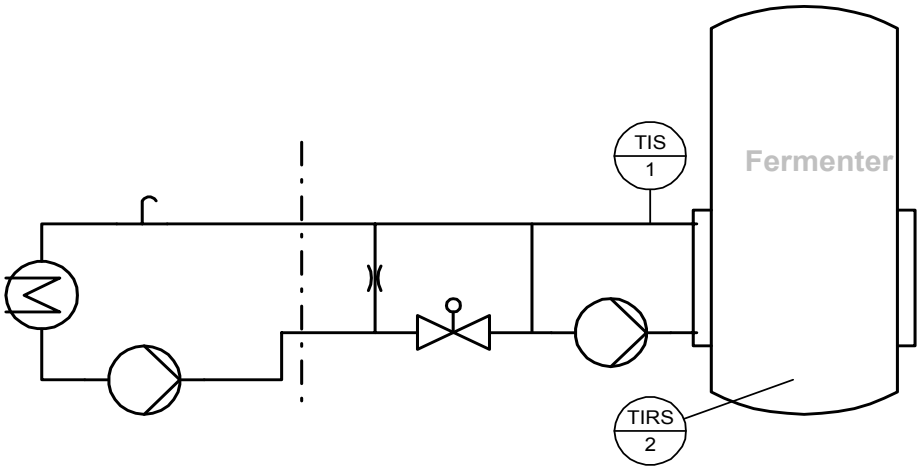

Figure 44: Heating and cooling system of the propagator. The separated area (left side) represents the cooling and heating aggregate. The latter is equipped with a pump for the cooling medium and temperature sensors. The cooling system is divided by a valve into two separately pumped circles, one for the cooling aggrgate and one for the cooling jacket of the propagator. If the valve is closed, the medium is pumped in each circle separately. If the circles are connected by opening the valve, the propagator is cooled directly by the cooling aggregate. The temperature of the propagator is controlled by the aggregate and the state of the valve dependent on the temperatur in the cooling jacket (1) and the propagator (2).

The closed loop control was subdivided into control loops for the propagator temperature and the temperature of the cooling jacket. Concerning the former, nominal value was the desired temperature of the yeast propagation. As input variable the difference between nominal and real temperature (see Figure 44 PT100 (2)) in the propagator was applied. Output variable of the controller was the nominal temperature in the cooling jacket. The response on a jump function showed no lag time (not shown). Hence, the controlled systems represented a P-T_1 element. Therefore, a PI controller was used [93, 104]. Parameters and other important conditions are given in Table 48.

Input variable for the control loop of temperature in the cooling jacket was the relation between nominal temperature, real temperature and medium temperature at the outflow of the aggregate. Output variable was the relation between opening and closing periods of the control valve. The relation was calculated analogue to Hege [62].

The aggregate nominal temperature was calculated with an offset of ±2°C to the nominal value of the cooling jacket, dependent on the situation (cooling or heating). Controllers for both cycles were implemented in the PLC as organisation bocks (OB) and system function blocks (SFB). Instruction list was used for programming of the PLC (IL, STL-IEC-1131). The PI block was called every minute by a timer OB. Every second the opening closing relation

was calculated based on the nominal value of the PI control and the opening period during the actual control cycle was determined.

5.1.1.4 Aeration and dissolved oxygen control

The dissolved oxygen concentration in propagation system A was controlled by a Siemens hardware control system SIPART DR20. Input variable of the controller was the nominal dissolved oxygen concentration in the propagator. Output variable was the opening angle of the control valve in the inflow pipe. So, control of dissolved oxygen concentration could be realised by variation of the airflow in the self aspirating aeration system.

The response to the jump function showed a small lag time (not shown). Hence, the controlled systems represented a P-T_2 element (lag time of second order). Medium for the experiments was wheat beer wort at 25°C with an oxygen saturation of 7.2 ppm [102]. Other relevant parameters were the same as in Table 48. Because of the aeration and the mixing effect of the Frings TRG aerator, an ideal distribution of dissolved oxygen was assumed. In accordance to Olsson and Piani [104] a PI controller was chosen. The parameters T_u and T_g for a P-T_2-system were determined and converted into proportional action coefficient (cP = 3.188) and integral action time (TI = 60s). With these parameters an accuracy in control of ±0.1 ppm dissolved oxygen concentration could be realised.

5.1.1.5 Implementation of PLC and the Human Machine Interface

A PLC (S7 314IFM) was used for manual and automatic control of of the propagation system. Integrated were modules for digital and analogue signal processing, a closed loop control cycle for temperature, single control level, and step by step control and data processing, respectively for the connected measurement devices. Instruction list in STEP 7 programming language was used.

The HMI was developed by the use of the software Siemens WinCC 5.0 and was designed using a top-down approach, whereby the user interface was defined first.

Colours of the user interface were chosen according to Charwat [27, 28, 29]. The start screen shows a graphical overview of the plant (light grey background). Inactive components (valve closed, motor off) are shown in dark grey color on a light grey background. Active components (valve open, motor on) are shown in green. All relevant states and variables, in particular the measured values, were logged by the HMI and could be shown graphically by opening a new window on the screen.

There were several scripts (ANSI C) implemented by the author of this thesis, which were executed cyclic. Data were logged in different cycles, i.e. every 10 s for values concerning aeration, every minute all values and triggered by a flag in the PLC, if connected measurement devices finished a measurement cycle.

The nominal values for propagator temperature during temperature scenarios was calculated from predefined setpoints by an Microsoft Excel spreadsheet cyclic and transferred every minute to the HMI, from where it was transferred to the PLC.

5.1.2 Propagation plant 2

The CCF with a volume of 1.5 hL was used for experiments D. The was equipped with a circulation pipe in closed circuit and an aeration unit. The suspension was pumped out of the cone and back into the tank below the filling level in radial direction. 60 L of barley malt wort were used. Batch-experiments were made at different temperatures (9, 16, 23, 30°C) with a nominal dissolved oxygen concentration of 2 mg/l. The apparent dissolved oxygen concentration varied inbetween 0 and 3 ppm due to pulsed aeration with a dual mode. A dissolved oxygen concentration of 2.0ppm was nominal value for a dual mode controller for aeration.

5.1.3 Propagation plant 3

The propagation plant 3 was used for experiments E. It consisted of two identical cylindroconical tanks (CCT) with a volume of 120 hL. Each tank possessed a circulation in closed circuit and an aeration unit. The suspension was pumped out of the cone and back into the tank below the filling level in radial direction. During circulation with 35 m^3/h the suspension was aerated with a flux of 1.5 m^3/h. Circulation (500 s) and pauses were pulse in a relation 2:1. Additionally both tanks were equipped wit a defoamer unit (fluid injection). Pressure in the tanks was controlled automatically, in order to achieve a low overpressure. Also, temperature was controlled to an setpoint value of 18-22°C. A turbidity measurement device was used to control yeast growth inbetween a scale of 0 – 100%. If a turbidity threshold of 80% was exceeded, temperature setpoint was decreased to 14°C and aeration was stopped. Every 96 minutes wort was delivered from the brewhouse. Each brew was inoculated with 30 hl yeast suspension. Thereupon the propagator was refilled with wort of the same brew. Each tank was used twice for inoculation, then tanks were switched.

5.1.4 Propagation plant 4

The propagation plant 4 was applied for experiments F. The plant consisted of three cylin droconical tanks (CCF) with a volume of 360 hL. All tanks were circulated in closed circuit with a flow of 150 hL/h. A venturi-pipe system in the circuit allowed an aeration rate (sterile air) of 120 – 600 L/h dependent on the state of yeast propagation. The medium was pumped out of the cone through the aeration unit and back into the tank below the filling level in radial direction. During the propagation a constant overpressure of 0.8 – 1.0 bar was applied. During the operating sequence two tanks were filled every day. They were aerated following a

standard procedure (8 h 480 L/h, 3 h 600 L/h, and 20 h or until pitching 120 L/h). Temperature was controlled on a nominal value of 15°C.

5.1.5 Propagation plant 5

The propagation plant for experiments G was composed of two stages. The first stage was a CCT with 95 hL filling volume whereby 10 hL inoculum were required. A lancet was used for aeration. Additionally, the tanks was circulated in closed circuit with a flow of 105 hL/h. The suspension was pumped out of the cone and back into the tank below the filling level in radial direction. With a timing device a proportion of 3:1 of aeration and circulation to pause was adjusted (Air flux 1.8 m^3/h). Temperature was controlled at a nominal value of 14°C.

The next day, 85 hL of the first stage were mixed with 160 hL wort in the second stage (CCF). Aeration and circulation were similar to the first stage. Temperature was controlled to 12°C. After 24 h the whole suspension was used for pitching.

5.1.6 Propagation plant 6

Propagation plant 6 was applied for experiments H. The construction was similar to propagation plant 1. In a CCF with a volume of 200 hL analogue to Figure 43 an aeration and mixing device was installed. Dissolved oxygen concentration was controlled by the air flow into the self aspirating aerator turbine. Temperature was controlled by a dual mode controller. Cooling medium was glycol.

5.2 Online measurement and calibration

The propagation system 1 was equipped with sensors for pH-value, oxygen, temperature, refraction index, turbidity, particle count, pressure, and airflow. Specifications of applied sensors and transmitters are given in Table 49. All signals are transformed to 4-20 mA and further processed in a PLC (S7-314IFM). If no specific transmitter is mentioned, the signal is transformed in an integrated transmitter device. Due to continuous aeration, bubbles interfered with measurement devices for turbidity (absorption of light) in the propagation tank.

Calibration buffer solutions from Merck (pH 4.01 and 7.00) were used for calibration of the pH-sensor. Oxygen sensors were calibrated with Na_2SO_3 solution for zero and air saturated water at 25°C for adjustment of the sensor to 8.25 ppm [102]. Turbidity sensors and particle count device were zero-calibrated with water. Cold water (5°C) and hot water (80°C) was used for calibration of the temperature sensors. Temperature of the sensors was adjusted with a calibration thermometer (±0.1°C).

5.3 Analytical methods

5.3.1 Offline measurement

For calibration of online sensors and in order to gain additional information the experiments were attended analytically as well.

During all experiments offline measurements were carried out for yeast cell count and gravity. In some experiments additionally ethanol concentration were measured. For the determination of the density of the propagated beer and the ethanol concentration a measurement device Scaba Automatic Beer Analyzer of Perstorp Analytical GmbH, Rodgau was used. Accuracy was specified with ±0.02% w/w for ethanolconcentration in a range of 0-7%. For density accutracy was specified with ±0.00005 g/mL in a range of 0.8000-1.2000 g/mL. Gravity was computed from density and temperature [107]. For experiments A and C ethanol measurement was neglected. In experiments A and C gravity was measured with with an aerometer.

Yeast count was determined using a haemocytometer (Merck, Darmstadt). The sample was diluted (dilution factor *f*) and the number of cells *n* in the haemocytometer (depth: 0.1 mm, area: 0.00025 mm^2, 16x16 squares) were counted. The yeast count

$$YC\ [Mio./mL] = n \cdot f \cdot \frac{4}{256} \tag{47}$$

was calculated referring to 1 mL. Two areas of the haemocytometer were counted in order to avoid outliers. If the results of both counts match together, the mean value of both counts was used for further calculation. Otherwise (> 5% difference) a new sample was prepared and counted. A systematical error of this method is specified in literature with ± 5% [54, 92]. Own experiments confirmed these results. During experiments B, E, F and H a cell counter (model 871 AL Systeme) was applied. The system was calibrated with with results of a haemocytometer. Here a systematical error of 170% could be compensated.

Yeast dry mass was determined gravimetrically. A sample was vacuum filtered and 4 g of the residuum dried for 3 h with 105°C. After cooling the sample in an exsicator, the dry mass was calculated from the yeast count and the differential weight (wet and dry sample). During the propagation process a specific dry mass of 4.0 to 4.5E-11 g/Cell occurred. Yeast harvested from fermentation tanks (CCF) or stored at cold temperatures turned out to be heavier with a mean specific dry mass of 5E-11 to 6E-11 g/Cell respectively. The results confirm literature data with dry masses of 2-6E-11 g/cell [22, 87,].

Free amino nitrogen (FAN) was determined with the Ninhydrin Method using a SKALAR device or alternatively with a HPLC. As the yeast could catabolise not only the determined

FAN as nitrogen source, for application in the process model the measured value was multiplied by 1.74 [102].

Zinc was measured using emission spectroscopy with inductive coupled plasma (ICP-OES).

5.3.2 Offline data processing

5.3.2.1 Specific growth rate

Experimental data out of the logarithmic state of the yeast propagation is the basis for the calculation of the specific growth rate μ:

$$y = ln\left(\frac{YC}{YC_0}\right) = \mu \cdot t \tag{48}$$

With YC is the yeast count, YC_0 the initial yeast count at inoculation and time t. This compensation function correlated significantly with the measurement values. The calculated specific growth rates were used for the determination of the temperature dependency of the biomass growth.

5.3.2.2 Biomass concentration

Biomass concentration

$$\text{Biomass}\,[\text{mmol/L}] = \frac{\text{YDM}\,[\text{g/Cell}] \cdot \text{YC}\,[\text{Mio. Cell/mL}]}{\text{BM}\,[\text{g/mol}]} \cdot 10^6 \frac{[\text{mL} \cdot \text{mmol}]}{[\text{L} \cdot \text{mol}]} \tag{49}$$

was calculated from yeast count with YDM = Yeast dry mass = $4 \cdot 10^{-11}$ g/cell, and BM = 25.01 g/mol [127] (Molar weight of the mean biomass composition). This conversion was necessary, because the molar concentration was used in the modelling. The mean biomass composition ($CH_{1.79}N_{0.15}O_{0.5}$) is adopted from literature [127].

5.3.2.3 Fermentable gravity and glucose equivalent

The fermentable part of the gravity represents the degradable sugars. The portion of the non fermentable carbohydrates are subtracted by the total measured gravity, in order to allow the value of the sugar concentration to reduce to zero. The real gravity

$$E_w\,[\%\ \text{w/w}] = \frac{p \cdot q + E_s}{1 + q} - 0{,}3 \cdot p \tag{50}$$

is calculated from the measured (apparent) gravity E_s with p = original gravity, 0.3 p = mean, non fermentable portion of the growth medium and q = 0,220 + p/1000 (attenuation coefficient).

For the application in the modelling approach the conversion of the fermentable gravity in a molar concentration as

$$\text{Substrate}\,[\text{mmol/L}] = (0{,}0413 \cdot E_w{}^2 + 9{,}9677 \cdot E_w + 0{,}0008)\,[\text{g/L}] \cdot \frac{10^{-3}}{180\ \text{g/mmol}} \tag{51}$$

was necessary. The applied function results from data for sugar solutions [133]. In the function, the molar weight of a glucose molecule (180 g/mol) was integrated and concentrations result as "glucose equivalents".

5.4 Microorganisms and medium

Applied microorganisms were brewing yeasts. Yeast belong to the protoascomycetae and are eucaryothic single cell organisms. Brewing yeast as well as bakers' yeast are classified as members of the *Saccharomycetaceae.* Characteristic is a asexual propagation [122]. The cells are round or elliptical. Diameters usually lie in a range of 5-12 µm [22, 102]. Figure 45 presents a microscopic picture of budding yeast cells during a propagation.

Bottom fermenting brewing yeast is classified in taxonomy as *Saccharomyces cerevisiae uvarum var. carlsbergensis* (*S. carlsbergensis*) [41]. In experiments A, D and G a bottom fermenting yeast of the strain W34/70 was applied. Experiments F were inoculated with a yeast strain W308. Top fermenting brewers' yeast is classified as *Saccharomyces cerevisiae* (*S. cerevisiae)*. In experiments C and E, a wheat beer yeast strain W68 of these group was propagated.

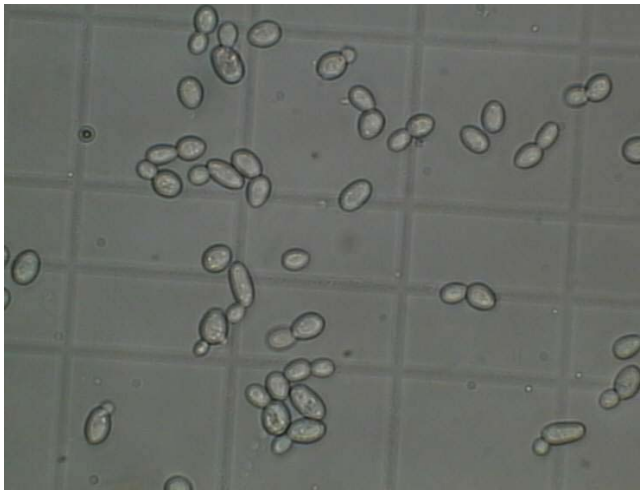

Figure 45: Microscopic picture of Saccharomyces cerevsiae uvarum var carlsbergensis (bottom fermenting yeast cell) in a haemocytometer. Budding yeast cells as well as single cells are shown. The area of single squares was 0.0025 mm^2.

As growth medium different malt worts were applied. The latter is a complex medium, with varying characteristics for each brewery and even each brew. For simplification in the following only substances were considered, which were relevant for yeast growth.

Usually malt wort consists of 11-12% dry mass (original gravity). A portion of 90 – 92% are carbohydrates. The amount of 70 - 80% of these are fermentable sugars as glucose, fructose, saccharose, maltose and maltotriose. Maltose represents the main portion [50]. Original gravities [% w/w] for the different experiments were 12.4 and 12.6% for experiments A and C (one experiment with 6.8%), 10.0 - 10.3% for experiments B and H, 11.3-11.5% for experiments D, 12.6 - 12.8% for experiments E, 12.2 - 12.3 for experiments F and 12.0 - 12.9% for experiments G.

Nitrogen compounds are the second main component in the malt wort with 4-5% w/w. A portion of 85-90% exists as FAN, peptides and proteins [48]. For yeast growth the availability of assimilable nitrogen components is of great relevance as nitrogen is needed for construction of new cell material. Therefore, for usual worts (FAN = 200 mg/L) the formation of new cell material is limited to a cell count of 80-110*10^6 cells/mL [6]. FAN was detected in a range of 210-220mg/L for experiments A and C, 170-190 mg/L in experiments B, D and H, 160-200 mg/L in experiments E and 190-195 mg/L in experiments F and G.

A growing yeast demands a wide range of trace elements for enzymatic and structural purposes. Usually, mineral compounds are not limiting in the beer wort, except for Zinc, which often fall short of a demanded concentration of 0.15 mg/L [50]. For experiments A, B and C, Zinc was added to a concentration of 0.2 mg/L. Zinc concentrations were measured in worts of 0.15-0.21 mg/L in experiments D and F, 0.07-0.08 mg/L in experiments E and 0.07 - 0.16 mg/L in experiments G and H.

5.5 Computational methods

5.5.1 Aquasim modelling software

Modelling and simulation was carried out using the software package AQUASIM 2.0 [116, 117]. AQUASIM allows the identification and simulation of aqueous systems. For each simulation the starting conditions including concentrations of biomass, gravity, nitrogen, ethanol and dissolved oxygen in the growth medium as well as the progression of the manipulated variables were required. During the parameter estimation procedure, in a first step f_{temp} (temperature coefficient for the substrate uptake rate) and t_{lag} (lag time coefficient) were fitted to the reference data of substrate concentrations. In a second step, the maximum specific oxygen uptake rate $q_{O2,max}$ was fitted to all reference data (substrate-, ethanol- and biomass concentrations). Parameter estimations were performed with a secant algorithm provided in AQUASIM [116, 117].

5.5.2 Parameter determination for temperature model (Newton approach)

In order to fit the models applied for the description of the temperature influence on biomass growth, a procedure according to Newton was applied. A vector

$$\vec{p} = (p_1, \ldots\ldots, p_m) \tag{52}$$

summarises all parameters of a model. The model itself represents a nonlinear function of this vector and a variable:

$$y = f(x; \vec{p}) \,. \tag{53}$$

A vector of parameters is now demanded, which allows an approximation of the function f to given data sets $P_k(x_k; y_k)$ with k = 1….n.

As a measure for accuracy of the description during the parameter estimation, the sum of squares due to error (deviation between measured data sets and model description)

$$\mathrm{SSE}\left(p_1, \ldots, p_m\right) = \sum_{k=1}^{n} \left(f\left(x_k; \vec{p}\right) - y_k\right)^2 \tag{54}$$

was applied.

APPENDIX

Additional Figures

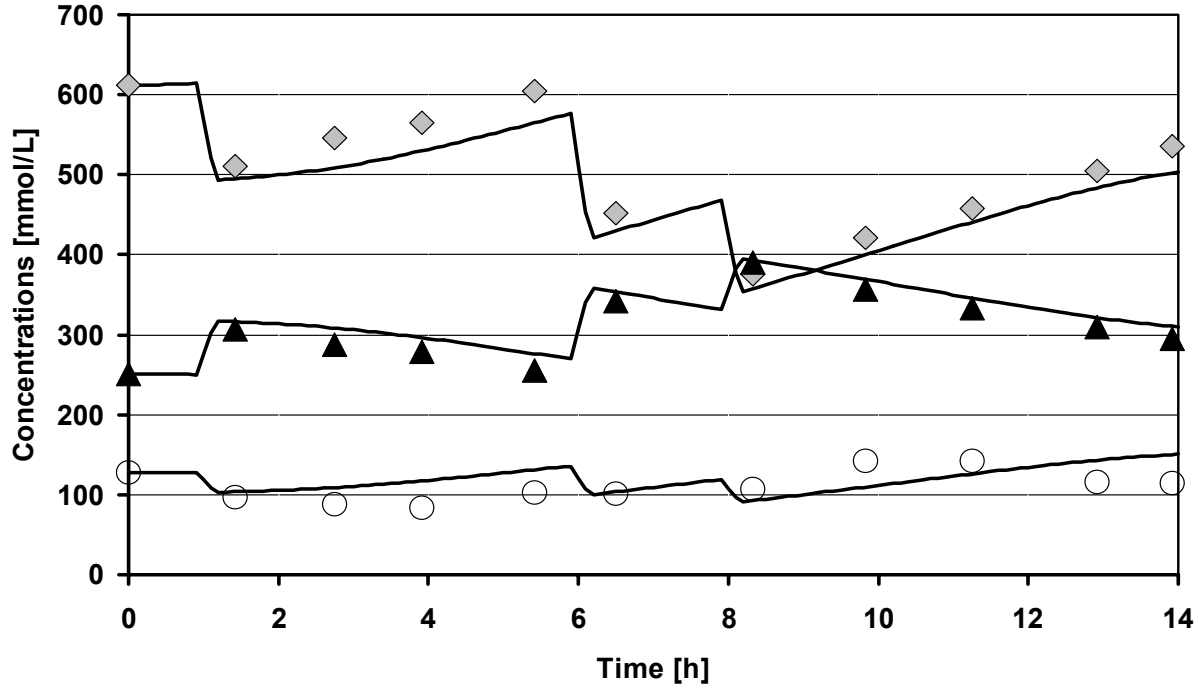

Figure 46: Sequencing batch propagation of experiments E. Propagations were carried out at 22°C. Presented are measurement values of concentrations of biomass (○), ethanol (◊) and substrate (▲). Lines indicate results of simulations.

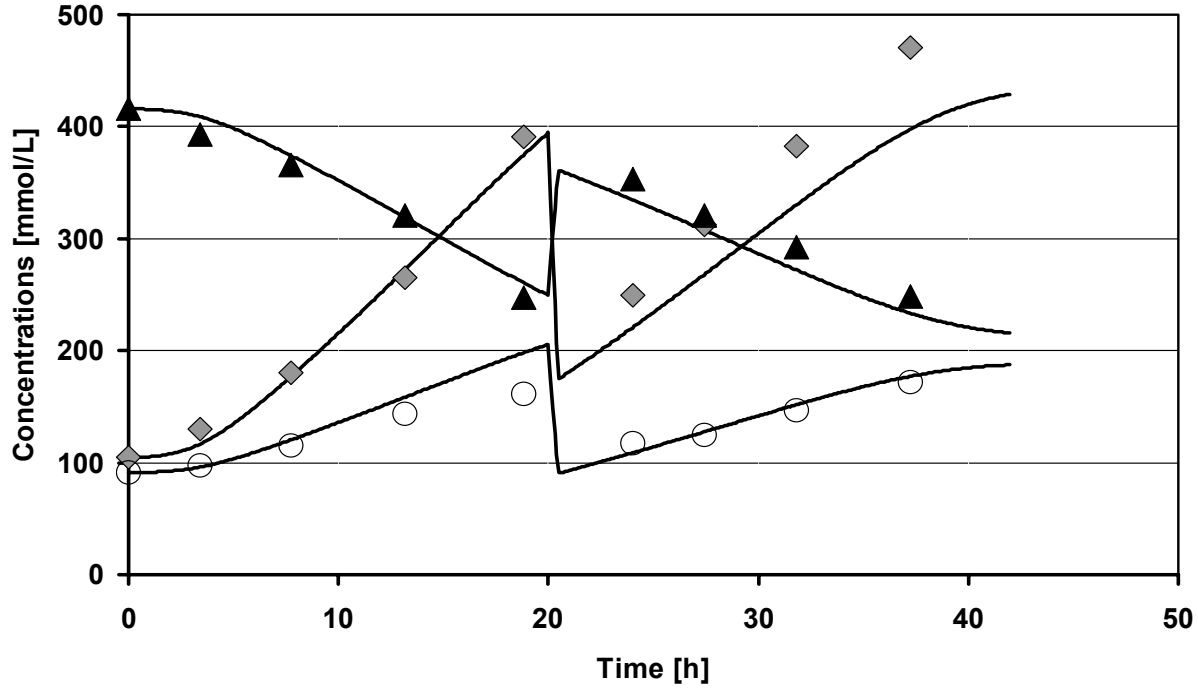

Figure 47: Sequencing batch propagation of experiments G. Propagations were carried out at 12°C and after doubling at 14°C. Measurement values of concentrations of biomass (○), ethanol (◊) and substrate (▲) are presented. Lines indicate results of simulations.

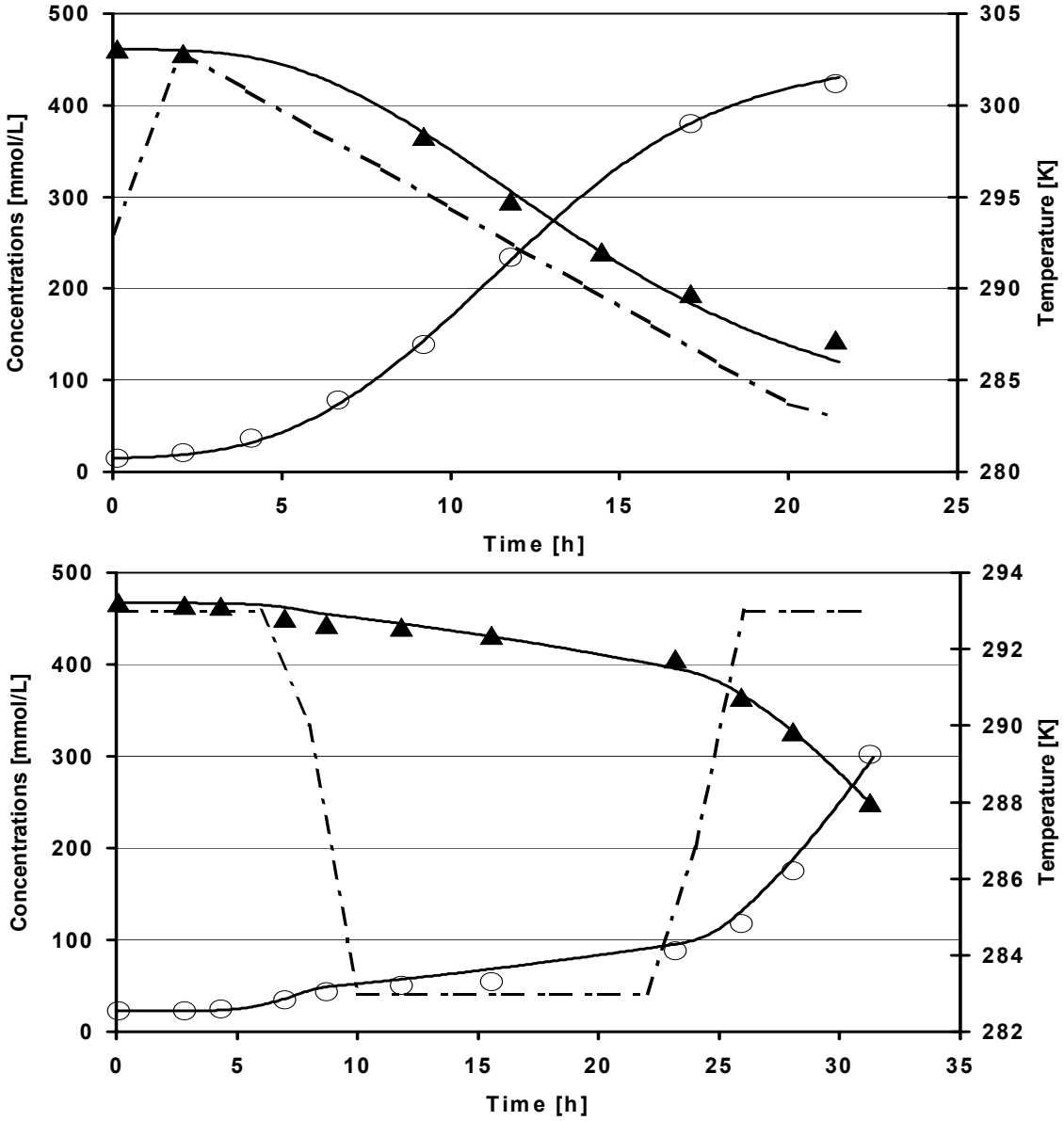

Figure 48: Temperature scenarios Black Box model. Measured concentration of biomass (○) and substrate (▲) are shown. Simulation results are indicated as lines. Temperature in the propagator is plotted as dashed line.

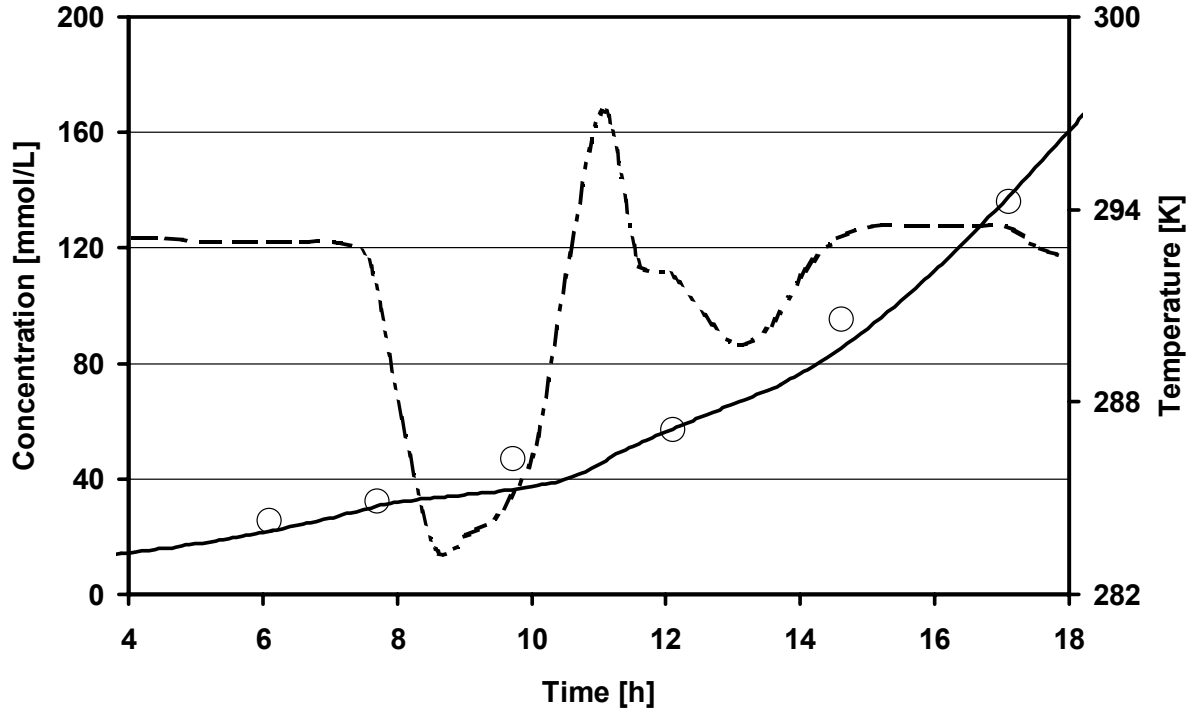

Figure 49: Disturbance in temperature control. Measured concentration of biomass (○) is shown. Simulation results (metabolic model) are indicated as lines. Temperature in the propagator is plotted as dashed line.

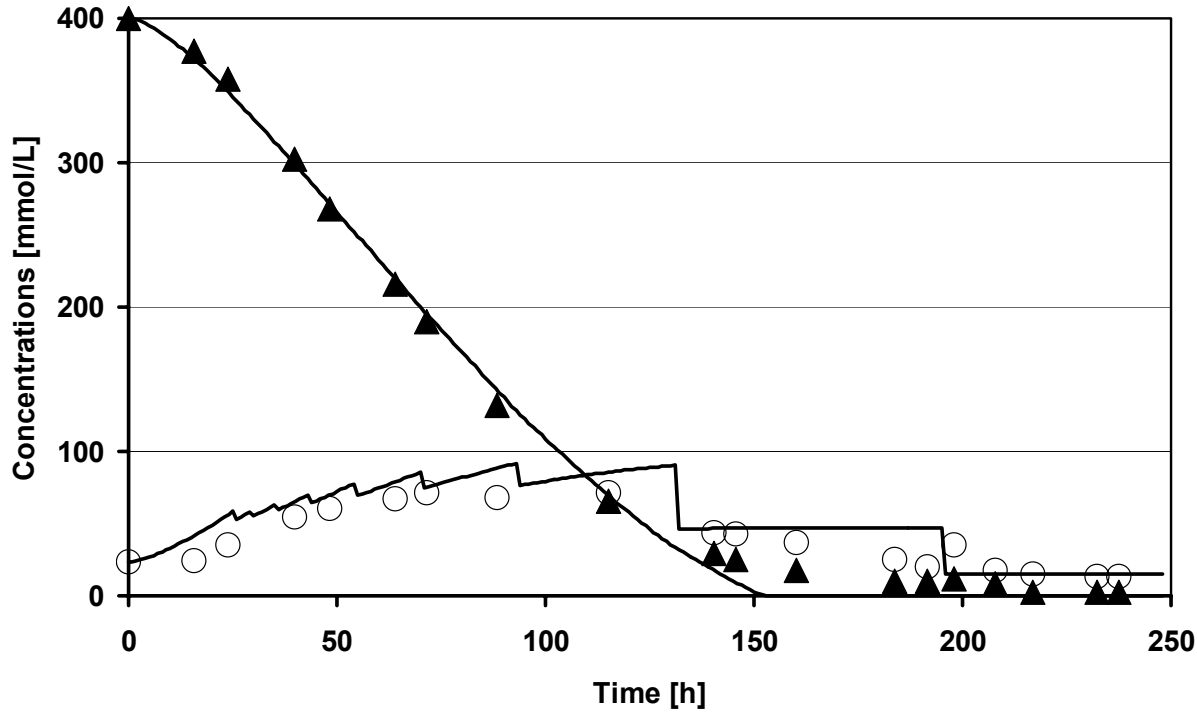

Figure 50: Fermentation run in a 10 hl CCF. Presented are measurement values for biomass (○▲) and substrate (▲). Lines indicate simulation results.

Validation of the models

Table 22: Estimated parameters for model based simulations of five propagation runs of experiments A (bootom fermenting brewers' yeast (W34/70). Propagations were carried out with 0.5ppm dissolved oxygen concentration and between 5°C and 30°C. Given are paramters for the Black Box model and the metabolic model.

	Black Box Model			Metabolic Model		
	f_{temp}	$q_{O2,max}$ [mmol/(mmol h)]	t_{lag} [h]	f_{temp}	$q_{O2,max}$ [mmol/(mmol h)]	t_{lag} [h]
5°C	0.0664	0.0058	0	0.0649	0.0063	0
10°C	0.1380	0.0091	11.1432	0.1270	0.0101	9.800
15°C	0.2079	0.0721	1.9088	0.2092	0.0615	1.6216
20°C	0.3432	0.1203	0.4815	0.2751	0.1108	0
30°C	0.8768	0.1348	1.2950	0.7050	0.1018	0

Table 23: Mean values of deviations between experiment and simulation and belonging standard deviations for experiments A.

	Mean Value of deviations [mmol/L]				Standard deviation [mmol/L]			
	Substrate	Substrate *	Biomass	Biomass *	Substrate	Substrate *	Biomass	Biomass *
Black Box Model								
5°C	6.04	2.73	11.27	5.10	7.02	2.44	19.61	5.50
10°C	3.79	3.79	4.84	4.84	2.77	2.77	4.07	4.07
15°C	6.58	6.10	7.70	6.07	5.45	4.38	6.87	5.84
20°C	5.21	1.53	2.41	2.60	9.95	2.21	1.86	1.97
30°C	14.82	3.43	9.92	1.58	20.55	3.52	15.32	1.08
Total	6.53	3.55	8.50	4.18	10.41	3.31	14.26	4.65
Metabolic Model								
5°C	7.46	3.02	9.31	5.50	8.31	2.71	13.99	5.92
10°C	3.96	3.96	4.25	4.25	2.74	2.74	3.78	3.78
15°C	6.82	6.68	7.98	6.21	4.75	4.09	7.28	6.03
20°C	4.31	3.60	2.47	2.58	4.49	4.47	1.80	1.94
30°C	3.58	3.63	4.00	3.32	3.69	3.89	2.97	2.03
Total	5.84	4.05	6.69	4.68	6.18	3.57	9.72	4.75

Table 24: Estimated parameters for model based simulations of five propagation runs of experiments B (bottom fermenting brewers' yeast). Propagations were carried out with 0.5 ppm dissolved oxygen concentration and between 8°C and 30°C. Malt germs as adjuncts were added for some propagations. Estimations were carried out only for the metabolic model.

	Yield $Y_{X/Sf}$ = 0.72 mol/mol			Yield $Y_{X/Sf}$ = 0.50 mol/mol		
	f_{temp}	$q_{O2,max}$ [mmol/(mmol h)]	t_{lag} [h]	f_{temp}	$q_{O2,max}$ [mmol/(mmol h)]	t_{lag} [h]
Without adjuncts						
8°C	0,1220	0,0038	0	0,1292	0,0098	0
15°C	0,2872	0,0027	3,386	0,3031	0,0042	0,9515
20°C	0,4836	0,0050	0	0,4923	0,0483	0
25°C	0,6328	0,0068	0	0,6371	0,0544	0
With adjuncts						
12°C	0,2515	0	0,4316	0,2891	0,0078	0,4669
17°C	0,3726	0,0059	0,2023	0,3715	0,04122	0,6675
20°C	0,5253	0,0133	0	0,5180	0,0649	0
25°C	0,7636	0,0152	0	0,7682	0,09157	0,1947
30°C	0,9495	0	0,4014	1,2398	0,0129	1,0440

Table 25: Mean values of deviations between experiment and simulation and belonging standard deviations for experiments B.

	Mean Value of deviations [mmol/L]				Standard deviation [mmol/L]			
	Substrate	Substrate *	Biomass	Biomass *	Substrate	Substrate *	Biomass	Biomass *
a) Without adjuncts								
8°C	7,55	7,97	4,95	7,99	7,84	7,04	4,15	6,61
15°C	7,67	7,7	2,23	4,29	5,69	7,73	2,33	4,38
20°C	3,66	4,44	5,68	7,28	3,07	3,72	5,54	5,28
25°C	6,81	7,04	12,96	13,63	7,47	7,41	10,78	9,41
30°C	10,64	13,9	10,41	3,40	8,53	13,09	8,84	2,94
Total	7,40	7,67	7,03	7,23	6,73	7,72	7,03	6,50
b) With adjuncts								
12°C	12,45	6,7	15,34	7,03	8,03	6,06	8,63	5,66
17°C	8,4	7,73	8,13	8,19	4,56	5,02	5,25	5,69
20°C	7,08	6,33	5,85	7,06	4,15	4,06	4,8	5,88
25°C	6,05	6,12	2,82	3,1	4,97	4,79	3,03	3,14
30°C	15,07	10,75	20,3	5,57	12,73	8,97	20,24	5,35
Total	9,44	7,46	10,65	7,78	7,44	5,51	10,02	6,57
Total a+b	8,91	7,57	8,91	7,51	7,12	6,70	8,84	6,45

Table 26: Estimated parameters for model based simulations of five propagation runs of experiments C (top fermenting brewers' yeast (W68). Propagations were carried out with 0.5 ppm dissolved oxygen concentration and between 8°C and 32°C. Parameters are mentioned for the Black Box model and the metabolic model.

	Black Box Model			Metabolic Model		
	f_{temp}	$q_{O2,max}$ [mmol/(mmol h)]	t_{lag} [h]	f_{temp}	$q_{O2,max}$ [mmol/(mmol h)]	t_{lag} [h]
8°C	0,0968	0,0051	0	0,0972	0,004	0
15°C	0,2833	0,0186	0	0,2873	0,0114	0
20°C	0,3342	0,0403	1,1688	0,4022	0,0288	0
27.5°C	0,7549	0,2141	4,3681	0,7531	0,1803	4,2634
32°C	1,1274	0,0305	0,8599	1,1982	0,0130	1,3030

Table 27: Accuracy experiments C (OG). Mean values of deviation between simulated and measured data and standard deviations are presented.

	Mean Value of deviations [mmol/L]		Standard deviation [mmol/L]	
	Substrate	Biomass	Substrate	Biomass
Black Box Model				
8°C	0,8	1,651	0,632	1,661
15°C	4,85	6,408	6,242	7,963
20°C	3,875	1,939	3,519	1,686
27.5°C	4,156	7,575	2,735	8,973
32°C	4,325	2,628	6,686	2,549
Total	3,406	3,660	4,087	5,362
Metabolic Model				
8°C	0,813	1,668	0,617	1,672
15°C	5,017	6,48	6,363	8,080
20°C	1,275	0,735	2,011	0,857
27.5°C	4,133	7,658	2,746	8,945
32°C	4,425	1,663	5,134	1,682
Total	2,869	3,299	3,764	5,463

Table 28: Estimated parameters for model based simulations of five propagation runs of experiments D (bottom fermenting brewers' yeast (W34/70). Propagations were carried out with 0.5ppm dissolved oxygen concentration and between 5°C and 30°C. Paramters are givenfor the Black Box model and the metabolic model.

	Black Box Model			Metabolic Model		
	f_{temp}	$q_{O2,max}$ [mmol/(mmol h)]	t_{lag} [h]	f_{temp}	$q_{O2,max}$ [mmol/(mmol h)]	t_{lag} [h]
9°C	0,1504	0,0111	12,76	0,1430	0,0144	13,2405
16°C	0,2616	0,1100	9,1208	0,2659	0,0705	9,235
23°C	0,5048	0,1637	3,9451	0,5525	0,1431	5,0093
30°C	0,9668	0,1286	2,9239	0,9846	0,0879	2,8242

Table 29: Accuracy experiments D. Mean values of deviation between simulated and measured data and standard deviations are presented.

	Mean Value of deviations [mmol/L]			Standard deviation [mmol/L]		
	Substrate	Biomass	Ethanol	Substrate	Biomass	Ethanol
Black Box Model						
9°C	7,92	5,41	9,60	7,54	5,91	9,32
16°C	4,7	5,79	7,12	4,58	4,49	6,61
23°C	1,75	2,4	7,87	2,64	3,61	7,92
30°C	3,55	3,56	3,46	2,43	3,58	3,40
Total	5,68	4,78	7,96	6,26	5,04	7,83
Metabolic Model						
9°C	9,58	4,44	11,19	8,22	4,00	9,09
16°C	4,55	4,95	5,88	4,65	4,87	6,97
23°C	4,65	6,35	8,38	4,66	7,24	7,07
30°C	2,3	3,32	3,32	2,41	3,48	3,48
Total	6,77	4,74	8,16	7,01	4,73	8,18

Modelling of temperature dependency

Table 30: Square root model with two parameters. Regarded are data points in the sub-optimal range (278-300,5 K).

	μ_{max}		f_{temp}		$q_{O2,max}$	
	Initial values	100 Iterations	Initial values	100 Iterations	Initial values	100 Iterations
b	0.022	0.0214	0.03	0.0273	0.015	0.0151
T_{min}	272	270.8888	272	270.3507	272	272.0330
SSE	0.0063	0.0038	0.0509	0.0377	0.0051	0.0051

Table 31: Square root model with four parameters. Regarded are data points in the whole temperature range (278-308 K).

	μ_{max}		f_{temp}		$q_{O2,max}$	
	Initial values	100 Iterations	Initial values	100 Iterations	Initial values	100 Iterations
b	0.0214	0.0266	0.0273	0.02782	0.0151	0.0209
T_{min}	270.8888	273.8528	270.3507	270.7616	272.0330	276.3958
c	0.25	0.1581	0.65	11.9800	0.5	0.2823
T_{max}	311	312.4639	311	308.1539	305.5	305.8223
SSE	0.0172	0.0095	0.0714	0.0609	0.0059	0.0030

Table 32: Bělehrádek Model with three parameters. Regarded are data points in the sub-optimal range (278-300,5 K).

	μ_{max}		f_{temp}		$q_{O2,max}$	
	Initial values	100 Iterations	Initial values	100 Iterations	Initial values	100 Iterations
			$\alpha := \alpha + 0{,}01$; $\alpha <= 55{,}5$;	for each α	$\alpha := \alpha + 0{,}01$; $\alpha <= 5$;	for each α
b	0.0214	0.0217	0.027	0.0017	0.0085	0.0123
T_{min}	270.8888	273.9228	270	-294.4498	277.99	277.9999
α	2	1.6900	2	55.49	1.1	1.34
SSE	0.0379	0.0035	0.038160	0.0226	0.005430	0.0037

Table 33: Bělehrádek Model with five parameters. Regarded are data points in the whole temperature range (278-308 K).

	μ_{max}		f_{temp}		$q_{O2,max}$	
	Initial values	1 Iteration	Initial values		Initial values	3 Iterations
b	0.0217	0.0227	0.0017	no	0.0123	0.0196
T_{min}	273.9229	275.6572	-294.4497	minimisation	277.9999	277.9986
c	0.2623	0.2243	0.4066	of	0.4432	0.2865
T_{max}	310.87279	310.9820	319.0269	SSE	305.1566	305.5983
α	1.6900	1.5454	55.49		1.34	1.7363
SSE	0.0141	0.0122	0.0517		0.0053	0.0029

Table 34: Schoolfield Model with four parameters (medium and high temperature range). Regarded values were μ_{max} and f_{temp} in the range 286-308 K, $q_{O2,max}$ in the range 286-305 K.

	μ_{max}		f_{temp}		$q_{O2,max}$	
	Initial values	10 Iterations	Initial values	10 Iterations	Initial values	10 Iterations
$r_{15°C}$	0.14	0.1337	0.23	0.2265	0.06	0.0632
ΔH^0	72000	79125.228	65000	61742.663	62000	65015.952
ΔH_H^0	250000	231101.68	250000	513434.54	750000	695886.37
$T_{0,5H}$	304	302.9821	308	308.5714	302	302.2559
SSE	0.0091	0.0068	0.0857	0.0487	0.0079	0.0046

Table 35: Schoolfield Model with four parameters (low and medium temperature range). Regarded values were μ_{max}, f_{temp} and $q_{O2,max}$ in the range 278-300,5 K.

	μ_{max}		f_{temp}		$q_{O2,max}$	
	Initial values	20 Iterations	Initial values	100 Iterations	Initial values	10 Iterations
$r_{15°C}$	0.14	0.3469	0.23	0.2235	0.06	0.1404
ΔH^0	57000	14076.057	61000	64469.925	55000	7485.2948
ΔH_T^0	-200000	-121820.07	-500000	-6926228.8	-300000	-237378.91
$T_{0,5T}$	279	290.7478	277	277.8989	283	288.9888
SSE	0.0069	0.0028	0.0242	0.0220	0.007993	0.0015

Table 36: Schoolfield Model with six parameters. Regarded values were μ_{max} and f_{temp} in the range 278-308 K and $q_{O2,max}$ in the range 278-305 K.

	μ_{max}		f_{temp}		$q_{O2,max}$	
	Initial values	50 Iterations	Initial values	1 Iteration	Initial values	5 Iterations
$r_{15°C}$	0.1338	0.1359	0.2265		0.1404	0.1429
ΔH^0	79125.228	78825.826	61742.663	no	7485.2948	6695.7988
ΔH_H^0	231101.68	227281.57	513434.54	minimisation	1112672.0	1100795.4
$T_{0,5H}$	302.9820	302.8947	308.5714	of	303.10335	303.1161
ΔH_T^0	-271149.57	-232085.88	-713399.45	SSE	-237378.91	-236498.15
$T_{0,5T}$	277.7551	277.6232	277.2053		288.9888	289.0924
SSE	0.0072	0.0071	0.0503		0.0019	0.0019

Table 37: Model of Mohr & Krawiec with two parameters (Arrhenius approach). Regarded values were μ_{max}, f_{temp} und $q_{O2,max}$ in the range 286-300.5 K.

A_2=0 !	μ_{max}		f_{temp}		$q_{O2,max}$	
	Initial values	100 Iterations	Initial values	100 Iterations	Initial values	100 Iterations
A_1	7.5	7.1879	4.5	4.5110	20	15.3362
E_{a1}	65000	61776.520	65000	67524.500	70800	59227.044
SSE	0.0063	0.0057	0.0232	0.0202	0.0105	0.0052

Table 38: Model of Mohr & Krawiec with four parameters. Regarded values were out of the sub optimal temperature range (278-300,5 K).

	μ_{max}		f_{temp}		$q_{O2,max}$	
	Initial values	100 Iterations	Initial values	1 Iteration	Initial values	3 Iterations
A_1	7.5	2.8842	4.5110	4.4512	15.3362	8.0656
E_{a1}	65000	16566.995	67524.500	66531.462	59227.044	19039.577
A_2	0.09	4.6601	0.006	0.0076	1	8.4942
E_{a2}	400000	138267.90	440000	401504.42	400000	280682.13
SSE	0.0070	0.0028	0.0227	0.0224	0.0049	0.0017

Table 39. Model of Mohr & Krawiec with six parameters. Regarded values were out of the whole temperature range (278-308 K).

	μ_{max}		f_{temp}		$q_{O2,max}$	
	Initial values	3 Iterations	Initial values	2 Iterations	Initial values	5 Iterations
A_1	2.8842	2.1071	4.4513	4.3151	8.0656	6.4398
E_{a1}	16566.995	1311.5936	66531.462	61463.045	19039.577	12260.401
A_2	4.6601	5.4180	0.0076	0.0116	8.4942	10.7866
E_{a2}	138267.90	132992.14	401504.42	410823.36	280682.13	219914.63
B	0.0003	0.0003	6 E-10	5.661 E-10	0.0002	0.0003
E_b	255000	244131.85	765000	757130.78	295000	284756.24
SSE	0.0124	0.0109	0.0781	0.0514	0.0037	0.0030

Table 40: Final parameters of the Schoolfield model for experiments A (metabolic model and Black Box model) and experiments B (metabolic model).

	$r_{15°C}$	ΔH^0	$\Delta H_H{}^o$	$T_{0,5H}$	$\Delta H_T{}^o$	$T_{0,5T}$
Experiments A						
Metabolic Model						
μ_{max}	0.13598108	78825.826	227281.57	302.89475	-232085.88	277.62329
f_{temp}	0.22648724	61742.663	513434.54	308.57142	-713399.45	277.20529
$q_{O2,max}$	0.14297069	6695.7988	1100795.4	303.11609	-236498.15	289.09242
Black Box model						
μ_{max}	0.13598108	78825.826	227281.57	302.89475	-232085.88	277.62329
f_{temp}	0.22648724	61742.663	513434.54	308.57142	-713399.45	277.20529
$q_{O2,max}$	0.18847571	-4746.2573	691431.158	304.23735	-290836.85	289.18388
Experiments B						
Metabolic model						
μ_{max}	0.2279	17697.82			-132739.88	289.4275
f_{temp}	0.33399506	56067.532			-10461132	274.1279
$q_{O2,max}$	0.04765152	44675.874			-343936.02	287.72579

Table 41: Estimated parameters for experiments A (metabolic model). 36 data sets for μ_{max}, f_{temp} and $q_{O2,max}$ are presented. Temperature T [K], $q_{O2,max}$ [mmol/(mmol h)].

	T	μ_{max}	f_{temp}	$q_{O2.max}$		T	μ_{max}	f_{temp}	$q_{O2.max}$
1	278	0.02512	0.06486	0.00630	19	288	0.116	0.24799	0.05087
2	278	0.0206	0.05772	0.00470	20	288	0.1318	0.24844	0.04898
3	281	0.05117	0.13714	0.007	21	290	0.1646	0.25116	0.08009
4	281	0.03882	0.09361	0.00997	22	293	0.2163	0.27515	0.11081
5	281	0.04766	0.10869	0.01363	23	293	0.235	0.36873	0.12844
6	283	0.06417	0.15510	0.01341	24	293	0.2374	0.35213	0.11942
7	283	0.05032	0.12702	0.01010	25	295	0.2938	0.44310	0.14195
8	283	0.06724	0.15439	0.01808	26	295	0.2893	0.41257	0.15028
9	286	0.1077	0.22577	0.03209	27	298	0.3309	0.61301	0.14930
10	288	0.1187	0.18522	0.05574	28	298	0.32	0.57082	0.13526
11	288	0.1348	0.20922	0.06150	29	298	0.3357	0.57106	0.14915
12	288	0.1381	0.25648	0.05082	30	300.5	0.3926	0.67593	0.17241
13	288	0.1334	0.19235	0.06608	31	300.5	0.3904	0.75288	0.16629
14	288	0.1428	0.23397	0.06233	32	303	0.3326	0.70495	0.10178
15	288	0.1269	0.22629	0.06937	33	303	0.3902	0.85510	0.07939
16	288	0.1183	0.21152	0.05343	34	305	0.2792	0.87588	0.01029
17	288	0.1403	0.22727	0.05792	35	305	0.3364	1.00438	0.01863
18	288	0.1491	0.23996	0.06752	36	308	0.2302	0.76113	0

Table 42: Estimated parameters for experiments A (Black Box model). 36 data sets for μ_{max}, f_{temp} and $q_{O2,max}$ are presented.

	T	μ_{max}	f_{temp}	$q_{O2.max}$		T	μ_{max}	f_{temp}	$q_{O2.max}$
1	278	0.02156	0.06638	0.00584	18	288	0.136	0.25493	0.06163
2	278	0.01696	0.05804	0.00346	19	288	0.133	0.20786	0.07210
3	281	0.03525	0.09347	0.01107	20	288	0.1134	0.17860	0.06325
4	281	0.0395	0.12298	0.00500	21	290	0.1589	0.24899	0.10464
5	281	0.04441	0.10935	0.01545	22	293	0.2192	0.34320	0.12028
6	283	0.06462	0.15451	0.02214	23	295	0.2919	0.44216	0.16502
7	283	0.06123	0.15481	0.01689	24	295	0.3172	0.46936	0.19065
8	283	0.0475	0.13795	0.00913	25	298	0.3536	0.57234	0.20013
9	286	0.11	0.23769	0.04044	26	298	0.3335	0.57056	0.17553
10	288	0.1406	0.23476	0.07262	27	298	0.2857	0.53065	0.14231
11	288	0.1291	0.27185	0.09249	28	300.5	0.3894	0.67347	0.20296
12	288	0.1487	0.24618	0.08414	29	300.5	0.3884	0.75204	0.19832
13	288	0.1333	0.19743	0.07371	30	303	0.3655	0.87683	0.13484
14	288	0.113	0.24830	0.07857	31	303	0.3898	0.84695	0.11017
15	288	0.1236	0.23222	0.06879	32	305	0.393	1.03032	0.05598
16	288	0.1489	0.25928	0.07249	33	305	0.3331	1.00324	0.04249
17	288	0.1294	0.24841	0.05828	34	308	0.2288	0.75886	0

Process control scenarios

Table 43: Accuracy of temperature control scenarios (Experiments A)

	Mean Value of deviations [mmol/L]		Standard deviation [mmol/L]	
	Substrate	Biomass	Substrate	Biomass
Black Box Model				
Scenario 1	5.9	3.18	7.67	2.21
Scenario 2	4.56	6.37	4.41	5.53
Total	6.45	6.21	5.83	5.94
Metabolic Model				
Scenario 1	7.29	8.54	6.18	7.47
Scenario 2	4.72	6.18	4.34	6.19
Total	6.66	7.18	5.96	6.77

Table 44: Accuracy of temperature control scenarios (Experiments B)

	Mean Value of deviations [mmol/L]		Standard deviation [mmol/L]	
	Substrate	Biomass	Substrate	Biomass
Scenario 1	4.10	8.30	4.76	10.57
Scenario 2	3.09	5.74	4.14	8.05
Total	3.80	7.06	4.53	8.99

Table 45: Accuracy of dissolved oxygen control scenarios (experiments A)

	Mean Value of deviations [mmol/L]		Standard deviation [mmol/L]	
	Substrate	Biomass	Substrate	Biomass
Black Box Model				
Scenario 1	5.49	7.85	4.84	6.59
Scenario 2	8.55	5.02	5.73	8.63
Total	8.58	6.87	6.8	8.41
Metabolic Model				
Scenario 1	4.86	6.87	4.67	8.74
Scenario 2	4.75	6.73	3.43	7.1
Total	5.34	6.87	4.94	7.61

Industrial Propagations

Table 46: Accuracy of industrial propagations (Experiments E-G). Mean values of deviation between simulated and measured data and standard deviations are presented.

	Mean Value of deviations [mmol/L]			Standard deviation [mmol/L]		
	Substrate	Biomass	Ethanol	Substrate	Biomass	Ethanol
Experiments E	4,41	33,24	6,48	4,85	27,54	8,14
Experiments F	7,09	7,73	6,6	7,61	9,24	9,18
Experiments G	5,93	10,65	10,92	4,0	11,03	5,06
Total	5,82	18,5	7,54	5,92	22,30	7,97

Table 47: Accuracies for model based simulations of experiments H

	Mean Value of deviations [mmol/L]		Standard deviation [mmol/L]	
	Substrate	Biomass	Substrate	Biomass
Propagation 1	3.29	3.78	4.82	4.89
Propagation 2	3.52	5.66	4.47	6.95
Propagation 3	2.96	4.83	3.78	6.03
Total	4.00	5.42	4.67	6.29

Tables to materials and methods

Table 48: Settings of the temperature controller and other relevant values.

	Symbol	Value for propagation system A	Unit
max. cooling/heater power		4000/2000	W
Stirring		1200 (25Hz)	rpm
filling level		0.125	m^3
flow rate of circulation pump (aggregate)		1.5	m^3/h
Parameter used			
proportional action coefficient	K_p	0.2	$°C^{-1}$
integral action time	T_n	45/60	h
derivative action time	T_v	0	h

Table 49: Specifications of applied sensors and transmitters for online measurement

	Manufacturer	**Sensor / Transmitter**	**Measurement range**	**Accuracy**
Temperature	Hartmann & Braun	PT 100	0-100°C	
Pressure	Endress + Hauser		0-4 bar abs.	ca. 1%
Extract	Krüss, Hamburg			
Density	Bopp & Reuther	DIMF 2.0 TRV		0.005
Turbidity	Monitek	22M	0-2000 AU	ca. 1%
Particle count	McNab		0-200 E+6 Cells/mL	ca. 1%
pH-value	Ingold Mettler Toledo	InPro3100/pH2100	0-14	ca. 0.05
Dissolved oxygen	Ingold Mettler Toledo	InPro6100/Ingold210	0-10 ppm	ca. 1%
Air Flow	Bopp & Reuther		0.05-0.3m^3/h	ca. 5%

REFERENCES

1 Adair, C., Kilsby, D.C., Whittall, P.T. (1989) Comparison of the Schoolfield (non-linear Arrhenius) model and the Square Root model for predicting bacterial growth in foods. Food Microbiology, Vol. 6, 1, 7-18.

2 Aiba, S., Shoda, M., Nagatani, M. (1968) Kinetics of product inhibition in alcohol fermentation. Biotechnology and Bioengineering, Vol. 10, 6, 845-864.

3 Alberts, B., Bray, D., Lewis, J., Raff, M., Roberts, K., Watson, J.D. (1994) Molecular biology of the cell, 3rd edition. Garland Publishing, New York.

4 Anderson, A. (1998) How brewers' yeast has been and is handled and treated. MBAA Tech. Q., Vol. 35, 1, 1-3.

5 Annemüller, G., Manger, H.-J. (1999) Die Belüftung der Hefereinzucht – maximal ist nicht gleich optimal! Brauwelt, Vol. 139, 21/22, 993–1007.

6 Annemüller, G., Manger, H.-J. (1998) Grenzen und Konsequenzen der Hefevermehrung in Bierwürze. Brauwelt, Vol 138, 49/50, 2478–2481.

7 Aries, V., und B.H. Kirsop. (1977). Sterol synthesis in relation to growth and fermentation by brewing yeasts inoculated at different concentrations. Journal of the Institute of Brewing, Vol. 85, 220-223.

8 Atkins, P.W. (1987) Physikalische Chemie, 1. Auflage. VCH Verlagsgesellschaft mbH, Weinheim.

9 Back, W., Bohak, I., Ackermann, T. (1993) Optimierte Hefewirtschaft, Verbesserung der physiologischen Eigenschaften von Anstell- und Dosierhefe mit Hilfe des Assimilationsverfahrens. Brauwelt, Vol. 133, 39, 1960–1963.

10 Back, W., Imai, T., Forster, C. Narziß, L. (1998) Hefevitalität und Bierqualität. Monatsschrift für Brauwissenschaft, Vol. 51, 11/12, 189–195.

11 Baltes, M. (1996) Entwurf eines metabolisch strukturierten Modells zur dynamischen Simulation des Katabolismus von *Saccharomyces cerevisiae*, PhD thesis, Universität Stuttgart.

12 Baker, C T H., Bocharov, G.A., Paul, C.A.H., Rihan, F.A. (1998) Modelling and analysis of time-lags in some basic patterns of cell proliferation. Journal of Mathematical Biology, Vol. 37, 4, 341-371.

13 Barford, J.P. (1990) A General Model for Aerobic Yeast Growth: Batch Growth. Biotechnology and Bioengineering, Vol. 35, 907–920.

14 Barford, J. P. (1981) A mathematical model for the aerobic growth of Saccharomyces cerevisiae with a saturated respiratory capacity. Biotechnology and Bioengineering, Vol. 23, 1735–1762.

15 Becker, T.M. (2002) Management of bioprocesses by means of modelling and cognitive tools. Habilitationsschrift, TU München.

16 Bělehrádek, J. (1926) Protoplasmic viscosity as determined by a temperature coefficient of biological reactions. Nature (London) Vol. 118, 478–480.

17 Bellgardt, K.-H. (2000) Some Modeling Basics. In: Bioreaction Engineering: Modeling and Control, K. Schügerl, K.-H. Bellgardt (eds.), Springer-Verlag Berlin Heidelberg New York, 3-5.

18 Bellgardt, K.-H. (1991) Cell Models. In: Biotechnology, 2nd, completely revised edition, edited by H.-J. Rehm and G. Reed, Vol. 4 Measuring, Modelling and Control, edited by K. Schügerl, VCH Verlagsgesellschaft mbH, Weinheim, Germany.

19 Berber, R., Pertev, C., Türker, M. (1999) Optimization of feeding profile for baker's yeast production by dynamic programming. Bioprocess Engineering, Vol. 20, 3, 263-269.

20 Bergter, F. (1983) Wachstum von Mikroorganismen: Experimente und Modelle. Chapter 9: Temperatur und Wachstum. Verlag Chemie, Weinheim.

21 Besli, N., Türker, M., Gul, E. (1995) Design and simulation of a fuzzy controller for fed-batch yeast fermentation. Bioprocess Engineering, Vol. 13, 3, 141-148.

22 Bronn, W.K. (1989/90) Technologie der Hefefabrikation – Backhefe. 14. Auflage, TU Berlin / Versuchsanstalt für Gärungsgewerbe und Biotechnologie, Berlin.

23 Burkhardt, L., Annemüller, G. (1998) Stoffdatenermittlung von Hefe. Teil 1: Untersuchungen zur Erfassung der Dichte von Hefesuspensionen und Hefezellen in Abhängigkeit von Hefetrockensubstanzgehalt und Temperatur. Monatsschrift für Brauwissenschaft, Vol.51, 1/2, 4-10.

24 Busturia, A., Lagunas, R. (1986) Catabolite Inactivation of the Glucose Transport System in *Saccharomyces cerevisiae*. Journal of Gen. Microbiology, Vol. 132, 379–385.

25 Caro, I., Pérez, L., Cantero, D. (1991) Development of a kinetic model for the alcoholic fermentation of must. Biotechnology and Bioengineering, Vol. 38, 742–748.

26 Cartwright, C.P., Rose, A.H., Calderbank, J., Keenan, M.H.J. (1989) Solute Transport. In: The Yeasts, Vol. 3, 5-56, 2nd edition, Academic Press, London.

27 Charwat, H.J. (1996a) Farbkonzept für die Prozessführung mit Bildschirmen (Teil 1). atp, Vol. 38, 5, 50–53.

28 Charwat, H.J. (1996b) Farbkonzept für die Prozessführung mit Bildschirmen (Teil 2). atp, Vol. 38, 6, 58–63.

29 Charwat, H.J. (1996c) Farbkonzept für die Prozessführung mit Bildschirmen (Teil 3). atp, Vol. 38, 7, 62–65.

30 Chmiel, H., Sonnleitner, B. (1991) Wachstum: Kinetik und Modelle. In: Bioprozeßtechnik 1. Einführung in die Bioverfahrenstechnik. H. Chmiel (Hrsg.). Gustav Fischer Verlag, Stuttgart, 139-190.

31 Cho, M.H. and Wang S.S. (1990) Practical method for estimating oxygen kinetic and metabolic parameters. Biotechnology Progress, Vol. 6, 164-167.

32 Cholerton. M. (1995) Advanced yeast propagation. Proc. Inst. Brew. Cent. South. Africa Sect., Vol. 5, 179-185.

33 Claes, J.E., van Impe, J.F. (2000) Combining yield coefficients and exit-gas analysis for monitoring of the bakers' yeast fed-batch fermentation. Bioprocess Engineering, Vol. 22, 3, 195-200.

34 Cortassa, S., Aon, M.A. (1994) Metabolic Control analysis of glycolysis and branching to ethanol production in chemostat cultures of Saccharomyces cerevisiae under carbon, nitrogen or phosphate limitations. Enzyme Microbiol. Technology, Vol. 16, 761-770.

35 Crabtree, H. G. (1929) Observations on the carbohydrate metabolism of tumors. Biochem. Journal, Vol. 23, 536-545.

36 Dantigny, P., Gruber, M. (1996) Transition rate kinetics from ethanol oxidation to glucose utilisation within a structured model of bakers' yeast. Applied Microbiology and Biotechnology, Vol. 45, 1/2, 199-203.

37 Dantigny, P., Molin P. (2000) Influence of the modelling approach on the estimation of the minimum temperature for growth in Belehradek-type models. Food Microbiology, Vol. 17, 597-604.

38 Dantigny, P. (1998): Dimensionless analysis of the microbial growth rate dependence on sub-optimal temperatures. Journal of Industrial Microbiology & Biotechnology, Vol. 21, 215-218.

39 De Ory, I., Romero, L. E., Cantero, D. (1998) Modelling the kinetics of growth of *Acetobacter aceti* in discontinuous culture : influence of the temperature of operation. Applied Microbiology and Biotechnology, Vol. 49, 2, 189–193.

40 Dittrich W., Göhde, W. (1969) Impulscytophotometrie bei Einzelzellen in Suspensionen. Z. Naturforschung, 24b, 360-361.

41 Donhauser, S. (1995) Charakterisierung von Hefearten und –stämmen. Bedeutung für die Herstellung ober- und untergäriger Biertypen. Brauwelt, Vol. 135, 50, 2644-2650.

42 Duboc, Ph., Marison, I., von Stockar, U. (1996) Physiology of *Saccharomyces cerevisiae* during cell cycle oscillations. Journal of Biotechnology, Vol. 51, 1, 57-72.

43 Duboc, P., Cascao-Pereira, L.G., von Stockar, U. (1998) Identification and Control of Oxidative Metabolism in Saccharomyces cerevisiae During Transient Growth using Calorimetric Measurements. Biotechnology and Bioengineering, Vol. 57, 5, 610-619.

44 Eils, H.-G., Eidtmann, A., Back, W. (2000) Maßnahmen zur Verbesserung der Hefetechnologie und Umsetzung in der Praxis, Brauwelt, Vol. 140, 15, 590-595.

45 Ejiofor, A.O. et al. (1994) Analysis of the respiro-fermentative growth of *Sacharomyces cerevisiae* on glucose in a fed-batch fermentation strategy for accurate parameter estimation. Applied Microbiology and Biotechnology, Vol. 41, 6, 664–669.

46 Emde, F. (2000) Eine Frage der Verteilung. Trend bei Misch- und Begasungssystemen. Chemie Technik, 4, 24-28.

47 Engasser, J.M., Marc, I., Moll, M., Duteurtre, B. (1981) Kinetic modelling of beer fermentation. Proc. EBC Congress, Vol. 18, 579-586.

48 Enari, T.M. (1974) Amino acids, peptids and proteins of wort. EBC Symposium, EBC Monograph I, 73-89.

49 Enfors, S.-O., Hedenberg, J., Olsson, K. (1990) Simulation of the dynamics in the Baker's yeast process. Bioprocess Engineering, Vol. 5, 191-198.

50 European Brewery Convention (EBC) (2000) Fermentation and Maturation. Manual of Good Practice. Fachverlag Hans Carl, Nürnberg.

51 Eyring, H. (1935) Activated complex in chemical reactions. Journal of Chemical Physics, Vol. 3, 107-115.

52 Fagervik, K. et al. (1995) Adaptive on-line simulation of bioreactors: fermentation monitoring and modelling system. Journal of Industrial Microbiology, Vol. 14, 403-411.

53 Fellner, M., Delgado, A., Becker, T. (2002) Functional neurons in dynamic neural networks for bioprocess modelling. Bioprocess and Biosystems Engineering, submitted.

54 Fiala, J., Lloyd, D.R., Rychtera, M., Kent, C.A., Al-Rubeai, K.M. (1999) Evaluation of cell numbers and viability of *Saccharomyces cerevisiae* by different counting methods. Biotechnology Techniques, Vol. 13, 787-795.

55 Gaden Jr., E.L. (2000) Fermentation Process Kinetics. Biotechnology and Bioengineering, Vol 67, 6, 629-635. Reprinted from J. of Biochemical and Microbiological Technology and Engineering, Vol. 1, 4, 413-429.

56 Geiger, E. (1993) Kontinuierliche Hefevermehrung. Brauwelt, Vol. 133, 16, 646-649.

57 Gervais, P., Martinez de Maranon, I. (1995) Effect of kinetics of temperature variation on *Saccharomyces cerevisiae* viability and permeability. Biochimica and Biophysica Acta, Vol. 1235, 52-56.

58 Giannuzzi, L., Pinotti, A., Zaritzky, N. (1998) Mathematical modelling of microbial growth in packaged refrigerated beef stored at different temperatures. International Journal of Food Microbiology, Vol. 39, 1/2, 101–110.

59 Grützmacher, J. (1991): Bedeutung des Sauerstoffs für die Betriebshefe, Brauwelt, Vol. 131, 23, 1986.

60 Gschwend-Petrik, M. (1983) Dynamische Untersuchungen zur Stoffwechselregulation und Ethanolbildung bei *Saccharomyces uvarum*, Dissertation, ETH Zürich.

61 Hartmeier, W.: Untersuchungen über die Kinetik der mikrobiellen Sauerstoff-Aufnahme und den Einfluß des Sauerstoff-Partialdruckes auf den Stoffwechsel von Saccharomyces cerevisiae, Dissertation, Fachbereich Lebensmitteltechnologie und Biotechnologie, Technische Universität Berlin, 1972

62 Hege, U. (1998) Eine Methode zur Regelung biotechnologischer Chargenprozesse mittels unscharfer Logik. Dissertation, TU München.

63 Heijnen J.J. (1994) Thermodynamics of Microbial Growth and its Implications for Process Design. Trends in Biotechnology, Vol. 12, 483–492.

64 Heijnen, J.J. (1996) Macroscopic Approach and Mathematical Modelling of Microbial Processes. In: BODL-Advanced Course Microbial Physiology and Fermentation Technology, Delft.

65 Heijnen, J.J. (1996) Metabolic Modelling. In: BODL-Advanced Course Microbial Physiology and Fermentation Technology, Delft.

66 Heijnen, J.J. (1996) Thermodynamics of chemotrophic growth and maintenance. In: BODL-Advanced Course Microbial Physiology and Fermentation Technology, Delft.

67 Heitzer, A., Kohler, H.-P.E., Reichert, P., Hamer, G. (1991) Utility of Phenomenological Models for Describing Temperature Dependence of Bacterial Growth. Applied and Environmental Microbiology, Vol. 57, 9, 2656-2665.

68 Herwig, C., von Stockar, U. (2002) A small metabolic flux model to identify transient metabolic regulations in *Saccharomyces cerevisiae*. Bioprocess Biosystems Engineering, Vol. 24, 6, 395-403.

69 Heyse, K.-U. (1995) Handbuch der Brauereipraxis, Hans Carl Verlag, Nürnberg.

70 Holzer, H. (1958) Aerobe Gärung und Wachstum, in: Neuere Ergebnisse aus Chemie und Stoffwechsel der Kohlenhydrate, Verlag Springer, Berlin – Göttingen – Heidelberg, 1958

71 Hutter, A., Oliver, S.G. (1998) Ethanol production using nuclear petite yeast mutants. Applied Microbiology and Biotechnology, Vol. 49, 5, 511-516.

72 Hutter, K.-J. (2000) Transparenz der Gärung und Kontrolle mit Hilfe der flußzytometrischen Analytik. Brauwelt, Vol. 140, 41, 1634-1641.

73 Hutter, K.-J., Remor, M., Müller, S. (2000) Biomonitoring der Betriebshefen in praxi mit fluoreszenzoptischen Verfahren. VII. Mitteilung: Untersuchungen zur flußzytometrischen Bestimmung des Glykogengehaltes der Betriebshefe. Monatsschrift für Brauwissenschaft Vol. 53, 5/6, 68-76.

74 Hutter, K.J., Müller, S. (1999) Prozeßoptimierung von Reinzucht- und Anstellverfahren mittels Flußzytometrie in sächsischen Brauereien. Monatsschrift für Brauwissenschaft, Vol. 52, 3/4, 40-48.

75 Hutter, K.-J., Müller, S. (1996) Biomonitoring der Betriebshefe in praxi mit fluoreszenzoptischen Verfahren - IV. Mitteilung: Zellzyklus und 3ß-Hydroxysterolgehalt. Monatsschrift für Brauwissenschaft, Vol. 49, 7/8, 234-239.

76 Hutter, K.-J., Herber, M., Lindemann, B. (1995) Biomonitoring der Betriebshefe in praxi mit fluoreszenzoptischen Verfahren I. Mitteilung: DNS-Gehalt und Zellzyklusanalysen verschiedener Betriebshefen. Monatsschrift für Brauwissenschaft, Vol. 48, 5/6, 184-190.

77 Hutter, K.-J., Eipel, H.E. (1978) DNA determination of yeast by flow cytometry. FEMS Microbiology Lett., Vol. 3, 35-38.

78 Imai, T., Ohno, T. (1995) Measurement of yeast intracellular pH by image processing and the change it undergoes during growth phase. Journal of Biotechnology, Vol. 38, 2, 165–172.

79 Jones, H.L. (1997) Yeast propagation – past present and future. Brewers' Guardian, Vol. 126, 24-27.

80 Kirsop, B.H. (1982). Developments in beer fermentation. Topics in Enzymology, Fermentation and Biotechnology, Vol. 6, 79-1051.

81 Koutsoumanis, K.P., Taoukis, P.S., Drosinos, E.H., Nychas, G.-J.E. (2000) Applicability of an Arrhenius model for the combined effect of temperature and CO_2 packaging on the spoilage microflora of fish. Applied and Environmental Microbiology, Vol. 66, 8, 3528-3534.

82 Krüger, E., Anger, H.-M. (1990) Kennzahlen zur Betriebskontrolle und Qualitätsbeschreibung in der Brauwirtschaft: Daten über Roh- und Hilfsstoffe, Halbfertig- und Fertigprodukte bei der Bierbereitung. Behr's Verlag, Hamburg, Germany.

83 Kruger, L. (1998) Yeast metabolism and ist effect on flavour: Part 1. Brewers' Guardian, Vol. 127, 4, 24-29.

84 Kruger, L. (1998) Yeast metabolism and ist effect on flavour: Part 2. Brewers' Guardian, Vol. 127, 5, 27-30.

85 Kunze, W. (1998) Technologie Brauer und Mälzer, 8., völlig neu bearb. Auflage, VLB Berlin.

86 Krzystek, L., Ledakowicz, S. (1998) Yield and maintenance coefficients in *S. cerevisiae* cultures. J. Chem. Technol. Biotechnol., Vol. 71, 3, 197-208.

87 Lehmann, J. (1997) Optimierung der Hefeassimilation und deren Einbindung in den Brauprozeß. Dissertation, TU München.

88 Lehninger, A.L., Nelson, D.L., Cox, M.M. (1994) Prinzipien der Biochemie, 2. Auflage, Spektrum Akademischer Verlag, Heidelberg Berlin Oxford.

89 Lentini, S.A. (1993) A Review of the Various Methods Available for Monitoring the Physiological Status of Yeast: Yeast Viability and Viatlity. Carlton and United Breweries Limited / Foster's Brewing Group, 287-293.

90 Maemura, H., Morimura, S., Kida, K. (1998) Effects of aeration during the cultivation of pitching yeast on ist characteristics during the subsequent fermentation of wort. J. Inst. Brew., Vol. 104, 207–211.

91 Manger, H.-J., Annemüller, G. (2000) Die Geschwindigkeit der Hefevermehrung in der Brauerei. Brauwelt, Vol. 140, 13/14, 520-525.

92 Manger, H.-J. (1998) Probleme bei der Bestimmung der Hefezellzahlen im Brauereibetrieb. Brauwelt, Vol.138, 18, 804-805.

93 Mann, H., Schiffelgen, H., Froriep, R. (1997) Einführung in die Regelungstechnik – analoge und digitale Regelung, Fuzzy-Regler, Regler-Realisierung, Software. Hanser Verlag, München, Wien, 7. Auflage.

94 Masschelein, C.A., Borremans, E., van de Winkel, L. (1994) Application of exponentially-fed-batch cultures to the propagation of brewing yeast. Proc. Conv. Inst. Brew. Asia Pac. Sect. 23, 104-108.

95 McLaren, J.I., Fischborn, T., Briem, F., Engelmann, J., Geiger, E. (1999) Zinkproblem gelöst? Brauwelt, Vol. 139, 45/46, 2159-2160.

96 Meszaros, A., Brdys, M. A., Tatjewski, P., Lednicky, P. (1995) Multilayer adaptive control of continous bioprocesses using optimising control technique. Case study: baker's yeast culture. Bioprocess Engineering, Vol. 12, 1/2, 1-9.

97 Methner, F.-J. (1999) Optimierte Hefepropagation mittels kontinuierlicher Belüftung. In: European Brewery Convention. Proceedings of the 27th congress, Cannes, France, 1999, 637-646.

98 Meyers Lexikon in XII Bd.7. Auflage, Leipzig: Bibliographisches Institut.

99 Mönch, D., Krüger, E., Stahl, U. (1995) Wirkung von Streß auf Brauereihefen. Monatsschrift für Brauwissenschaft, Vol. 48, 9/10, 288-299.

100 Mohr, P.W.; Krawiec, S. (1980) Temperature characteristics and Arrhenius plots for nominal psychrophiles, mesophiles and thermophiles. Journal of General Microbiology, Vol. 121, 311-317.

101 Müller, S., Hutter, K.-J., Bley, T., Petzold, L., Babel, W. (1997) Dynamics of yeast cell states during proliferation and non proliferation periods in a brewing reactor monitored by multidimensional flow cytometry. Bioprocess Engineering, Vol. 17, 5, 287-293.

102 Narziß, L. (1995) Abriß der Bierbrauerei. 6., neubearbeitete Auflage, Ferdinand Enke Verlag, Stuttgart.

103 Nielsen, J., Villadsen, J. (1994) Bioreaction Engineering. Plenum Press, New York.

104 Olsson, G., Piani, G. (1993) Steuern, Regeln, Automatisieren - Theorie und Praxis der Prozeßleittechnik.Hanser-Verlag und Prentice-Hall International, Wien, London.

105 Peters, U., Hege, U., Enders, T., Becker, T., Delgado, A., Denk, V. (1997) On-line Messung und Regelung wichtiger Produktparameter bei der industriellen Fermentation. Chemie Ingenieur Technik, Vol. 69, 1225–1226.

106 Petrova, M., Koprinkova, P., Patarinska, T. (1997) Neural Network modelling of fermentation processes. Microorganism cultivation model. Bioprocess Engineering, Vol. 16, 3, 145-149.

107 Pfenninger, H. (1993) Brautechnische Analysenmethoden Band II, Freising.

108 Pham, H.T.B., Larsson, G., Enfors, S.-O. (1998) Growth and Energy Metabolism in Aerobic Fed-Batch Cultures of *Saccharomyces cerevisiae*: Simulation and Model Verification. Biotechnology and Bioengineering, Vol. 60, 4, 474-482.

109 Pirt, J.S. (1975) Principles of Microbe and Cell Cultivation. Blackwell Scientific Publications, Oxford, 211-218.

110 Podgornik, A., Koloini, T., Raspor, P. (1997) On-Line Measurement and Analysis of yeast Flocculation. Biotechnology and Bioengineering, Vol. 53, 2, 179-184.

111 Popova, S. (1997) Parameter identification of a model of yeast cultivation process with neural network. Bioprocess Engineering, Vol. 16, 4, 243-245.

112 Presser, K.A., Ross, T., Ratkowsky, D.A. (1998) Modelling the growth limits (growth/ no growth interface) of *Escherichia coli* as a function of temperature, pH, lactic acid concentration and water activity. Applied and Environmental Microbiology, Vol. 64, 5, 1773–1779.

113 Ratkowsky, D.A., Olley, J., McMeekin, T.A., Ball, A. (1982) Relationships between temperature and growth rate of bacterial cultures. Journal of Bacteriology, Vol. 149, 1-5.

114 Ratkowsky, D.A., Lowry, R. K., McMeekin, T.A., Stokes, A. N., Chandler, R.E. (1983) Model for bacterial culture growth rate throughout the entire biokinetic temperature range. Journal of Bacteriology, Vol. 154, 1222-1226.

115 Ratkowsky, D.A., Ross, T., McMeekin, T. A., Olley, J. (1991) Comparison of Arrhenius-type and Bělehrádek-type models for prediction of bacterial growth in foods. Journal of Applied Bacteriology, Vol. 71, 452-459.

116 Reichert, P. (1994) Concepts Underlying a Computer Program for the Simulation of Aquatic Systems. Schriftenreihe der EAWAG No. 7, Switzerland.

117 Reichert, P. (1998) Aquasim 2.0 - User Manual, Swiss Federal Institute for Environmental Science and Technology (EAWAG), Switzerland.

118 Reinhardt, C., Völker, B., Martin, H.-J., Kneiseler, J., Fuhrmann, G.F. (1997) Different activation energies in glucose uptake in *Saccharomyces cerevisiae* DFY1 suggest two transport systems. Biochimica et Biophysica Acta, Vol. 1325, 126-134.

119 Rizzi, M., Baltes, M., Theobald, U., Reuss, M. (1997) In Vivo Analysis of Metabolic Dynamics in *Saccharomyces cerevisiae*: II. Mathematical Model. Biotechnology and Bioengineering, Vol. 55, 4, 592-608.

120 Rose, A.H., Vijayalakshmi, G. (1993) Baker's yeast. In The Yeasts, 2nd Ed. Vol. 5: Yeast Technology. A.H. Rose and J.S. Harrison, eds, Academic Press, London, 357-398.

121 Scheffers, W.A., van Dijken, J.P. (1987) Redox Control in Yeast. In: Monograph XII, E.B.C.-Symposium on Brewers' Yeast , Vuoranta (Helsinki), Finland, November 1986. Verlag Hans Carl, Nürnberg, Germany.

122 Schlegel, H.G. (1992) Allgemeine Mikrobiologie, 7., überarbeitete Auflage, Georg Thieme Verlag Stuttgart New York,

123 Shi, H., Shimizu, K. (1998) On-Line Metabolic Pathway Analysis Based on Metabolic Signal Flow Diagram. Biotechnology and Bioengineering, Vol. 58, 2/3, 139-148.

124 Schmid, R.; Sapunov, V.N. (1982) Non-formal kinetics, Kapitel: Dependence of reaction rate on temperature. Verlag Chemie, Weinheim.

125 Schoolfield, R. M., Sharpe, P. J. H., Magnuson, C. E. (1981) Non-linear regression of biological temperature-dependent rate models based on absolute reaction-rate theory. Journal of Theoretical Biology, Vol. 88, 719–731.

126 Sharpe, P. J. H., DeMichele, D.W. (1977) Reaction kinetics of poikilotherm development. Journal of Theoretical Biology, Vol. 64, 649–670.

127 Sonnleitner, B., Käppeli, O. (1986) Growth of saccharomyces cerevisiae is controlled by its limited respiratory capacity: Formulation and verification of a hypothesis. Biotechnology and Bioengineering, Vol. 28, 6, 927-937.

128 Strauß, G. (1990) Modellbildung des Wachstums von Backhefe (*Saccharomyces cerevisiae*) im Fed-Batch-Airliftreaktor. Dissertation, Universität Hannover.

129 Sweere, A.P.J., Giesselbach, J., Barendse, R., de Krieger, R., Honderd, G., Luyben, K.C.A.M. (1988) Modelling the dynamic behaviour of *Saccharomyces cerevisiae* and ist application in control experiments, Applied Microbiology and Biotechnology, Vol. 28, 2, 116-127.

130 Teissier, P., Perret, B., Latrille, E., Barillere, J. M., Corrieu, G. (1996) Yeast concentration estimation and prediction with static and dynamic neural network models in batch cultures. Bioprocess Engineering, Vol. 14, 54, 231-235.

131 van Gulik, W. M., Heijnen, J. J. (1995) A Metabolic Network Stoichiometry Analysis of Microbial Growth and Product Formation, Biotechnology and Bioengineering, Vol. 48, 681-698.

132 van Hoek, P., van Dijken, J.P., Pronk, J.T. (1998) Effect of specific growth rate on the fermentative capacity of bakers' yeast. Applied and Environmental Microbiology, Vol. 64, 11, 4226-4233.

133 VDI-Wärmeatlas Berechnungsblätter für den Wärmeübergang (1987) Verein Deutscher Ingenieure VDI Gesellschaft Verfahrenstechnik und Chemieingenieurwesen (Hrsg.), 8. Auflage, VDI-Verlag GmbH, Düsseldorf.

134 Verdun, C., Postma, E., Scheffers, W. A., van Dijken, J. P. (1992) Effect of benzoic acid on meatbolic fluxes in yeast: A continious culture study on the regulation of respiration and alcoholic fermentation, Yeast, 8, 501–517.

135 Volk, N., Lübbert, A. (1999) Modellgestützte Optimierung von Fermentationsprozessen, Vortrag Nr. 20, In: Kurzfassung der Referate der internen Arbeitssitzung des DECHEMA-Arbeitsausschusses „Technik biologischer Prozesse“

der DECHEMA Deutsche Gesellschaft für Chemisches Apparatewesen, Chemische Technik und Biotechnologie e.V. und des GVC-Fachausschusses „Bioverfahrenstechnik“ der GVC, Erfurt, 11.– 12.05.1999.

136 von Nida, L. (1996) Aerobe Hefeherführung. Brauwelt, Vol. 136, 36, 1685–1688.

137 Votruba, J., Kminek, M., Palatova, M. (1995) Education of Beer Brewing Physiology and Technology Using PSI Simulation Language. In: Preprints of the 6th Int. Conference on Computer Applications in Biotechnology, Garmisch-Partenkirchen, Germany, May 14-17, 1995.

138 Wackerbauer, K., Evers, H., Kunerth, S. (1996) Hefepropagation und Aktivität der Reinzuchthefe, Brauwelt, Vol. 136, 37, 1736–1743.

139 Wackerbauer, K., Tayama, T., Kunerth, S. (1997) Neuere Erkenntnisse des Einflusses der Hefelagerung auf die Gäraktivität und Vitalität von Hefen in nachfolgenden Gärungen. Monatsschrift für Brauwissenschaft, Vol.50, 7/8, 132-137.

140 Walker, G. M. (1998) Yeast, Physiology and Biotechnology, John Wiley & Sons, Chichester.

141 Weete, J. D. (1989). Structure and function of sterols in fungi. Advances in Lipid Research, Vol. 23, 115-167.

142 Wijtzes, T., de Wit, J.C., Huis in`t Veld, J.H.J., van`t Riet, K., Zwietering, M.H. (1995) Modelling bacterial growth of *Lactobacillus curvatus* as a function of acidity and temperature. Applied and Environmental Microbiology, Vol. 61, 7, 2533–2539.

143 Wolf, K.-H., (1991). Kinetik in der Bioverfahrenstechnik. Behr’s Verlag, Hamburg.

144 Zepf, M., Geiger, E., Nieten, I. (2000) Parametersteuerung bei der aeroben Hefevermehrung. Brauwelt, Vol.140, 44, 1849-1851.

145 Zhang, Z., Scharer, J., Moo-Young, M. (1997) Mathematical Model for aerobic culture of a recombinant yeast. Bioprocess Engineering, Vol. 17, 4, 235-240.

146 Zheng-Xiang, W., Zhuge, J., Fang, H., Prior, B.A. (2001) Glycerol production by microbial fermentation: A review. Biotechnology Advances, Vol. 19, 3, 201-223.

Curriculum Vitae of Tomas Kurz

1970 Born May, 11th in Stuttgart, Germany as the youngest of three sons of Margot and Erich Kurz. Mother tongue german.

1976 Primary school until 1980

1980 Grammar school until 1989. Finished with general qualification for university entrance (Abitur)

1989 Military service until 1990.

1990 Industrial placement in a brewery (Dinkelacker-Schwabenbräu AG, Stuttgart) until 1991.

1991 Study of brewing and beverage technology at the Technische Universität München-Weihenstephan until 1997.

1997 Doctoral thesis at Technische Universität München, Germany, at the Chair of Fluid Mechanics and Process Automation, until 2002.